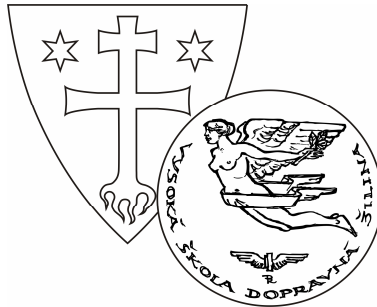# UNIVERSITY OF ŽILINA

TRANSCOM 2009

8-th EUROPEAN CONFERENCE
OF YOUNG RESEARCH AND SCIENTIFIC WORKERS

PROCEEDINGS

SECTION 6
MACHINES AND EQUIPMENTS. APPLIED MECHANICS

ŽILINA June 22 - 24, 2009
SLOVAK REPUBLIC

UNIVERSITY OF ŽILINA

TRANSCOM 2009

8-th EUROPEAN CONFERENCE
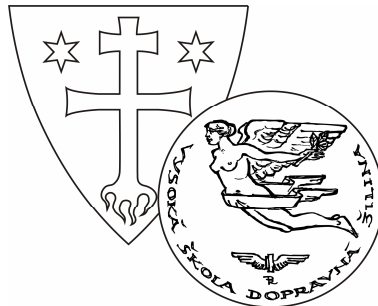OF YOUNG RESEARCH AND SCIENTIFIC WORKERS

under the auspices of

Prof. Ing. Ján Mikolaj, PhD.
Minister of Education, Slovak Republic

&

Prof. Ing. Ján Bujňák, PhD.
Rector of the University of Žilina

SECTION 6

MACHINES AND EQUIPMENTS. APPLIED MECHANICS

ŽILINA June 22 - 24, 2009
SLOVAK REPUBLIC

TRANSCOM 2009
8-th European conference of young research and scientific workers

TRANSCOM 2009, the 8th international conference of young European researchers, scientists and educators, aims to establish and expand international contacts and co-operation. The main purpose of the conference is to provide young scientists with an encouraging and stimulating environment in which they present results of their research to the scientific community. TRANSCOM has been organised regularly every other year since 1995. Between 160 and 400 young researchers and scientists participate regularly in the event. The conference is organised for postgraduate students and young research workers up to the age of 35 and their tutors. Young workers are expected to present the results they had achieved.

The conference is organised by the University of Žilina. It is the university with about 13 000 graduate and postgraduate students. The university offers Bachelor, Master and PhD programmes in the fields of transport, telecommunications, forensic engineering, management operations, information systems, in mechanical, civil, electrical, special engineering and in social sciences.

SECTIONS AND SCIENTIFIC COMMITTEE

1. TRANSPORT AND COMMUNICATIONS TECHNOLOGY
Scientific committee: Baumann S. (D), Cenek P. (SK), Droździel P. (PL), Janáček J. (SK), Jánošíková Ľ. (SK), Kremeňová I. (SK), Novák A. (SK), Palúch S. (SK), Rievaj V. (SK), Řezáč M. (CZ), Schnieder E. (D), Surovec P. (SK), Žarnay P. (SK)

2. ECONOMICS AND MANAGEMENT
Scientific committee: Bartošová V. (SK), Blašková M. (SK), Březinová O. (CZ), Duncan F.H. (USA), Hittmár Š. (SK), Kos B. (PL), Kucharčíková A. (SK), Lyakin A. (RUS), Rostášová M. (SK), Rybakov F. (RUS), Strenitzerová M. (SK), Strišš J. (SK), Tomová A. (SK)

3. INFORMATION AND COMMUNICATION TECHNOLOGIES
Scientific committee: Bärwald W. (D), Dado M. (SK), Drozdová M. (SK), Hanuliak I. (SK), Keil R. (D), Klimo M. (SK), Kolev P. (BG), Kotsopoulos S. (GR), Madleňák R. (SK), Matiaško K. (SK), Spalek J. (SK), Vaculík J. (SK), Vaculík M. (SK), Vrček N. (HR)

4. ELECTRIC POWER SYSTEMS. ELECTRICAL AND ELECTRONIC ENGINEERING
Scientific committee: Altus J. (SK), Blažek V. (D), Čápová K. (SK), Dobrucký B. (SK), Dodds S.J. (GB), Santarius P. (CZ), Vittek J. (SK)

5. MATERIAL ENGINEERING. MECHANICAL ENGINEERING TECHNOLOGIES
Scientific committee: Adamczak S. (PL), Bokůvka O. (SK), Borkowski S. (PL), Dzimko M. (SK), Guagliano M. (I), Kunz L. (CZ), Meško J. (SK), Nicoletto G. (I), Palček P. (SK), Skočovský P. (SK), Takács J. (H)

6. MACHINES AND EQUIPMENTS. APPLIED MECHANICS

Scientific committee: Dekýš V. (SK), Gerlici J. (SK), Kalinčák D. (SK), Malenovský E. (CZ), Medvecký Š. (SK), Merkisz J. (PL), Nemček M. (CZ), Pawelczyk M. (PL), Sága M. (SK), Zapoměl J. (CZ), Žmindák M. (SK)

7. CIVIL ENGINEERING

Scientific committee: Bouchair H. (F), Dmitrovskaja L. (RUS), Garbuz A. (UA), Ižvolt L. (SK), Melcer J. (SK), Ivanov J. (BG), Teleman E.C. (RO), Vičan J. (SK), Zolotov M. (UA)

8. SOCIAL SCIENCES

Scientific committee: Banáry B. (SK), Baštinec J. (CZ), Cabanová V. (SK), Gulová L. (CZ), Kráľová Z. (SK), Růžičková M. (SK), Šindelářová J. (CZ), Vikoren V. (N)

9. SECURITY ENGINEERING. FORENSIC ENGINEERING

Scientific committee: Danihelka P. (SK), Horák R. (CZ), Navrátil L. (CZ), Poledňák P. (SK), Reitšpís J. (SK),   Seidl M. (SK), Šenovský M. (CZ), Šimák L. (SK), Vasiliev D. (BG), Zamiar Z. (PL)

ORGANIZING COMMITTEE

CHAIRPERSON   Bokůvka Otakar

EXECUTIVE SECRETARY   Vráblová Helena

MEMBERS   Bábel J., Belan J., Braciník P., Brída P., Brumerčík F., Dobrotková M., Dubcová Z., Frajtová-Michalíková K., Harušinec J., Hnátová Z., Houšková L., Imrišková E., Jánošíková G., Kačiaková B., Kardoš M., Kormancová M., Krasňan M., Kuzmová M., Ladovský T., Ližbetinová L., Mihalov K., Močková M., Mráz M., Murín M., Neslušan M., Ondrejka R., Pachová S., Pavelková I., Pilát P., Potkan T., Remek Ľ., Smetana M., Sršníková D., Stránska S., Štofková K., Tulejová L., Valentíková E., Varmus M., Vaško A., Vaško M., Záborský M.

SECTION 6   MACHINES AND EQUIPMENTS, APPLIED MECHANICS

REVIEWERS:

Bronček Jozef
Brumerčík František
Dekýš Vladimír
Gerlici Juraj
Grenčík Juraj
Handrik Marián
Hlavňa Vladimír
Jandačka Jozef
Kalinčák Daniel
Král Metod
Kučera Ľuboš
Lack Tomáš
Lábaj Ján
Malcho Milan
Mikulík Marian
Sága Milan
Sapietová Alžbeta
Stuchlý Vladimír
Toporcer Emil
Vaško Milan
Žmindák Milan

Note:

Authors are responsible for language contents of their papers

CONTENTS

8

The Influence of Properties of Selected Fuels on Injection Parameters and Vibroacoustic Injector Signal

[*] Ambrozik T., Łagowski P.

[*] Kielce of University of Technology, Faculty of Mechatronics and Machine Building, Chair of Heat Machines, Al. 1000-lecia PP 7, 25-314 Kielce, e-mail: silspal@tu.kielce.pl

Abstract. The paper presents the research results and the analysis of the influence of the basic physical properties of the mineral fuels, biofuels and their blend with diesel oil (ON) with 30% ester content (B30) used to fuel AD3.152 UR engine on the basic stream parameters of atomizing fuel: the mean volumetric and superficial diameter of a drop the initial speed of the fuel outflow from the atomizer, the velocity of stream front the atomizer, injected fuel charge and the voltage of vibroacoustic signal of injector during engine work cycle. Investigations were carried out at the test bench, which included measurement system for fast changing quantities. The research shows that physical and chemical properties of engine fuel influence the mentioned stream parameters of atomizing fuel and vibroacoustic signal of injector.

Keywords: atomizer, combustion engine, injector, vibroacoustic signal.

1. Introduction

Building engines with higher unit power and with the best technical and economic indeexes a very important economic task. Designing and manufacturing engines brings many complicated problems connected with the necessity of improvement and optimisation the combustion process and with reduction maximum gas pressure in the cylinder and the fuel in the fuel system at the same time. The resolution of mentioned problems should be realised by assuring the proper injection and fuel atomization characteristics, which are one of the important factors influencing the natural environment pollution and noise emission. The intensive research on supply systems in the self ignition engines resulted in precise injection, which causes that the engine fulfil the exploitational requirements with minimizing the negative influence on the natural environment.

2. Test stand and measuring range

Testing were carried out at the test bench, which included AD3.152 UR engine, water brake and also a control and measurement unit to control the stand and take readings of the engine and brake work parameters. The stand was equipped with a system to take measurements of important fast changing quantities: pressure in cylinder, pressure in the pipe injection, the injector needle lift. Besides the test bench contain the piezoelectric charge accelerometer B&K 4371V, which used to measurement to vibration acceleration. The diagram of the research stand is shown in Fig. 1. and the Basic technical data of sensor are presented in table 1.
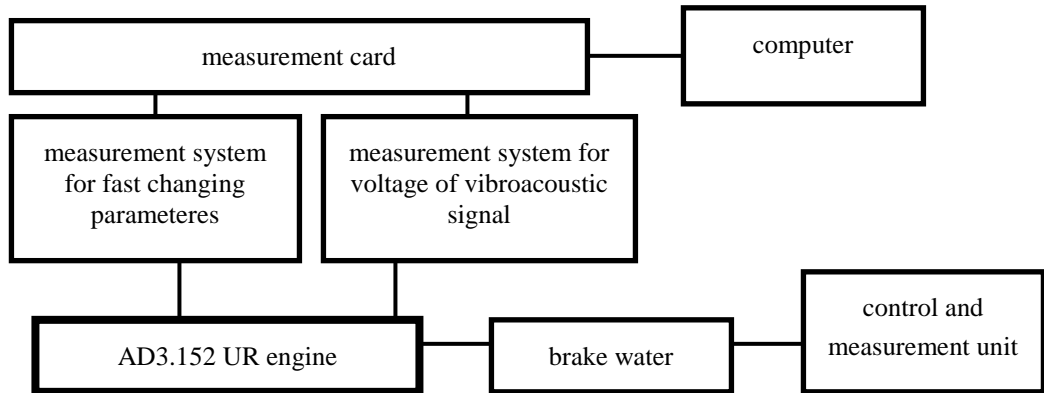
Fig. 1. Block diagram of the research stand

The piezoelectric charge accelerometer B&K (model 4371S)		
Parameter	Units	Value
Charge sensitivity	pC/ms-2	1,02
	pC/g	10
Frequency range	Hz	0,1÷12600
Mounted Resonance Frequency	kHZ	42
Residual nosie level	mg	0,24
Operating temperature range	0C	-74÷250
weight	gram	11

Tab. 1. Basic technical data of the piezoelectric charge accelerometer [10]

The engine under investigation was the self ignition AD3.152 UR with fuel directly injected into the combustion chamber located in the piston crown. During investigation the engine fuelled by diesel feul Ekodiesel Ultra D, rapeseed oil fatty acids methyl esters (FAME) and their blend with diesel fuel B30 (30% FAME).

Received result of investigation when the engine was fuelled by biofuel and B30 compared with results was received when the engine was fuelled by diesel fuel. During of investigation the engine was operated external speed characteristic and manufacturing settig engine. Physical and chemical properties of the examined fuels are presented in Table 2.

Parameter	Ekodiesel Ultra D diesel oil	FAME plant fuel
Cetane number	51.4	51
Calorific value, MJ/kg	43.2	36.7
Density at 15°C, g/cm^3	0.8354	0.883
Kinematic viscosity, mm^2/s (~40°C)	2.64	4.47
Ignition temperature, °C	63	above 130
Cold filter blocking temperature, °C	-23	-14
Average elementary composition, %: C	87.2	76.8
H	12.7	12.1
O	0	11
Sulphur content S, mg/kg	9	8.1
Water content, mg/kg	43.8	113
Particulate matter content, mg/kg	5	18

Tab. 2. Basic physical and chemical properties of engine fuels used in investigations [3,4]

The measurements of the pressure in the cylinder, in the pipe injection, the injector needle lift and the vibroacustic signal were made for 50 engine work cycles. The engine operated in the external speed characteristics, at the rotational speed from 1000 to 2200 rpm.

The received results were as follows:
- the mean pressure in the cylinder,
- the mean pressure in the pipe injection,
- the mean injector needle lift,
- the mean tension amplitude of the vibroacustic signal of the injector.

3. Analysis and results investigation

The knowledge of physical properties, technical data of tested engine and the experimentally made indicator diagrams of pressures in the cylinder, pipe injection and injector needle lift enabled to compute the velocity and the dose of a fuel flowing out of the atomizer during the engine work cycle. The velocity of a fuel flowing out of the atomizer was computed from the formula:

$$w = \mu \sqrt{\frac{2 \cdot \Delta p}{\rho_{pal}}} \ , \ [m/s] \tag{1}$$

where:

μ – coefficient of a fuel outflowing from the atomizer,

$\Delta p = pw - pc$, [MPa] – difference between the pressure in the atomizer hole and the pressure of working medium in the cylinder,

ρ_{pal}, [kg/m3] – density of injected fuel.

The knowledge of hour fuel consumption a fuel dose was computed [1]:

$$g_c = \frac{G_h}{30 \cdot n \cdot i} \ , \ [kg/cykl \ pracy] \tag{2}$$

where:

i – number of cylinders,

G_h – hour fuel consumption,

n – rotational speed of the crankshaft [rpm].

n [obr/min]	N_e [kW]	$\mu_{śr}$	w_{max} [m/s]	$10^{-6} \cdot g_c$ [kg/cykl]	p_{wmax} [MPa]	α_w [°OWK]	d_{32} [µm]
1000	16,509	0,56	117,09	47,733	20,422	14,063	35.7
1200	19,935	0,52	108,39	45,648	20,417	18,281	38.12
1400	23,402	0,58	128,83	45,032	23,254	18,281	38.15
1600	26,58	0,65	150,78	43,514	27,92	18,281	36.06
1800	29,531	0,73	177,61	45,277	27,922	18,281	35.42
2000	32,399	0,75	188,12	45,156	29,679	18,281	36.51
2200	26,786	0,57	144,12	37,045	29,814	22,5	41.30

Tab. 3. The results of measurement and calculations of fuel injection parameters for the AD3.152UR engine operated in external speed characteristics and fuelled by diesel fuel (ON) with angle of the fuel injection advance 17 CA deg and with flow section of atomizer taps f = 246 10-9 m2

n [obr/min]	N_e [kW]	$\mu_{śr}$	w_{max} [m/s]	$10^{-6} \cdot g_c$ [kg/cykl]	p_{wmax} [MPa]	α_w [°OWK]	d_{32} [µm]
1000	16,42	0,6	119,69	51,94	19,80	14,063	37,90
1200	19,829	0,57	115,17	51,64	20,23	18,28	41,65
1400	23,28	0,64	139,63	51,48	23,73	18,28	39,51
1600	26,439	0,7	163,17	50,17	26,90	18,28	38,00
1800	29,37	0,76	185,32	51,64	29,35	18,28	36,25
2000	31,802	0,79	199,00	50,46	31,32	18,28	35,21
2200	26,979	0,69	163,12	42,25	27,92	19,69	38,76

Tab. 4. The results of measurement and calculations of fuel injection parameters for the AD3.152UR engine operated in external speed characteristics and fuelled by rapeseed oil fatty acids methyl esters (FAME) with angle of the fuel injection advance 17 CA deg and with flow section of atomizer taps f = 246 10-9 m2

n [obr/min]	N_e [kW]	$\mu_{śr}$	w_{max} [m/s]	$10^{-6} \cdot g_c$ [kg/cykl pracy]	p_{wmax} [MPa]	α_w [°OWK]	d_{32} [µm]
1000	16,552	0,54	108,08	50,72	19,26	14,063	39,66
1200	20,112	0,58	119,92	49,69	20,38	15,47	39,21
1400	23,464	0,64	141,64	48,56	23,54	15,47	37,84
1600	26,649	0,68	160,02	49,4	26,45	16,875	37,50
1800	29,793	0,66	161,85	46,06	28,66	18,28	39,10
2000	32,062	0,69	167,65	45,93	30,74	18,28	38,64
2200	27,253	0,63	155,45	38,61	29,12	18,28	40,20

Tab. 5. The results of measurement and calculations of fuel injection parameters for the AD3.152UR engine operated in external speed characteristic and fuelled by the blend of 30% of FAME and 70% of diesel fuel with angle of the fuel injection advance 17 CA deg and with flow section of atomizer taps f = 246 10-9 m2

n [rpm]	The mean vibroacustic signal of the injector for the engine, U [mV]		
	ON	FAME	B30
	for 50 work cycles of the engine	for 50 work cycles of the engine	for 50 work cycles of the engine
1000	238	230	218
1200	267	253	239
1400	286	297	269
1600	320	351	287
1800	345	328	297
2000	343	326	302
2200	340	320	293

Tab. 6. The mean vibroacustic signal of the injector for the engine operated in external speed characteristic and angle of injection advance 17CA deg fuelled by ON, FAME and B30
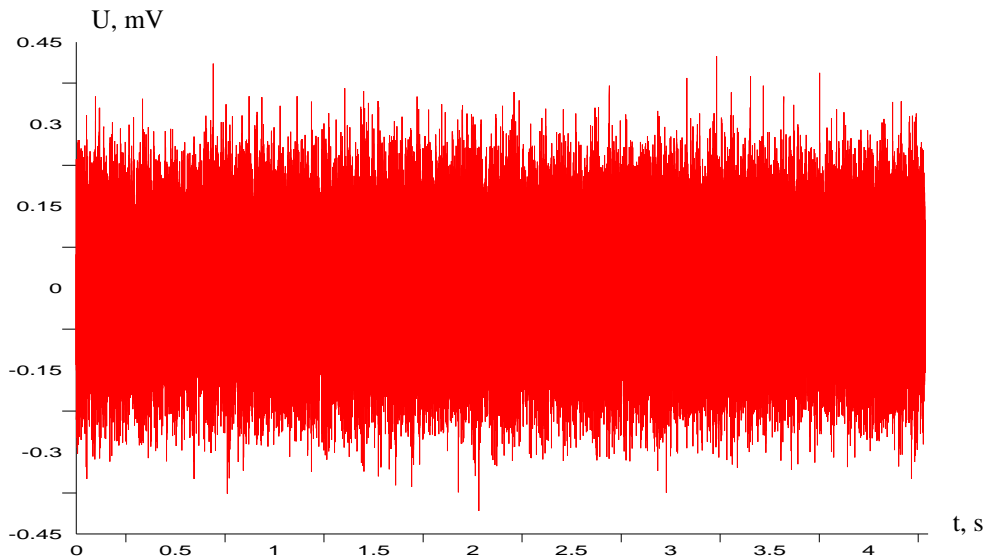

Fig. 2. The exemplary course of the vibroacustic signal in the injector (U) in function with time for 50 work cycles of the engine operated in external speed characteristic, fuelled by FAME, at the rotational speed 1400 rpm.

4. Conclusion

The analysis of research results allows to draw following conclusions: / To sum up, the investigations showed that:

- maximum pressures in the cylinders were about 10% higher when the engine was fuelled by biofuels for the engine operated in external speed characteristics,
- higher (at about 12%) doses of biofuels than mineral fuels were obtained,
- the mean amplitudes of the vibroacustic signal of the injector were lower (at about 10-15%) when the engine was fuelled by B30 in comparison with ON and FAME,
- the maximum speed of the fuel outflowing from the atomizer in the engine fuelled by tested fuels and operated in external speed characteristics was changing in the range from about 108 m/s to about 200 m/s. The outflow velocities were higher when the engine was fuelled by FAME than when it was fuelled by diesel fuel (ON). It can be explained by the higher kinematic viscosity of biofuel (4,47mm2/s). The velocity of outflowing fuel was changing in an extensive borders, so three forms of stream disintegration can appear. The basic disintegration form was atomization, during which large part of fuel is splited into drops,
- the fuel dose used during one engine work cycle was lower for the engine fuelled by diesel oil than for the engine fuelled by FAME and its blend B30. Higher fuel doses were received for the engine operating at lower rotational speed (1000-1400 rpm).
- for the engine operated in external speed characteristics and fuelled by commercial diesel fuel at lower rotational speed (n=1000 rpm to n=1800 rpm) the mean diameter of the drop d32 is lower than for the engine fuelled by FAME. When the engine was fuelled by biofuels the mean diameter of the drop became smaller (from 41μ to 35μ) when the rotational speed became higher (from 1200 rpm to 2000 rpm). The reduction of the mean diameter of the drop size indicates smaller fuel atomization. Surface tension and viscosity forces counteract drops disintegration, therefore the disintegration process lasts to the moment, when forces that stabilize the drop become bigger than forces that cause its disintegration.
- it is expedient and relevant to continue the research on pressing and fuel injection processes in the case when the engine is fuelled by biofuels and its blend with diesel fuel. The important task is to estimate the parameters of injection fuel process and noise emission caused by the engine injection system.

References

[1] AMBROZIK A.: *Wybrane zagadnienia procesów cieplnych w tłokowych silnikach spalinowych.* Politechnika Świętokrzyska, Kielce 2003.

[2] AMBROZIK A., AMBROZIK T., ŁAGOWSKI P.: *Wpływ obciążenia silnika AD3.152 UR na charakterystyki wydzielania ciepła podczas procesu spalania.* Susiec 2008.

[3] AMBROZIK A., AMBROZIK T., KURCZYŃSKI D., ŁAGOWSKI P.: Sprawozdanie z grantu: „Modelowanie wydzielania ciepła i emisji NO ze spalinami w silniku o zapłonie samoczynnym zasilanym olejem napędowym i paliwami pochodzenia roślinnego", nr grantu: 4 T12D 053 28, Kielce 2008.

[4] AMBROZIK A., AMBROZIK T., KRUCZYŃSKI S., ORLIŃSKI S.: Wpływ właściwości paliw mineralnych i roślinnych na prędkość narastania ciśnienia w przewodzie wtryskowym i emisję akustyczną wtryskiwacza. Motrol, 2007.

[5] FALKOWSKI H., HAUSER G., JANISZEWSKI T., JASKUŁA A.: *Układy wtryskowe silników wysokoprężnych.* WKiŁ, Warszawa 1989.

[6] IDZIOR M., LIJEWSKI P.: Possibilities of description of spraying fuel quality with CI engines injectors with investigation method of the stream parameters of atomizing fuel. Journal of Kones Internal Combustion Engines, 2002.

[7]   ЛЫШЕВСКИЙ А.С.: Процессы распыливания топлива дизельными форсунками. Москва, Машгиз, 1963.

[8]   ORZECHOWSKI Z., PRYWER J.: *Rozpylanie cieczy*. WNT, Warszawa 1991.

[9]   РАЗЛЕЙЦЕВ Н.Ф.: *Моделирование и оптимизация процесса сгорания в дизелях*. Издательское объединение „Вища школа", Харьков 1980.

[10] http://www.bruel.com.pl/

The Model of a Single Plate: The Basis of Thermoacoustic Engines

[*] George Andrei, [*] Dan Andrei, [**] Rafal Golebski
* University "Dunărea de Jos" Galaţi, Faculty of Mechanical Engineering,
Thermodynamics and Thermal Engines Department, Domnească Street, No. 47, 800008, Galaţi,
Romania, E- mail: {george.andrei, dan.andrei}@ugal.ro
** Częstochowa University of Technology, Faculty of Mechanical Engineering and Computer Science,
Institute of Machines Technology and Production Automation, Al. Armii Krajowej 21 42-200
Częstochowa, Poland, E-mail: rafal@itm.pcz.pl.

Abstract. In this article the author presents a model developed by Nicholaus Rott [6] and used the first time by Gregory Swift [7]. This model presents how a simple plate introduced in a standing wave can influence the fluid near the plate. The model represents the basis of the thermoacoustic engines [3], [4], [5], [7], [8].

Keywords: Acoustics, Thermoacoustics, Thermoacoustic Engine.

1.   Introduction

This article present a model developed by Nicholauss Rott [6] and used the first time by Gregory Swift [7] in one of his publications. The purpose of this work is to descript a simple example where the acoustic and thermodynamic effects are nearly distinct. We will consider a fluid supporting an acoustic plane standing wave [3, 4, 5], [7] and a single small solid plate aligned parallel to the direction of vibration of the standing wave. We will present here how the standing wave is modified by the presence of the plate.

This simple effect, produced by the interaction between sound wave and solid boundary, are the basis of all thermoacoustic engines phenomena. To derive this basis effect with as few complications as possible, we will make many simplifying assumptions.

2.   The single plate model

Consider a solid plate of length Δx, width $\Pi/2$, and negligible thickness, as shown in fig. 1. The length Δx is aligned along the x axis, and there is an ordinary acoustic standing wave directed along x in the fluid around the plate with the pulsation ω. The acoustic pressure [2, 3, 4, 5], [7], [8] is:

$$p = p_A \sin(x / \bar{\lambda})\cos(\omega t), \tag{1}$$

and the acoustic velocity:

$$v = -(p_A / \rho_0 c)\cos(x / \bar{\lambda})\sin(\omega t), \tag{2}$$

where:
pA is the pressure amplitude at the pressure antinodes of the standing wave [N/m^2];
$\bar{\lambda} = c / \omega = \lambda / 2\pi$ is the radian length of the wave [rad];

c is the sound speed of the fluid [m/s]; $\omega = 2\pi f$ is the angular frequency [s-1]; f is the frequency [Hz]; λ is the wave length [m]; t is time [s].

We have defined the width as *Π/2* because a cross section perpendicular to x through the plate a perimeter Π and we will see later that the heat flux along the plate is proportional to *Π*.
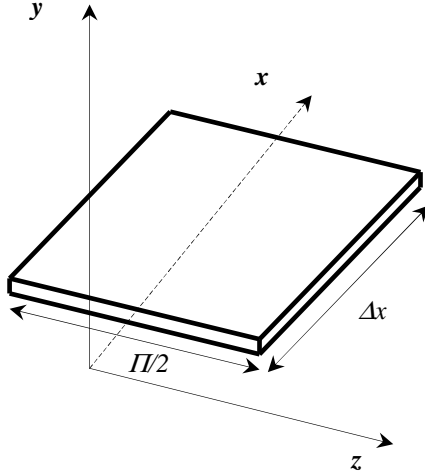

Fig.1. The geometry of the simplest thermoacoustic example

We will assume that an expansion to first order in the acoustic amplitude suffices for all thermodynamic and acoustic variables (pressure, velocity, temperature, density, entropy), and we adopt the usual complex notation for time-oscillatory quantities.

For example, the pressure p will be written:

$$p(x,t) = p_0 + p_1(x)e^{i\omega t}, \qquad (3)$$

with p1 (and similarly the other small oscillating amplitudes) a function of position, and all the time dependence appearing in the factor eiωt.

The average values (subscript 0) will be real, but the small amplitudes (subscript 1) will in general be complex, reflecting time phasing of the oscillating quantities.

We will use the complex exponential method of solution of linear differential equations, and the convention that the real parts of this complex solution represent the actual, physical solution. In this notation, the acoustic standing wave has the pressure given in (3) and x component of velocity:

$$u = u_1 e^{i\omega t}; \text{ with } p_1 = p_A \sin(x/\lambda) \equiv p_1^s(x); \ u_1 = i(p_A / \rho_0 c)\cos(x/\lambda) \equiv i u_1^s(x). \qquad (4)$$

To avoid confusing minus signs later, we take $0 < x < \lambda/4$ so that we define p_1^s and u_1^s as positive real functions of x. The superscript "s" refers to standing waves.

2.1. Oscillatory temperature

Without the plate

In the absence of the plate, the sound wave is adiabatic, and so there is an oscillating temperature T1 related to the pressure p_1 by: $T_1 = (\partial T / \partial p)_s p_1$. In [2], [3], [4] and [7] we show that:

$$T_1 = \beta T_0 p_1 / \rho_0 c_p, \qquad (5)$$

where: β is the thermal expansion coefficient, $\beta = -(\partial \rho / \partial T)_p / \rho$; ρ_0 is average density [kg/m^3]; T_0 is average temperature [K] and cp is the constant-pressure heat capacity per unit mass [J/kgK].

We have to note that: Since $\beta T_0 / \rho_0 c_p$ is positive and real, T1 and p1 are in phase in an ordinary sound wave; for ideal gases, it is easy to show that:

$$\beta T / \rho_0 c_p = (\gamma - 1)T_0 / \gamma p_0 . \tag{6}$$

We now introduce the plate [3], [4], [5], as shown in figure 1, into the standing wave and begin our thermoacoustic calculation by first finding the temperature of the fluid near of the plate:

$$T = T_0 + T_1 e^{i\omega t} . \tag{7}$$

We will see that the plate modifies the original, unperturbed temperature oscillations of equations (5) in both magnitude and phase. For fluid we defined [2, 3, 4, 5], [7, 8]: the thermal penetration depth, $\delta_k = \sqrt{2a_g / \omega}$, is roughly the distance that heat can diffuse through the fluid during a time $1/\omega$; ag is the thermal diffusivity [m^2/s]; ω is the pulsation [Hz]; kg is the thermal conductivity of gas [W/mK]; $a_g = k_g / \rho_0 c_p$. For example [8] in air at the frequency f = 1000 Hz, δk = 0,1 mm. To make rapid progress, we need several assumptions:

1. We assume that a steady state exists;
2. We assume that the plate is short enough ($\Delta x << \lambda$) and far enough from the both velocity and pressure nodes that p_1 and u_1 can be considered uniform over the entire plate;
3. The fluid is considered ideal gas, so it has zero viscosity, so u_1 does not depend on y;
4. The plate has a large enough heat capacity per unit area that its temperature does not change appreciably at the acoustic frequency;
5. We neglect temperature dependence of the thermophysical properties of the fluid and plate;
6. We assume that the plate has a given mean-temperature gradient in the x direction:

$$\nabla T_0 = \underbrace{\frac{dT_0}{dx}}_{\nabla T_0}\vec{e}_x ;$$

7. We neglect the plate's thermal conductivity and the fluid's thermal conductivity in the x direction;
8. We also take the mean fluid temperature $T_0 (x)$ to be independent of y and to be the same as that of the plate.

To calculate the oscillating fluid temperature T1 we begin with the general equation of the heat transfer (entropy equation) [3], [4], [7], with the assumptions made becomes:

$$\rho \frac{Ds}{Dt} = \frac{\delta \dot{Q}_v}{T} + \rho \dot{s}_i ; \delta \dot{Q}_v = \rho T \left(\frac{\partial s}{\partial t} + v \cdot \nabla s \right) = \nabla \cdot (k\nabla T) + \text{terms quadratic in velocities}; \tag{8}$$

with $\delta \dot{Q}_v = div\vec{q}$ and $q = -k\nabla T$; $\dot{Q}_v$ is the volume density to the heat flux [W/m3] ; q is the density to the heat flux [W/m2]; k is the thermal conductivity [W/mK] .

This equation shows that the entropy at a point changes in time due to the convective flow of entropy, conduction of heat, and generation of entropy by quadratic terms (equals to zero by assumptions made). Keeping only first-order terms, and neglecting thermal conduction along x, equation (8) becomes [3], [4], [7]:

$$\rho_0 T_0 \left(i\omega s_1 + u_1 \frac{ds_0}{dx} \right) = k_g \frac{d^2 T_1}{dy^2} \text{ or } T_1 + i\frac{\delta_k^2}{2}\frac{d^2 T_1}{dy^2} = \frac{T_0 \beta}{\rho_0 c_p} p_1^s - \frac{\nabla T_0}{\omega} u_1^s . \tag{9}$$

Here

$$\delta_k^2 = 2k_g / \rho_0 c_p \omega. \tag{10}$$

To calculate the solution T1(y) we use the boundary conditions:
1. Boundary condition imposed by the plate T1(0) = 0,
2. Oscillatory temperature far from plate has a finite value T1(∞) = finite.

The solution is:

$$T_1 = \left(\frac{T_0 \beta}{\rho_0 c_p} p_1^s - \frac{\nabla T_0}{\omega} u_1^s \right) \left(1 - e^{-\frac{(1+i)y}{\delta_k}} \right). \text{ So: } \Re e \left(1 - e^{-\frac{(1+i)y}{\delta_k}} \right) = 1 - e^{-\frac{y}{\delta_k} \cos\left(\frac{y}{\delta_k} \right)},$$

$$\Im m \left(1 - e^{-\frac{(1+i)y}{\delta_k}} \right) = e^{-\frac{y}{\delta_k} \sin\left(\frac{y}{\delta_k} \right)}. \tag{11}$$

The terms in this equation are easily interpreted. The fluid far from the plate, y >> δ_k, makes negligible thermal contact with the plate. In that case we have:

$$T_1 \to \underbrace{\frac{T_0 \beta}{\rho_0 c_p} p_1^s}_{I} - \underbrace{\frac{\nabla T_0}{\omega} u_1^s}_{II}. \tag{12}$$

The first term here is simply due to the adiabatic compressions and expansions of the fluid. The second term comes from the mean-temperature gradient in the fluid (∇T_0). As the fluid oscillates along x with displacement amplitude $x_1 = u_1^s / \omega$ the temperature at a given point in space oscillates by an amount $\Delta T_0 u_1^s / \omega$ even if the temperature of a given piece of fluid remains constant. The actual temperature oscillations are just a linear superposition of these two effects.

In this case we replace T1 = 0 in equation (12), so [3, 4]:

$$\nabla T_0^{crit} = T_0 \beta \omega p_1^s / \rho_0 c_p u_1^s, \text{ or } \nabla T_0^{crit} = T_0 \beta c^2 tg(x / \lambda) / c_p \lambda, \tag{13}$$

there is a critical mean-temperature gradient (equations (4) show that $p_1^s / u_1^s = \rho_0 ctg(x / \lambda)$).

For this ∇T_0^{crit} the temperature oscillations at a point are zero; the fluid properties and standing wave geometry conspire so that the temperature changes due to the pressure oscillations cancel those due to the displacement oscillations.

The critical temperature gradient is important because it is the boundary between the heat pump and prime mover functions of thermoacoustic engines, and $\nabla T_0 \cong \nabla T_0^{crit}$ for efficient engine performance.

For ideal gases:

$$\gamma - 1 = T_0 \beta^2 c^2 / c_p. \tag{14}$$

Substituting both these results into equation (13) we have:

$$\nabla T_0^{crit} = (\gamma - 1) T_0 tg(x / \lambda) / \lambda. \tag{15}$$

3. Conclusion

For an engine we want to have a very little value for T_0/λ (so to a very little value for ∇T_0^{crit}) to obtain a big value for the wave length (λ).

In the full expression of T_1 the "y" dependent part of equation (11), $\left(1 - e^{-(1+i)y/\delta_k}\right)$, is complex. It approaches one "1" for $y >> \delta_k$ and zero "0" for $y << \delta_k$ where the plate imposes the condition $T_1 = 0$. Most importantly, for $y \cong \delta_k$, its magnitude is still of the order of one "1", but it has a substantial imaginary part.

References

[1] BEJAN, A. *Advanced Engineering Thermodynamics*. Wiley, second edition, 1997.

[2] ANDREI, G. *Approche théorique a l'étude des échangeurs de chaleur dans les systèmes thermoacoustiques*, Rapport de Stage, Institut de Physique Nucléaire d'Orsay, France, Juillet 2005.

[3] ANDREI, G. *Thermoacoustic systems used in the heat transfer*, 2nd PhD Rapport, „Dunarea de Jos" University of Galaţi, january, 2006.

[4] ANDREI, G. *Acoustical and Thermal Studies of the heat exchangers in the thermoacoustic systems*, PhD Thesis, "Dunarea de Jos University", Galati, Romania, 2008.

[5] ANDREI, G. THERMEAU,J., P., BALTEAN,D., ANDREI, D. *The heat flux andacoustic power produced by a single plate introduced into a standing wave*, 2nd International Conference on Thermal Engines and Environmental Engineering MET IME, Galaţi, Proceedings in Section A, Pag. 277-284, 7-9 juin, 2007.

[6] N Rott, *Thermoacoustics* . Advanced in Applied. Mechanics, 20 :135-175, 1980.

[7] SWIFT, G.W. *Thermoacoustic engines* , J. Acoust. Soc. Am. Vol. 84, 1145-1180, 1988.

[8] SWIFT, G.W. *Thermoacoustics: A unifying perspective for some engines and refrigerators*, Condensed Matter and Thermal Physics Group, Los Alamos National Laboratory, fifth draft, 29 may 2001.

20

Identification of a Manipulator Model
Using the Input Error Method

[*]Leszek Cedro, Dariusz Janecki

[*] Assoc. Prof. Dariusz Janecki, DrSc. Leszek Cedro, Kielce University of Technology, Faculty of Mechatronics and Machinery Design, Division of Computer Science and Robotics, tel/fax. +48/41/3424504, Al. Tysiąclecia PP 7, 25-314 Kielce, Poland email: lcedro@eden.tu.kielce.pl, djanecki@tu.kielce.pl

Abstract. The problem of parameter identification for a four-degree-of-freedom robot was solved using specially developed differential filters [1]. The data were fine-tuned using the input error method [2].

Keywords: identification, differential filters.

1. Introduction

The rapid developments in computer hardware and software and, consequently, the common use of computers to control processes have aroused wide interest in mathematical modeling, control processes and, accordingly, control system identification.

The method of identification applied in the analysis involves fine-tuning of the inverse model. The method can be used only for such values of the input signals that are determined from the measurement data. Identifying a dynamic system by means of the input error method (Fig. 1) requires looking for a model that generates the same input as the object. Only in the case of model reversibility is such a procedure possible. This reversibility is true for linear minimum-phase models and a certain class of non-linear models where the input is determined basing on the output data.

Let us assume, for instance, that the object is described by means of a differential equation:

$$f(y^{(n)}, y^{(n-1)},..., y, \theta) = x . \tag{1}$$

where f is a certain known function. Thus, the identification error is defined as:

$$e = x - \hat{x} ,$$
$$\hat{x} = f(y^{(n)}, y^{(n-1)},..., y, \hat{\theta}) . \tag{2}$$

A drawback of this method is that derivative estimates need to be determined. An advantage, on the other hand, is that it is not necessary to solve the differential equations describing the model at each step of iteration.
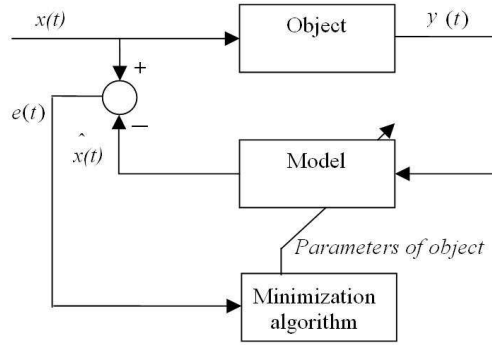
Fig. 1. A block diagram of the process of estimation of the inverse model parameters

The fundamental problem related to the implementation of the input error method and its generalization is the necessity to determine the estimates of signal derivatives. This is achieved by applying differential filters.

2. A mathematical model of a robot manipulator

The analysis was conducted for a manipulator with four degrees of freedom, the structure of which is presented in Fig. 2.
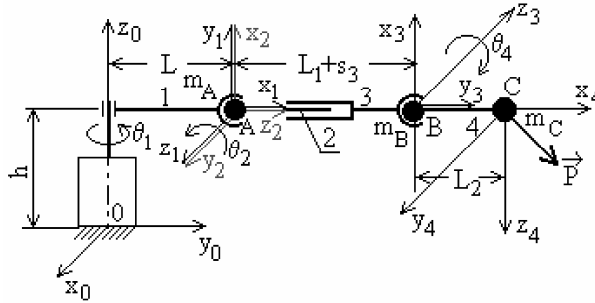

Fig. 2. Manipulator model

Let us determine the velocities of points A, B and C.

$$U_{ij} = T_1 \cdot T_2 \cdots T_{j-1} \cdot \Theta \cdot T_j \cdot T_{j+1} \cdots T_i$$

$$\vec{r}_A^{(1)} = \vec{r}_B^{(3)} = \vec{r}_C^{(4)} = [0,0,0,1]^T$$

(3)

The kinetic energy of the system is:

$$K_{1A} = \frac{1}{2} U_{11} \vec{r}_A^{(1)} m_A \vec{r}_A^{(1)^T} U_{11}^T = \frac{1}{2} m_A L^2 \dot{\theta}_1^2$$

$$K_{3B} = \frac{1}{2} \sum_{j=1}^{3} \{ U_{3j} \vec{r}_B^{(3)} m_B \vec{r}_B^{(3)^T} U_{3j}^T \} \dot{q}_j^2 = \frac{1}{2} m_B \{ [L + (L_1 + s_3)\cos\theta_2]^2 \dot{\theta}_1^2 +$$

$$+ (L_1 + s_3)^2 \dot{\theta}_2^2 + \dot{s}_3^2 \}$$

(4)

22

$$K_{4C} = \frac{1}{2} \sum_{j=1}^{4} \{ U_{4j} \vec{r}_C^{(4)} m_C \vec{r}_C^{(4)T} U_{4j}^T \} \dot{q}_j^2 = \frac{1}{2} m_C \{ [L + (L_1 + s_3) \cos\theta_2 + L_2 \cos(\theta_4 - \theta_2)]^2 \dot{\theta}_1^2 +$$

$$+ [(L_1 + s_3)^2 + L_2^2 + 2(L_1 + s_3) L_2 \cos\theta_4] \dot{\theta}_2^2 + \dot{s}_3^2 + L_2^2 \dot{\theta}_4^2 \}$$

$$K = K_{1A} + K_{3B} + K_{4C}$$

The potential energy of the system is:

$$\Pi = \Pi_{1A} + \Pi_{3B} + \Pi_{4C} = -(m_A + m_B + m_C) gh - (m_B + m_C) g(L_1 + s_3) \sin\theta_2 +$$

$$+ m_C g L_2 \sin(\theta_4 - \theta_2) \tag{5}$$

PD controllers were used to ensure stable operation of the system and generation of a signal required for the identification process. As a result, a set of closed-loop equations was derived. The manipulator dynamics could then be defined by applying the Lagrange equations.

$$\frac{d}{dt} \frac{\partial K}{\partial \dot{\theta}_1} - \frac{\partial K}{\partial \dot{\theta}_1} + \frac{\partial \Pi}{\partial \theta_1} = \tau_1, \ \tau_1 = K_{p1}(\theta_{r1} - \theta_1) - K_{d1} \dot{\theta}_1$$

$$\frac{d}{dt} \frac{\partial K}{\partial \dot{\theta}_2} - \frac{\partial K}{\partial \dot{\theta}_2} + \frac{\partial \Pi}{\partial \theta_2} = \tau_2, \ \tau_2 = K_{p2}(\theta_{r2} - \theta_2) - K_{d2} \dot{\theta}_2$$

$$\frac{d}{dt} \frac{\partial K}{\partial \dot{s}_3} - \frac{\partial K}{\partial \dot{s}_3} + \frac{\partial \Pi}{\partial s_3} = \tau_3, \ \tau_3 = K_{p3}(s_{r3} - s_3) - K_{d3} \dot{s}_3 \tag{6}$$

$$\frac{d}{dt} \frac{\partial K}{\partial \dot{\theta}_4} - \frac{\partial K}{\partial \dot{\theta}_4} + \frac{\partial \Pi}{\partial \theta_4} = \tau_4, \ \tau_4 = K_{p4}(\theta_{r4} - \theta_4) - K_{d4} \dot{\theta}_4$$

3. Simulation of the manipulator model

This section discusses the results of a simulation of closed-loop equations including a robot model with PD controllers. The collected data will then be used in the identification algorithm.

First, the pre-determined signal was defined: $[\theta_{r1} \ \theta_{r2} \ s_{r3} \ \theta_{r4}]$. The signal was assumed to be a properly delayed step function (each arm with a different delay) passing through an additional low-pass filter with a boundary frequency $\Omega_g = 0.025 \, [rad]$. The filtering was responsible for limiting the signal spectrum.
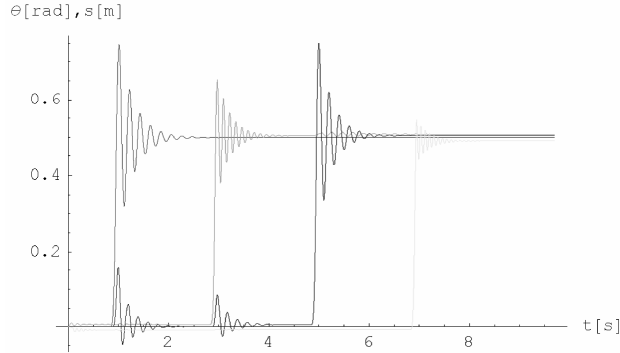

Fig. 3. Responses of $\theta_1, \theta_2, s_3, \theta_4$

23

The responses are not satisfactory from the point of view of regulation. The aim of the study was to generate signals to be used in the identification process. It is advisable that the pre-determined signals and the controller parameters be carefully selected so that the signals provide sufficient information about the object dynamics.

4. Identification

Let us recall that the robot mass and arm length are the unknown parameters denoted as $\chi = [m_A, m_B, m_C, L, L_1, L_2]$. The method used for the parameter identification is represented graphically in Figure 1. It is assumed that the measurement data concerning the trajectories of the generalized variables and the necessary input signals are available. The estimate of the input signals, $\hat{\tau}^f$, is determined basing on the current estimates of the object parameters $\hat{\chi} = [\hat{m}_A, \hat{m}_B, \hat{m}_C, \hat{L}, \hat{L}_1, \hat{L}_2]$. These equations have the same structure as Eq. (6); yet, the unknown parameters, χ, are replaced by the estimates, $\hat{\chi}$, the generalized variables are replaced by variables filtered through a low-pass filter, and their derivatives (which are not measured) are replaced by their estimates obtained by using relevant differentiating filters. Let us assume that the boundary frequency of the differentiating filters is: $\Omega_g = 0.2 \, [rad]$. The identification requires determining the estimates of the parameters responsible for the quality factor minimization.

$$J(\hat{\chi}) = \frac{1}{T} \int_0^T (\hat{\tau}^f - \tau^f)^2 \, dt \,, \qquad (7)$$

where τ^f is an input signal filtered with a low-pass filter.

The identification procedure is commenced for the following initial values: $\hat{\chi} = [51 \quad 26 \quad 16 \quad 0.85 \quad 0.65 \quad 0.25]$. The final values of the parameters are determined after 1340 iterations of the minimization algorithm. The estimates $\hat{\chi} = [49.9201 \quad 25.0225 \quad 14.9591 \quad 0.800161 \quad 0.600063 \quad 0.200312]$ slightly depart from the real values of the parameters, $\chi = [50 \quad 25 \quad 15 \quad 0.8 \quad 0.6 \quad 0.5]$.

5. Conclusion

In contrast to the conventional output error method, which involves comparing and estimating input signals, the input error method is considerably faster. The identification procedure does not require solving a series of differential equations in each iteration of the algorithm minimizing the quality factor.

It should be noted that the spectrum of the pre-determined signals is limited. In spite of the fact that the robot system is a non-linear system, the following relationship is obtained for the filtered signals: $\hat{\tau}^f \cong \tau^f$, if $\hat{\chi} = \chi$. As the slight differences are due to the system non-linearity and quantization errors, the equation can be solved approximately.

References

[1] JANECKI, D., CEDRO L. *Differential Filters with Application to System Identification*, TRANSCOM 2007, Żilina.

[2] GIERGIEL J.,UHL T. *Identyfikacja układów mechanicznych*, PWN Warszawa 1990.

24

Investigation of the Influence of Air Pressure in Car Tires on Effectiveness of Their Suspension System

[*]Roman Filipiak, [**]Marian Josko
*University of Technology, Institute of Working Machines and Motor Vehicles, Poznan,
Address to correspondence - ul. Gornoslaska 63a/6, 62800 Kalisz, Poland, firo_r@poczta.onet.pl,
roman.filipiak@doctorate.put.poznan.pl
** University of Technology, Institute of Working Machines and Motor Vehicles, Piotrowo 3, 60965
Poznan, Poland, marian.josko@put.poznan.pl

Abstract. It happens that the results of car examination, made in different diagnostic stations in different conditions are not similar. In this paper it was analyzed the influence of air pressure in tires on reliability of the car's technical examination, especially considering passenger cars. The purpose of this work is an experimental evaluation of influence of air pressure in car tires on effectiveness of suppressing vibrations by suspension system, which has effected on general car condition and safety in road traffic.

Keywords: diagnostic line, pressure in tires, car vehicles, effectiveness of suppression, suspension method EUSAMA.

1. Introduction

The main objective of a car suspension system is to ensure good adhesion of car wheels to the road and possibly the highest comfort of traveling for its users. Proper functioning of the suspension system has direct influence on the safe movement of a car on the road, it is also the condition of appropriate operation of other safety systems, e.g. braking system.

To examine shock absorbers installed in a car, and in fact, vehicle suspension, are used practically two methods: the method of free vibrations and the method of forced vibrations. The first method includes the evaluation of vibrations (specifically, the number of vibration semi-periods) of a motorcar body caused by throwing down the body from the stationary state.

In newer types of free vibrations method, the loading force of a wheel on the ground is measured [1]. The second method includes forcing vertical vibrations of a wheel with the frequency of 16-25 Hz [2].

Those methods make use of a well known fact of high sensitivity of the suspension system vibrations amplitude to the suppression in the resonance zone. Those methods include the method suggested by BOGE Company. A never variation of the second method of vehicle shock absorbers examination method is the method called EUSAMA (an acronym of an original name of the European Association of Shock Absorbers Manufacturers). The values recorded in this method are the static load forces as well as dynamic load forces of a road wheel on the road (the plate of the forcing equipment).

In this paper, the maximum permissible total mass of vehicles is expressed in tones [t], and the pressure in tires is given in bars [bar]. This is connected with the universality of those units in technical examinations and scaling of the examination equipment in the said units.

2. Examination station

Tests were performed in a regional vehicle examination centre. It was performed on a station type TUZ-1 by Unimetal [3-5]. This is a station used for performing technical tests of vehicles (with a maximum permissible mass – mpm up to 3,5t) suspension systems suppression efficiency. This equipment consists of two separate measuring sets (vibrating), a control – indication unit and a computer [6-11].

Vehicle suspension system technical examination result depends on:
▪ The technical condition of an examined vehicle,
▪ Design and performance of the station,
▪ Present technical condition of the examination stand,
▪ Surrounding conditions (temperature, pollution of tires or plates of vibrating sets),
▪ Human factor (care of performance the examination, correctness of setting the wheels on the plates, etc.).

The result of technical examination of vehicle suspension system depends on many factors, whose influence is difficult to maintain on the stable level. Suspension system examination results might differ from the objective state – actual state. So, it is crucial to assess the influence the conditions might have on the measurement and its results. It is obvious that the change of tire pressure influences the suppression of vehicle suspension system. There is a requirement of keeping the pressure in tires on the level close to the nominal one (approximately 2 bars). However, there is no detailed information about the magnitude of the said pressure changes influence on suppression of suspension systems in various vehicles. Due to this, a detailed aim of those examinations is assessment of tires pressure (in given vehicles) on the values of EUSAMA indicator, which has been assumed as a measure of vehicle suspension technical condition.

3. Description of examinations objects

There were two vehicles subject to technical examination, Fiat Punto, year of manufacture 2006 and Skoda Fabia manufactured in 2006. They are vehicles with maximum permissible mass up to 3,5t. They both had efficient chassis systems, including the suspension systems. Tires met technical requirements which permitted the vehicles to traffic. The tires dimensions were compliant with manufacturers' requirements. The examination was performed in a short time (three weeks) in order to reduce the impact of possible changes resulting from normal operation of vehicle (the use of suspension system elements) on the test.

4. The course and test conditions

In this work the EUSAMA indicator value was assumed as a measure of suspension suppression and it results from the percentage relation of minimum wheel pressure on the test plate during vibrations in the resonance scope to the static pressure of the wheel [1].

The tests included checking the efficiency of suspension system suppression specified by the EUSAMA metric within the scope from the half of nominal pressure in a tire to the pressure higher than the nominal, with an increment by 0.2 bars. Nominal pressure in both vehicles was 2.0 bar. The pressure in the tests was adjusted by means of a pressure control and adjustment device – type PA-10K. This is an attested electronic device with microprocessor automatic equipment for adjustment and control of the pressure especially in car vehicles tires.

Vehicle wheels were located centrally on the examination station for checking the suspension system suppression effectiveness (measuring plate) – Fig. 1. During the tests a driver was not inside the car.

Fig. 1. Vehicle wheel location on measuring plates.

5. Test results

In the Tab. 1 there are results of tire pressure influence on the efficiency of suspension system suppression (the values of EUSAMA indictor) in Fiat Punto, manufacturing year – 2006.

Pressure [bar]	Front axle [%] Side		Rear axle [%] Side	
	Left	Right	Left	Right
1,0	79	76	54	60
1,2	77	75	48	54
1,4	73	73	44	49
1,6	66	66	36	40
1,8	61	61	31	34
2,0*	54*	56*	26*	31*
2,2	48	48	16	25
2,4	44	44	11	19
2,6	39	38	8	16
2,8	35	34	3	11
3,0	32	32	1	8

*values referring to the nominal pressure

Tab. 1. Results of suspension system examination of Fiat Punto, manufacture year – 2006.

The next vehicle tested on the TUZ-1 test station, in which the influence of tire pressure on EUSAMA indicator was examined was Skoda Fabia combi (estate car). The Tab. 2 consists of the results of this vehicle suspension system test.

Pressure [bar]	Front axle [%]		Rear axle [%]	
	Side		Side	
	Left	Right	Left	Right
1,0	80	81	75	74
1,2	79	81	73	76
1,4	78	81	74	73
1,6	75	76	71	71
1,8	73	74	67	66
2,0*	70*	71*	61*	61*
2,2	65	69	57	58
2,4	63	64	54	54
2,6	59	61	50	50
2,8	57	59	47	46
3,0	54	55	43	42

*values referring to the nominal pressure

Tab. 2. Results of suspension system examination of Skoda Fabia, manufacture year –2006.

6. Tests results analysis

The results gathered in Tab. 1 and Tab. 2 were presented in a graphic manner for both of the examined vehicles in Fig. 2 and Fig. 3.
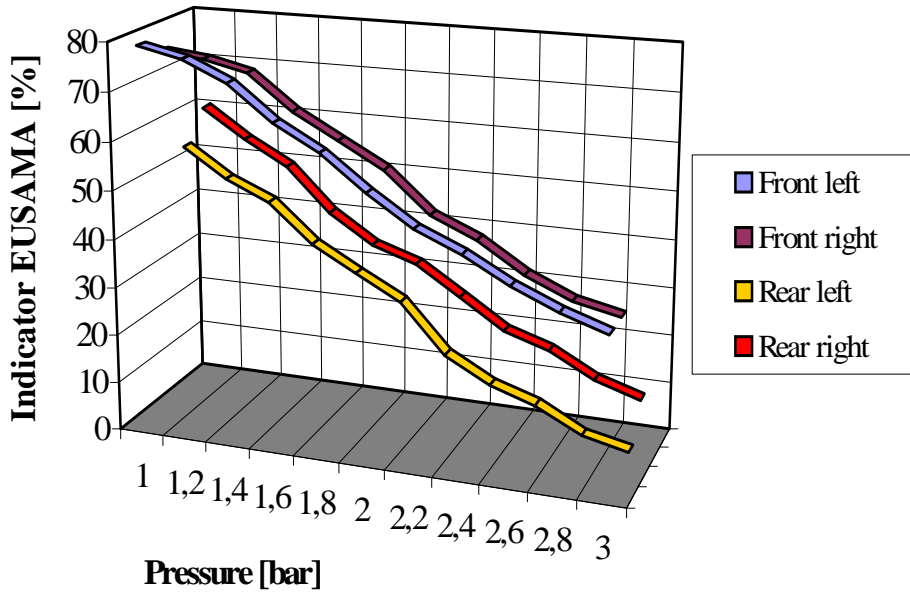
Fig. 2. The relationship between the tire pressure and the EUSAMA indicator for Fiat Punto 2006 suspension system
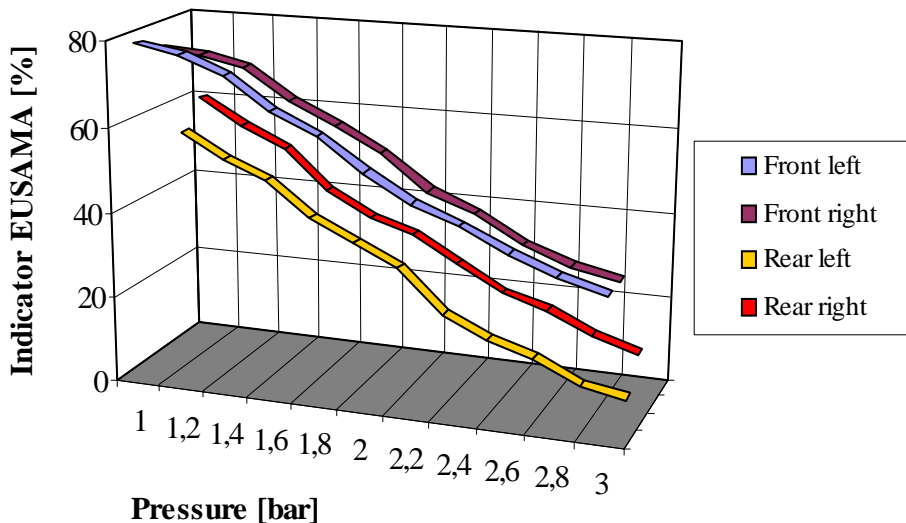
Fig. 3. The relationship between tire pressure and the EUSAM indicator for Skoda Fabia combi (estate car) 2006 suspension system.

As it can be seen from the diagrams in Fig. 2 and Fig. 3, the tendency of suspension system suppression effectiveness, expressed by EUSAM indicator, is very clear. The tire rigidity which is changing together with the tire pressure has a clear influence on the values of the aforementioned indicator. It signifies suspension system susceptibility to changes of pressure in tires. The consequence of that might be qualification during suspension system technical examination to the condition not conforming to the actual state.

Examining vehicle suspension system suppression effectiveness in different tire pressure values, one might come to the conclusion that with the increase of tire pressure, the effectiveness of suspension system suppression decreases. In case of tire pressure of 3.0 bar, the rigidity of a tire increases considerably and its suppression is much lower than in case of a tire not inflated to the nominal pressure, which is expressed by a lower value of EUSAMA indicator.

Based on the results of conducted examinations, one might come to the conclusion that in case when a basic principle of preparing a car i.e. adjusting proper tire pressure recommended by a manufacturer prior to the technical examination, is not met, the assessment of the suspension system might not be credible – this is proved both by the measurements and the diagrams made on their basis.

Analyzing obtained relations in the Fig. 2 and Fig. 3, one might notice that the difference of EUSAMA indicator value between the axles of Skoda Fabia is lower in comparison to the earlier examined vehicle – Fiat Punto. This is to some extent caused by higher loads of the rear axle of Skoda Fabia on the road, because this is a vehicle with an estate car body, which means higher load on the rear axle. One might also spot that in Skoda Fabia, the difference of EUSAMA indicator value on one axle between the extreme tire pressure values is lower than in Fiat Punto vehicle. This shows that the suspension system of this vehicle is less susceptible to the changes of tire pressure changes.

7. Conclusion

Based on the conducted tests and achieved results, one might form the following statements:

- As the tire pressure increases, the EUSAMA indicator value for suspension systems of both vehicles has a decreasing tendency.

As a result of tire pressure change within the scope of 1.0-3.0 bar, the difference between the lowest and the highest suspension suppressing efficiency indicator value exceeds 50% for both of the examined vehicles.

- The value of the EUSAMA indicator depends on the static pressure of a wheel on the ground.

References

[1] SITEK, K. *Car diagnostics. Publishing house Car*, Warsaw 1999.

[2] BOCHEŃSKI C. *The supervisory investigations of cars, (collective work)*. WKiŁ, Warsaw, 2000.

[3] Records technicals - motive line diagnostic Uniline 2000. Publishing house, UNIMETAL, 2007.

[4] Records technicals - motive line diagnostic Uniline 3000. Publishing house, UNIMETAL, 2007.

[5] Records technicals - motive line diagnostic Uniline 5000. Publishing house, UNIMETAL, 2007.

[6] Records technicals - motive. Device to control of effectiveness of suppression of suspension of vehicle about dmc to 3,5 t. type TUZ-1/L. Publishing house, UNIMETAL, 2005.

[7] Records technicals – motive. The device to extorting pull at the carriageable wheels for control of rooms in elements of suspension and the arrangement of managerial vehicle about dmc do 3,5t type SZ-3.5. Publishing house, UNIMETAL, 2007.

[8] Records technicals – motive. The universal device to extorting pull at the carriageable wheels of vehicle for control of rooms in elements of suspension and the managerial arrangement type SZ-16. Publishing house, UNIMETAL, 2007.

[9] ŻÓLTOWSKI B., ĆWIK Z. *Lexicon of technical diagnostics*. Publication ATR, Bydgoszcz 1996.

[10] Website: http://www.unimetal.pl-czerwiec, 2007.

[11] Website: http://www.heka-online.de-czerwiec, 2007.

Analysis of the Meshing Conditions of a Worm Gear Drive

Rafał Gołębski *

* Czestochowa University of Technology, Faculty of Mechanical Engineering and Computer Science, Institute of Machines Technology and Production Automation, Al. Armii Krajowej 21 42-200 Czestochowa, Poland, E-mail: rafal@itm.pcz.pl

Abstract. The knowledge of the toothing profiles of the worm and the wormwheel is necessary for the analysis of the course and conditions of meshing. The determination of relationships that occur between the teeth profiles of the worm and the wormwheel and the parameters defining their working surfaces is thus indispensable in this case.

Keywords: Worm gear, cone-derivative worm, Archimedes' worm, involute worm

1. Introduction

When analyzing the worm gear shown in Fig. 1 in terms of the mating of the worm with the wormwheel is can be stated that the worm plays a role similar to that of a rack mating with a cylindrical gear – the momentary axis of rotation is in this case a straight line perpendicular to the worm axis and parallel to the wormwheel axis.
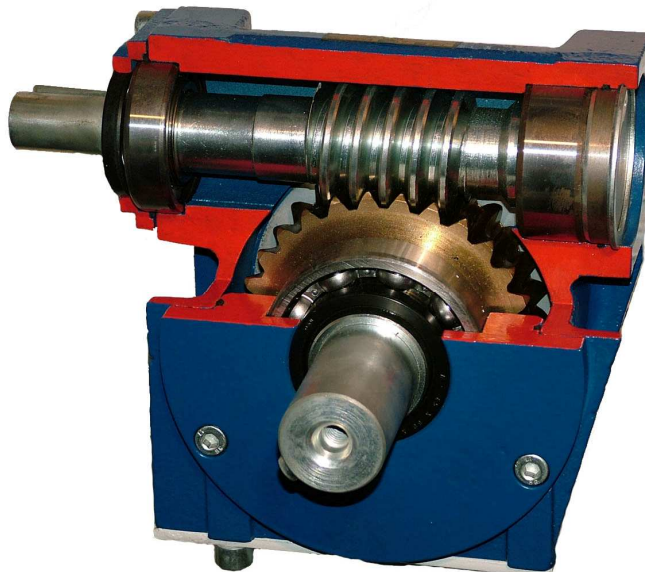

Fig. 1.   A cylindrical worm gear [1]

The geometric locus of axes of rotation for the wormwheel will be the rolling plane, while for the worm – the rolling cylinder with a teeth pitch equal to the teeth pitch of this worm, which is a constant quantity. It should be added that, in contrast to cylindrical toothed

gears, in worm gears a slip occurs on the rolling line. However, owing to the fact that the pitch of the worm and the pitch of the wormwheel are identical, the name "rolling wheel" for the wormwheel and the name "rolling surface" for the worm are preserved.

2. Mating of the worm with the wormwheel

The detailed analysis of the toothing is quite often not possible, or is uneconomic; therefore, it is crucial to understand the influence that the type of worm and some toothing parameters can exert on the system of the line of contact and the extent of the toothing region.

The shape of the contact line and its position, as well as the toothing region extent depend on many factors, of which the following can be ranked among the main ones:
- type of worm
- lead angle and tooth profile angle
- wormwheel rim shape
- number of worm and wormwheel teeth
- position of the toothing pitch point.

The position and shape of the line of contact is influenced most decisively by the type of worm – Fig. 2. The toothing shape variation is different and depends on different worm variants. In gears with worm of a concave tooth profile, both the toothing shape and the course of the line of contact is markedly different from that occurring in gears with worms of rectilinear helical surfaces, or with cone-derivative worms. Figure 2 shows the projection of the line of contact for two different worms, which are Archimedes' worm and the involute worm. In both cases, these are single-coil worms with a small lead angle; whereas, with increasing helical line lead angle the differences between the involute worm and Archimedes' worm become greater.
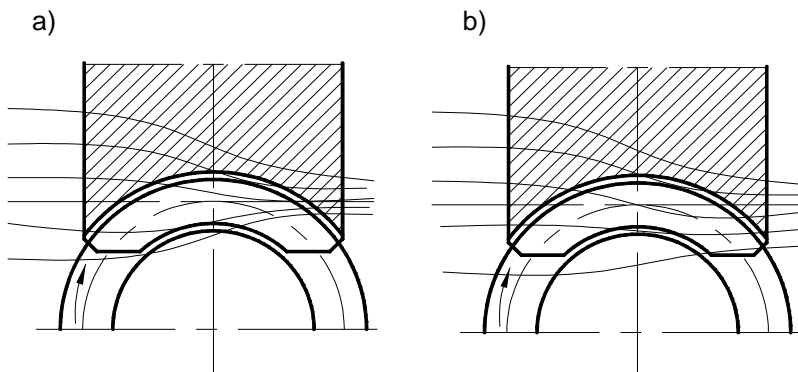
a)   b)

Fig. 2. The course of the line of contact between worm teeth and wormwheel teeth [2]: a) Archimedes' worm, b) involute worm.

If a theoretical hypothesis of an ideal gear, that is the one where the mating elements are sufficiently rigid and executed practically with no deviations and there is no need for lubrication, is analyzed, the conclusion can be drawn that such toothing in both gear elements would be most advantageous, which is as close as possible to the nominal surfaces satisfying the basic principle of meshing within the entire meshing region – Fig. 3.
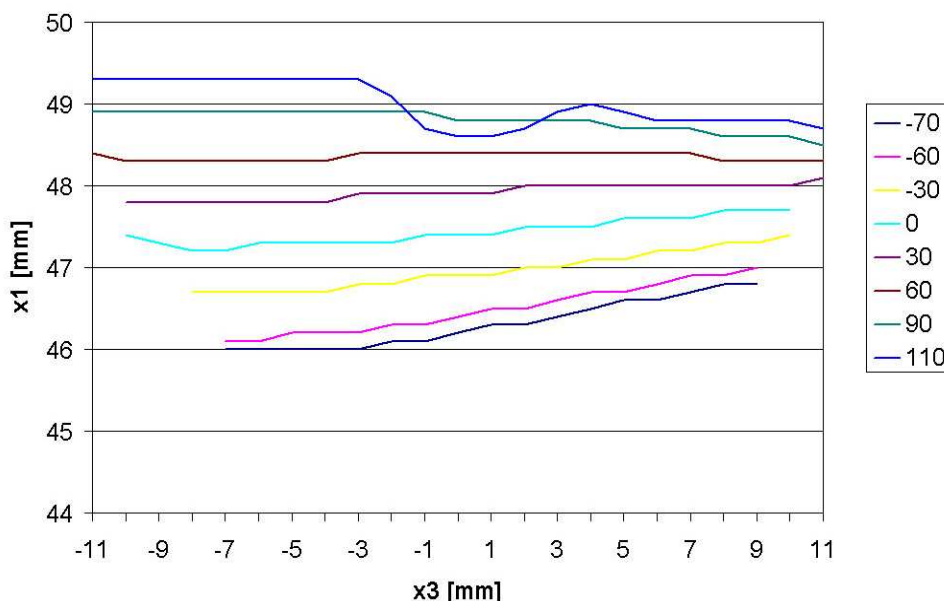
Fig. 3. The illustration of the correct position of the line of contact as a function of the angle of gear rotation (the legend on the right-hand side is expressed in [°]) [1].

In the case of coupled gears, where the gear tooth surface are of an envelope nature in relation to one another, theoretically a linear tooth contact occurs; therefore, when analyzing the gear it is generally assumed that the contact between worm teeth and wormwheel teeth is linear. In reality, though, it is not possible. Individual gear elements always exhibit some flexibility and, as practice and calculations show [1], the errors of gear assembly or execution, even in the case of mating of surfaces of mutually envelope character, will transform the linear tooth contact into a punctual one that can move to the outer worm wheel face, which could cause accelerated wear or breaking of wormwheel teeth. When making a gear it should be made sure to create the best possible conditions for lubrication of mating gear elements. In the worm gear, the friction work is particularly great, therefore assuring the proper lubrication of the gear, and especially preventing the teeth from being removed from the oil at the time of they entering into meshing, is crucial for the whole gear mating process.

As practice and performed calculations show [1], the errors of gear assembly or execution, even in the case of mating of surfaces of mutually envelope character, will transform the linear tooth contact into a punctual one that can move to the outer worm wheel face, which could cause accelerated wear or breaking of wormwheel teeth. Therefore, worm gears should be executed and assembled very accurately, and any possible errors should be used as the parameters for locating the contact and the trace of fitting of the gear.

3. Conclusion

In the case of the analyzed worm surface and the kinematics of machining determined for it, there is only one linear-contact surface coupled with this surface, whereas there may be any number of surfaces with a punctual contact with it. This creates definitely grater possibilities in the design and engineering of worm gears, but, at the same time, the solution of the task in that case becomes more difficult.

Indeed, in the analysis of mutually coupled surfaces it is sufficient to limit the task to the determination of the mating tooth surfaces, whereas in the case of the punctual contact it is necessary to design the construction and the technology of execution of gear elements, while allowing additionally for the analysis of their meshing, that is the determination of the actual points of contact between the mating elements. Gears with linear tooth contact are sensitive to execution and assembly errors which are actually not possible to be excluded in the gear execution process; they can only be minimized. Punctual-contact gear, on the other hand, will be less sensitive to such errors.

References

[1] GOŁĘBSKI R.: Analiza geometryczna przekładni ślimakowej walcowej (The geometric analysis of the cylindrical worm gear). A doctoral thesis. Czestochowa University of Technology, 2006

[2] MARCINIAK T.: Przekładnie ślimakowe walcowe (Cylindrical worm gears). The PWN Publisher, Warsaw 2001

Stress Analysis Evaluation in the Contact Patch of a Railway Wheel Tread and a Rail Head

[*]Jozef Harušinec, [*]Tomáš Lack, [*]Juraj Gerlici
[*]University of Žilina, Faculty of Mechanical Engineering, Department of Transport and Handling Technology, Univerzitná 1, 01026 Žilina, Slovakia, {Jozef.Harusinec, Tomas.Lack, Juraj.Gerlici}@fstroj.uniza.sk

Abstract. The paper deals with the issue of wheel / rail contact stresses analysis. The stress analysis can be solved by different methods: experimental and simulation – computational. From the range of experimental methods, the photo- elastimetry method is known and utilized. We are interested in the contact solutions with the help of the Finite element method methodology. There is a need for this special couple bodies deformations, contact patch and contact stressing analysis in detail. The results of strain – stress computations by the Hertz and the Strip method are available for comparison.

Keywords: wheel /rail contact patch, stress analysis, photo-elastimetry, finite element, Kalker method.

1. Introduction

In general, we can divide the contact issue into a point contact (that can be carried out in one point, two points, or more than two points) and a contact in a contact patch. We will search and assess this type of contact mainly in normal and tangential directions. Although there is a need for the contact patch and contact stresses between railway wheel and rail assessment, it is necessary to judge more types of methods proposed for the evaluation and verification of this case. For the purpose of suitable computational method choice, it is useful to carry out a comparable computation with the couple of two cylinders with their simple radii.

2. Rail /Wheel Contact Analysis

An important parameter which influences the power effect of a wheel on the rail is the size and shape of the contact area as well as the normal stress distribution which has the impact on it. Nowadays various methods are used to find out the size of contact areas and stresses. It is necessary to mention the Hertz method as one of the oldest and up to date used methods. It provides acceptable results for a large area in spite of many simplifications. Another representative is the stripe method which is thanks to its results close to reality and it is used in the following calculations, or the Kalker's method for the performance of more detailed and precise "half spaces contact" evaluation. Nowadays, another group of calculation programme systems (ANSYS, MSC.MARC, ADINA...) is used to a certain extend. The systems work on the base of the Finite elements method theory. Searching for the contact problems solution with the help of FEM is the subject of the paper too. The analytical computational methods capabilities were mainly in the past completed or enhanced by experimental methods of contact stresses evaluation on the base of visualization.

2.1. Experimental Methods

The photo-elastimetry method is based upon the principle of the light refraction during the transition through the object manufactured from a transparent material on which the external load acts. There it is possible to perform the tests on the test rig as it is shown below. The advantage is the smart gaining of the results, the disadvantage is, that it is possible to analyze the stress only in one plane.
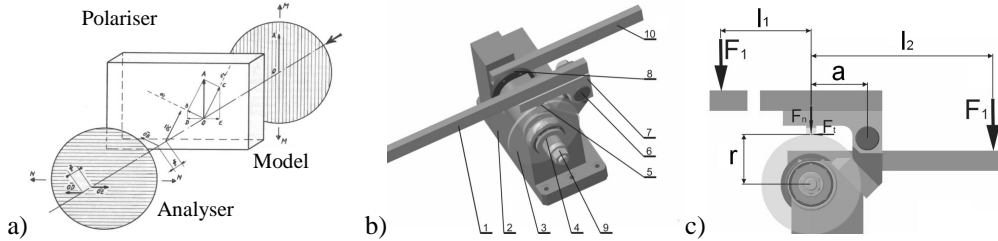

Fig. 1. The polarization phenomenon principle and the test rig for experimental stresses evaluation.

Description: 1 – lever, 2 – frame, 3 – test disc, 4 – clutch, 5 – prism, 6 – pin, 7 – arm, 8 – a wheel for torque moment transmission, 9 – locknut , 10 – lever for torque moment generation, l_1, l_2, and, r are arms [m], on that act the forces F_1, F_2, F_n, F_t [N].

These principles were utilized in the past at the Department of Transport and Handling Technology. The model was compounded from the cylinder phi 200x8 and 500x8 and the prism 45x45x8 manufactured from EPOXI E110 and EPOXY E13. Mechanical and load parameters were known. Similar to them we carried out the model computation with the help of ANSYS programme package. The stress distribution in comparison to the experimental research is shown in the Fig. 2.
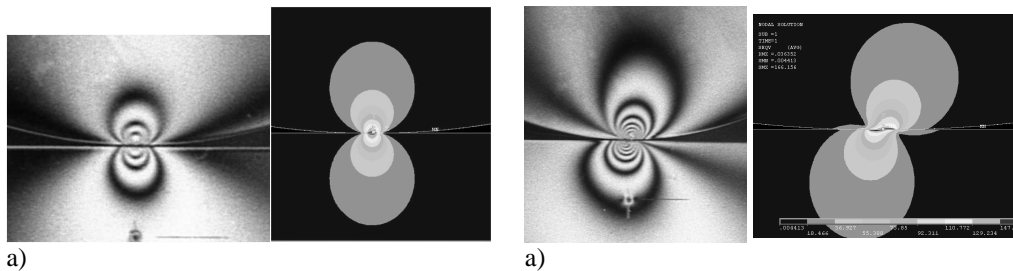

Fig. 2. The normal and tangential stress distribution visualized by the experiment and assessed by the computation with the programme ANSYS.

Fig.2a) shows the couple of normal stress evaluations and Fig.2b) shows the tangential stress distribution. The shapes of both stress distribution figures of experimental results correspond to the shapes gained by the computation.

2.2. Analytical Computational Methods

The above mentioned methods can be divided from the point of view of the possibility to evaluate the surface stresses only and surface and inner body stress evaluation into two ranges. The methods of half space contact evaluation (hertzian and quasihertzian) can be included in the first group. They are very fast and useful for computations of vehicle dynamics. The Finite element method is much slower but the internal stress distribution can be evaluated.
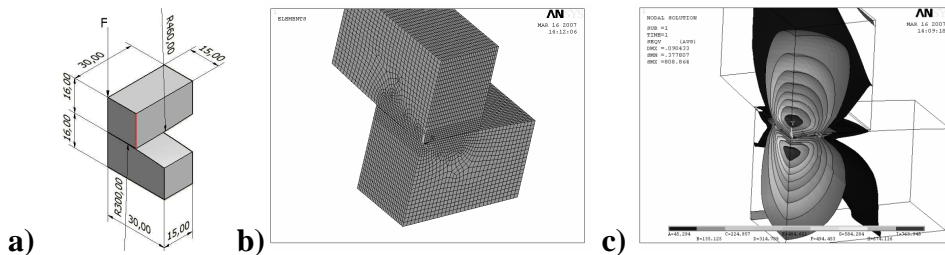
Fig. 3. The FEM element, meshed FEM model normal stress distribution assessed by the computation with the programme ANSYS.

The computations were carried out on two cylinders of 300 mm radius (rail) and 425 mm radius (wheel) cylinders.

2.3. Results Comparison

In the Tab.1 there is the list of computational results. The FEM models had been compounded from different types of FEM [1].

Nr.	FEM Element	Semi-axis a [mm]	Semi-axis b [mm]	Ellipse area S [mm²]	Middle pressure p_S [MPa]	Max. pressure p_{max} [MPa]	CPU time [min]
1	SOLID185 /1mm/m	7,93	6,000	149,48	668,993	1225	10
2	SOLID185 /0,5mm/m	7,743	6,000	145,878	685,5	1231	27
3	SOLID185 /0,25mm/m	7.25	5.520	125,727	795,337	1235	184
4	SOLID187 /1mm/f	8,439	6,000	159,07	628,65)	1211	25
5	SOLID187 /0,5mm/f	7,86	6,000	148,158	674,95	1205	135
6	SOLID187 /0,25mm/f	7,7433	5,985	145,582	686,87	1203	486
	Hertz method	**7,1937**	**5,4197**	**122,48**	**816,43**	**1224,65**	**15**

Tab. 1. Results gained from four various models.

The schematic layout of wheel /rail position
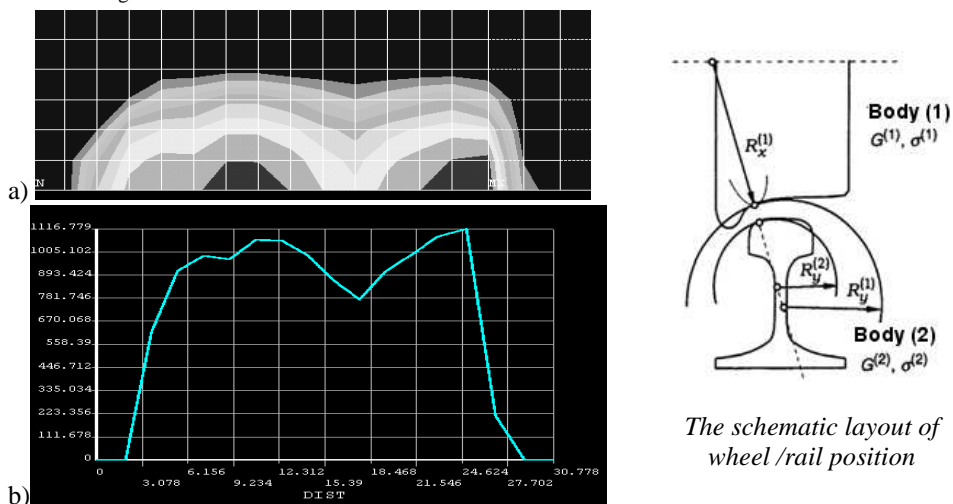
Fig. 4. Stress distribution of the real shapes rail and wheel evaluation (a), contour of maximum stress b).

3. Conclusion

From the range of experimental methods, the photoelastimetry method was utilized. The results gained by this method for the tested model correspond to the results of analytically gained results. This method has its advantages and disadvantages. The Finite element method was tested for the purpose of a contact stress distribution evaluation. The results in addition to the ellipse axis parameters and contact pressure distributions include the stress parameters under the body surface. The assessed CPU time of FEM analyses were from 10 minutes to 8 hours. For the purpose of surface and internal stress evaluation, it is effective to use the FEM based method, but it is needed to pay attention to input parameters and finally to increase the precision of a computational model. For better results evaluation it is suitable to create an algorithm and to build the code in MATLAB system. With the help of this programme we will be able to assess the parameters, which is not easily possible with the postprocessor of ANSYS programme.

Acknowledgement

References

[1] ANSYS Release 11, Documentation for users.

[2] BAUD, R., V., HEIDELBERGER, K. *Polarisationsoptishe Tensometrie*. Technishe Rundschau, Bern 1955.

[3] GERLICI, J., LACK T. *Contact of a railway wheelset and a rail*. (In Slovak). ISBN 80-8070-317-5. EDIS – Publishing house of the University of Žilina 2004.

[4] HARUŠINEC, J., LACK, T., GERLICI, J. *Steady-state stress analysis of railway wheel /rail contact with the help of FEM*. In: proceedings of international conference "TRANSCOM 2007", ISBN 978-80-8070-696-8, proceedings, Section 7, pp.65-70, EDIS – Publishing house of the University of Žilina 2007.

[5] HARUŠINEC, J., GERLICI, J., LACK, T. *A rail /wheel contact analysis with the help of the Finite element method*. (In Slovak) In: proceedings of the 18-th international conference „PRORAIL 2007", Part I., pp. 173-180, EDIS, ISBN 978-80-89276-06-6, Žilina 2007.

[6] HARUŠINEC, J., LACK, T., GERLICI, J.: *Stress conditions in the railway wheel tread and rail head contact area*. (In Slovak). In: proceedings of the international conference "Dynamics of rigid and deformable bodies". ISBN 978-80-7414-030-3. Pp. 43-52. J. E. Purkyně University, Ústí nad Labem. 2008.

[7] LACK, T., GERLICI J.: *Contact area and normal stress determination on railway wheel / rail contact*. Communications Scientific letters of the University of Žilina, 1/2005, Pp. 38-45, ISSN 1335-4205, EDIS – Publishing house of the University of Žilina 2005.

[8] LACK, T., GERLICI, J., HARUŠINEC, J. *An Accurate evaluation of contact stress fields of rail and wheel*. . (In Slovak) In: proceedings of the international conference "Dynamics of rigid and deformable bodies". ISBN 978-80-7044-914-1. Pp. 127-136. J. E. Purkyně University, Ústí nad Labem 2007.

[9] SÁGA, M., VAVRO, J., KOPECKÝ, M. *Computer analysis and synthesis of mechanical systems (In Slovak: Počítačová analýza a syntéza mechanických sústav)*. ISBN 80-968605-4-2. Žilina, ZUSI, 2002.

[10] SHACKLETON, P., IWNICKY, S. *Comparison of wheel–rail contact codes for railway vehicle simulation: an introduction to the Manchester Contact Benchmark and initial results*. Vehicle System Dynamics Vol. 46, Nos. 1–2, January–February 2008, 129–149, ISSN 1744-5159, Taylor & Francis 2008.

[11] TELLISKIVI, T., OLOFSSON, U.: *Contact mechanics of measured wheel-rail profiles using the finite element method*. In.: Proc Instn Mech Engrs Vol 215 Part F, pp. 65-72. IMechE 2001.

[12] WRIGGERS, P. *Finite element algorithms for contact problems*. Archives of computational methods in engineering, State of the art reviews. ISSN: 1134-3060. Vol. 2,4 (1995). Pp.1-49, CIMNE, Barcelona 1995.

Research on Influence of Professional Preparation for a Car Mechanic on Skills for Performing Repairs of Vehicles

[*]Daniel Kołodziejski, [**]Marian Jósko

[*] Poznan University of Technology, Institute of Working Machines and Motor Vehicles, Piotrowo 3, 60-965 Poznan, Poland, danila.transport@wp.pl

[**] Poznan University of Technology, Institute of Working Machines and Motor Vehicles, Piotrowo 3, 60-965 Poznan, Poland, marian.josko@put.poznan.pl

Abstract. The purpose of this article is to present the professional preparation of a car mechanic according to car mechanics themselves. It presents the influence of human factor, which conditions the improvement of service and repair processes at service stations of car vehicles. It compares the levels of practical and theoretical preparation of graduates of professional basic and professional secondary schools. Moreover it studies, the following issues: assessment of time assigned for professional training, necessity to take part in additional courses, choice of profession according to interests and willingness to work as a car mechanic.

Keywords: human factor, educational system, professional preparation, questionnaire research.

1. Introduction

With system and economical transformation in Poland within the last dozen of years, there has been a change in the way how students of professional secondary schools are prepared to perform their profession including the profession of a car mechanic. The observation of this way shows, that qualifications acquired by graduates of those schools do not meet the requirements of present garages in Poland. The previous system of service and repairs of car vehicles comprised homogenous vehicles in respect of the brand. Those vehicles were characterized by low technological complication. Present system of service and repairs of car vehicles comprises not only vehicles, which are diversified from the perspective brands, models or the age, but also vehicles which are technologically advanced. This enforces changes in the education of future car mechanics on the level of secondary schools educating the profession of a car mechanic.

The purpose of this article is to present the influence of human factor, particularly professional preparation, on the quality of works performed at service and repair stations. The research referred to assessment of professional preparation in practical and theoretical aspect with reference to opinions of graduates of schools preparing for the profession of a car mechanic.

2. The characteristic of present educational system

In the present educational system a future car mechanic is expected to show a professional flexibility, which can be achieved by basic and extended education. In the observed way of education, a scarcity of present model of professional education is noticed [1].

The quality of services and repairs at service stations of car vehicles is influenced by factors that can be reduced to three main groups [2,3]:

- human,
- technical (technological),
- economic.

This article focuses on the human factor presented in Fig. 1 characterized by, among others, the following elements: psychophysical, the ability to solve problems or the quality of professional preparation. The factor of professional preparation is particularly analyzed taking into consideration opinions of graduates of schools educating car mechanics.
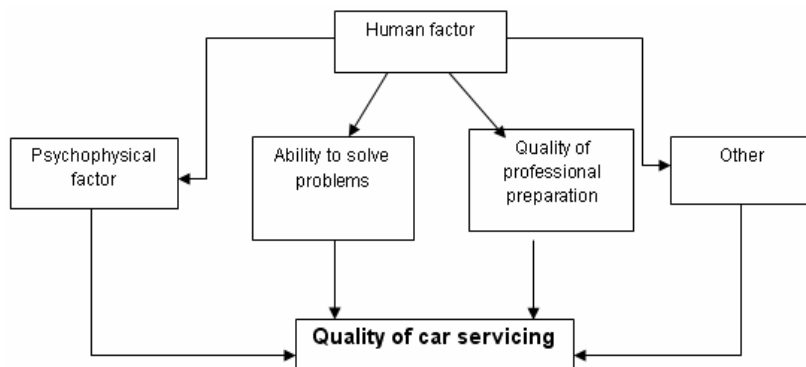
Fig. 1. Selected elements of human factor on quality of service and repair stations.

Differences in practical and theoretical preparations in professional basic schools and professional secondary schools educating car mechanics were presented.

3. Research on influence of theoretical professional preparation

A questionnaire research was carried out to assess the professional preparation. Graduates of professional basic schools and professional secondary schools, which prepare for the profession of a car mechanic, took part in the research. The research was carried out in 42 schools: 39 professional secondary schools and 36 professional basic schools. The research comprised period of time between 2006 and 2008. In the research 2196 graduates of professional secondary schools and 1782 graduates of professional basic schools which educate the profession of a car mechanic took part.

The research had a form of questionnaire with closed and open questions. The closed questions were characterized according to nominal alternative scales (with bi-partite classification) and a gradual scaling of attitudes was applied. In this case a rank scale was used, where the answer was scaled according to the nominal scale [3].

The first question referred to the preparation level of the graduates of secondary schools to perform the profession of a car mechanic in theoretical aspect. The second question referred to the same group of graduates but from the perspective if practical aspect. To determine the level of self-assessment of competence a five-point Likert item [4,5] was applied.

The sequence of the rising scale of assessment:
1: very low level,
2: low level,
3: medium level,
4: good level,
5: very good level.

The results presented in Fig. 2 show that both practical and theoretical preparation are assessed at second and third rank in five-point scale of answers. Such results show medium or low level of preparation of graduates of professional secondary and professional basic schools for the profession of a car mechanic.
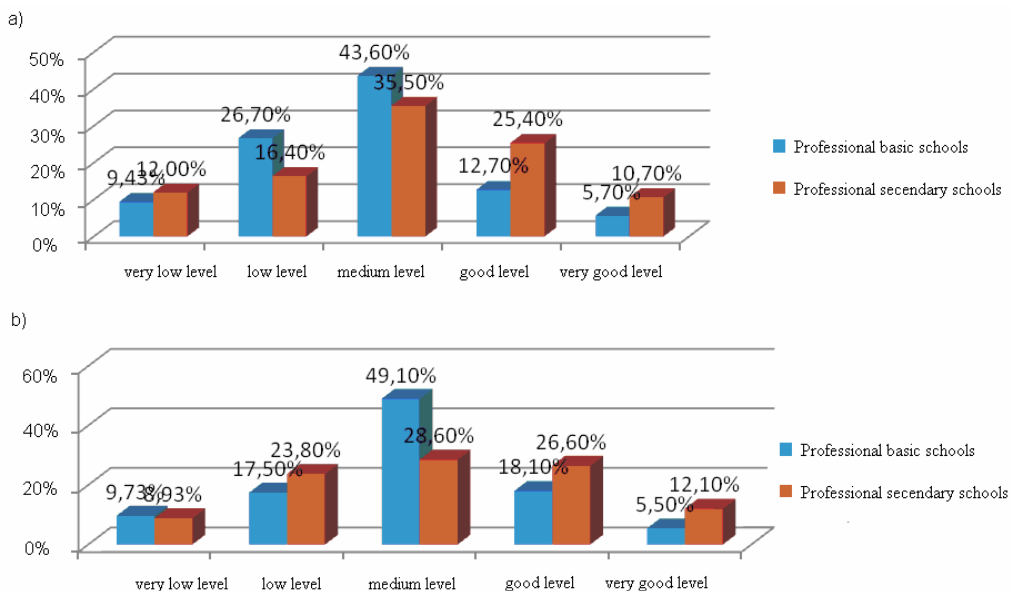
a)

b)

Fig. 2. Distribution in percentage of responses of graduates of professional secondary schools for question referring to the level of professional preparation for the profession of a car mechanic:
a) level of theoretical preparation, b) level of practical preparation.

4.   Ancillary research

Next step was a second part of the questionnaire research, whose aim was to assess time assigned for practical education of the profession and required for additional trainings. It was checked if students chose the school according to their interests and if they plan to work as car mechanics. The following questions were included in the questionnaire:
- Do you think that time assigned for practical education of the professional is sufficient for a future car mechanic?
- Do you think that before starting work as a car mechanic you should take additional courses?
- Did you choose the profession of a car mechanic according to your interests?
- Do you plan to work as a car mechanic after graduation?

This part of the questionnaire consisted of closed questions, which were characterized according to nominal alternative scales (with bi-partite classification). Students could only give affirmative or negative answer (Yes, No). For the fourth question tripartite classification was applied comprising the following answers: Yes, No, I have no opinion. Fig. 3 presents the results.
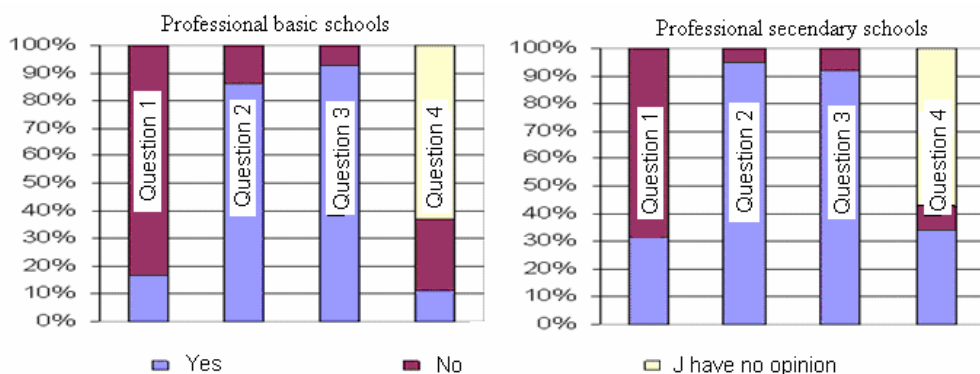
Fig. 3. Distribution in percentage of responses of students of professional secondary and professional basic schools to the question about time assigned for practical education of the profession, necessity to take additional training, choice of the profession according to interests and plan to work as a car mechanic.

5. Conclusion

- During the research invariable quality of education in the period of research perceived by graduates was confirmed,
- Most of inquired persons assess both their theoretical knowledge and practical skills on second on third level in five-point classification,
- Relatively low percentage of graduates plan to work as car mechanics , although with reference to the research, they chose the profession according to their interests,
- Students of professional secondary schools and students of professional basic schools show deficiencies in practical preparation and express necessity to attend courses improving their qualifications.

References

[1] BEDNARCZYK, H. *Zadania zawodowe i kształcenie mechaników*. Instytut Technologii Eksploatacji, Radom 1996.

[2] LEGUTKO, S. *Podstawy eksploatacji maszyn i urządzeń*. Wydawnictwo Szkolne i Pedagogiczne, Warszawa 2004.

[3] SMALKO, A. *Podstawy eksploatacji technicznej pojazdów*. Oficyna Wydawnicza Politechniki Warszawskiej, Warszawa 1998.

[4] KACZMARCZYK, S. *Badania marketingowe*. Polskie Wydawnictwo Ekonomiczne, Warszawa 2003.

[5] BRZEZIŃSKI J. *Metodologia badań psychologicznych*. Wydawnictwo Naukowe PWN, Warszawa 2003.

Pressure and Flow Measurement in a Nonconventional Energetic System

[*]Andrej Kovalčík

[*]University of Zilina in Zilina, Faculty of Mechanical Engineering, Department of Automotive Technology, Univerzitná 1, 01026 Žilina, Slovakia, andrej.kovalcik@fstroj.uniza.sk

Abstract. The paper deals with a pressure and flow measurement in a nonconventional energetic system, in which a combustion engine is implemented. A working medium (lithium bromide liquid + water) flows in the cooling system of a combustion engine and a nonconventional energetic system.

Keywords: pressure, flow, nonconventional energetic system, absorption cooling system, combustion engine, working medium.

1. Introduction

The energetic system is classified among absorption cooling systems. A working medium is mixture of the lithium bromide liquid with water.

There is an analysis of course of pressure in particular branches of a nonconventional energetic system (see Fig. 1).
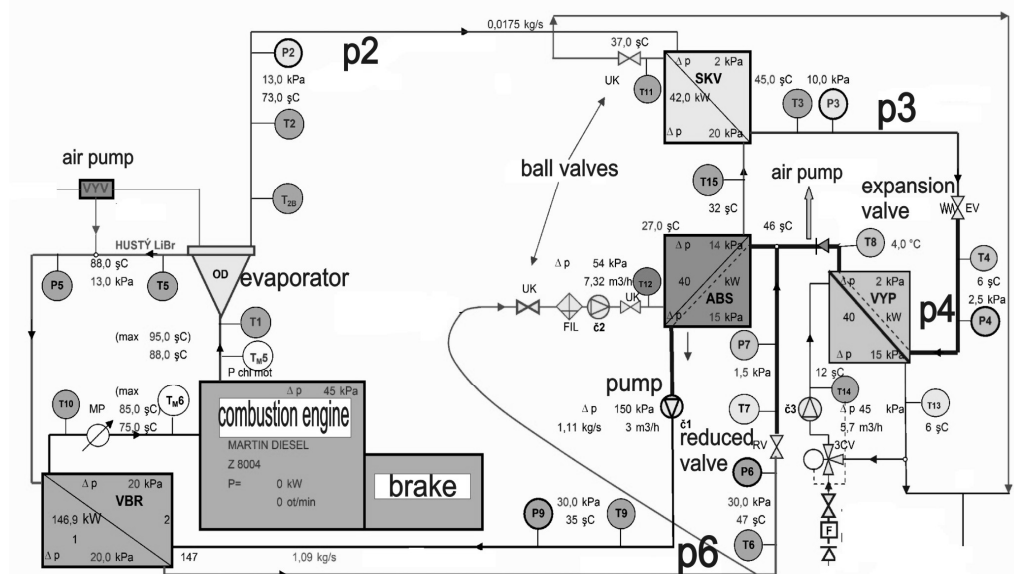
Fig. 1. Block scheme of the nonconventional energetic system.

2. Manipulation with a pump, expansion and reduced valve

All of measurement practiced on a test unit of the nonconventional energetic system. Manipulation with a pump - the change of rotation speed and the change of position of the expansion and reduced valve.

Fig. 2 shows the impact of a hydrostatic height of liquid on pressure sensors while the test unit is in sleep mode. The change of flow of liquid (resulting from the change of the pump rotation speed) is shows in Fig. 3. The max flow of liquid was achieved in the time of 780 s. Fig. 4 shows course of pressure and flow caused by the manipulation with the expansion and reduced valve. The expansion valve is fully open in the time of 1500 s. The reduced value is continually regulated from the time of 1575 s (see Fig. 4). Fig. 5 illustrates the change of pressure and flow of liquid after turning-on an air pump in the time of 2160 s.
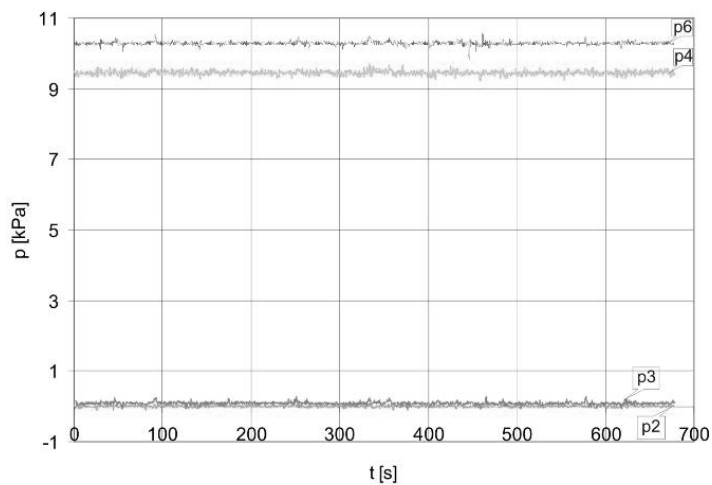
Fig. 2. The test unit in sleep mode.
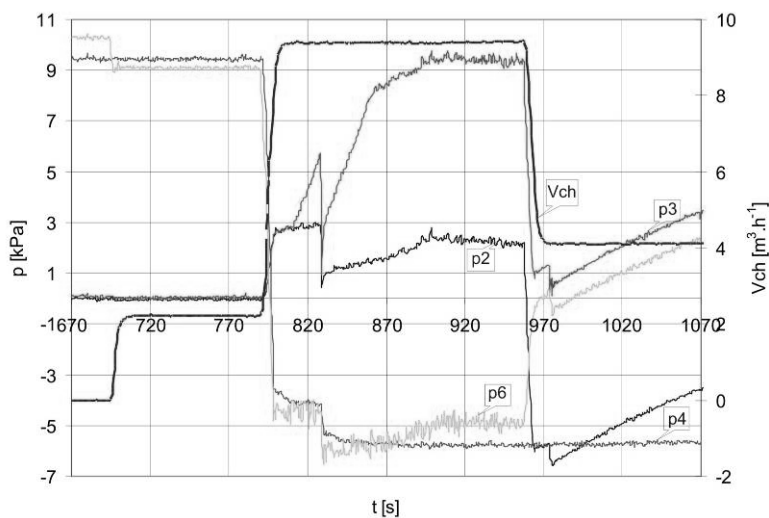
Fig. 3. The flow of liquid.
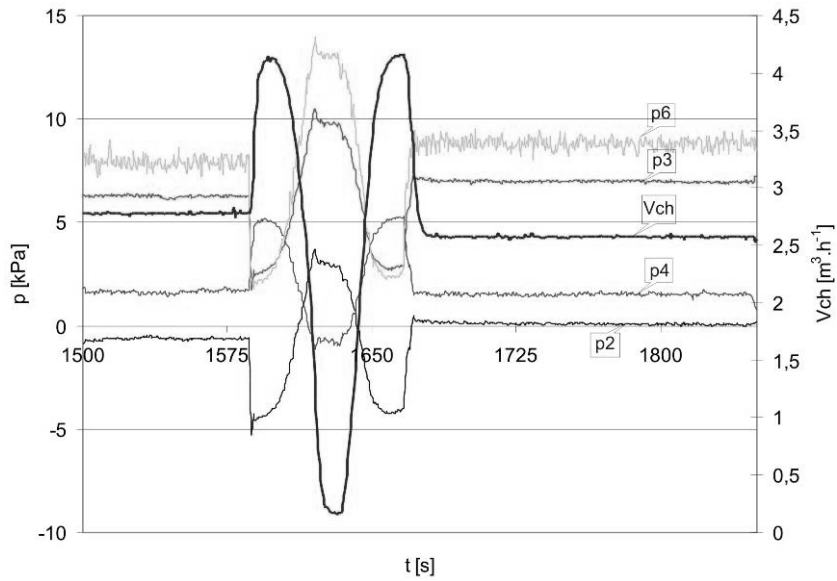
Fig. 4. Manipulation with an expansion and reduced valve.
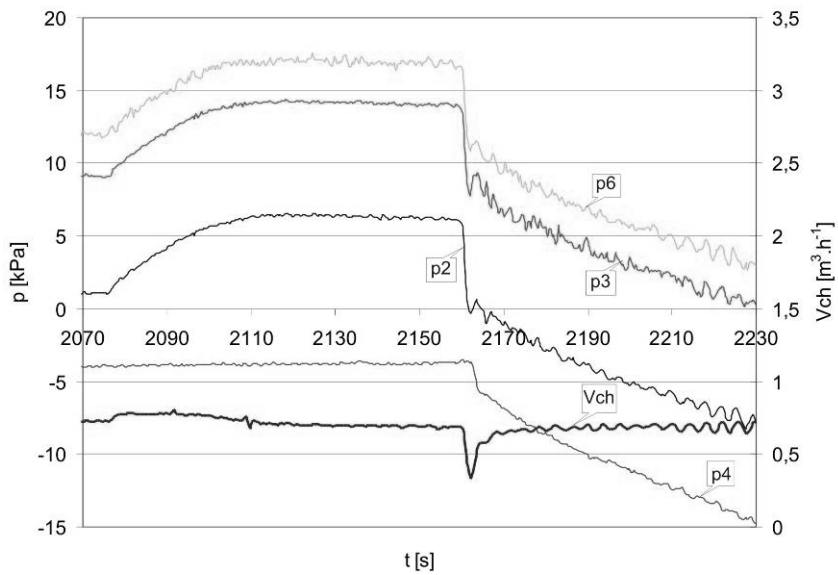
Fig. 5. Turning – on an air pump.

3. Conclusion

The paper contains a file of pressure and flow liquid measurement. In the presented Figs. it can be seen an effect of manipulation by controls on nonconventional energetic system and effect of controls on physical quantities.

Acknowledgement

References

[1]   HLAVNA V. et. al.: *A non-conventional energetic unit*. EDIS University of Zilina, 2008.

Combined Cycle Plants for Cogeneration in Industrial Power Station

[*]Andrej Kovalčík, Dušan Sojčák, Daniela Zvarková
[*]University of Žilina, Faculty of Mechanical Engineering, Department of Automotive Technology,
Univerzitna 1, 01026 Žilina, Slovakia, andrej.kovalcik@fstroj.uniza.sk

Abstract. The article shows short description of combined cycle plants for cogeneration in industrial power station. It involves a gas turbine and steam turbine as important equipment for transport of energy. There is short discussion about an effect of the most important design conditions and parameters.

Keywords: gas turbine, steam turbine, HRSG – heat recovery steam boiler, design conditions, design parameters.

1. Introduction

The thermodynamic advantage of a combined-cycle applies not only for use in a power plant that produces power alone, but also for those which provide heat or process steam as well. Fig.1 shows the flow diagram of such an installation with a backpressure turbine.

The thermodynamic superiority of the combined-cycle plant over a conventional power plant is even more pronounced in cogeneration plants than it is in plants used only to generate electricity. The drop between the average heat input to the process and that of the exhausts is greater in a combined-cycle plant than in a steam power plant.

If both types of power plants have to supply heat at the same temperature level, the loss in temperature drop is the same in both cases but. the relative loss in combined-cycles is smaller because the total drop available is larger. The following combined-cycle installations can be considered for cogeneration plants:

- combined-cycle plant with a backpressure turbine,
- combined-cycle plant with an extraction/condensing turbine,
- gas turbine with a waste heat boiler.

Though the gas turbine with a waste heat boiler is no longer a genuine combined-cycle plant (it operates without a steam turbine), it can be viewed as a limit case. All installations can be equipped with supplementary firing, which might even be of considerable advantage for the cogeneration process because it offers a much greater design and operating flexibility than available with waste heat utilization alone. The production of steam or thermal energy can be controlled independently of the electrical power output because the gas turbine assumes control of the power output and the auxiliary firing handles control of the steam or heat generation. Cogeneration plants can be classified into three categories as follows:

- industrial power stations to supply process steam to industrial plants,
- thermal power stations to supply thermal energy to district heating systems,
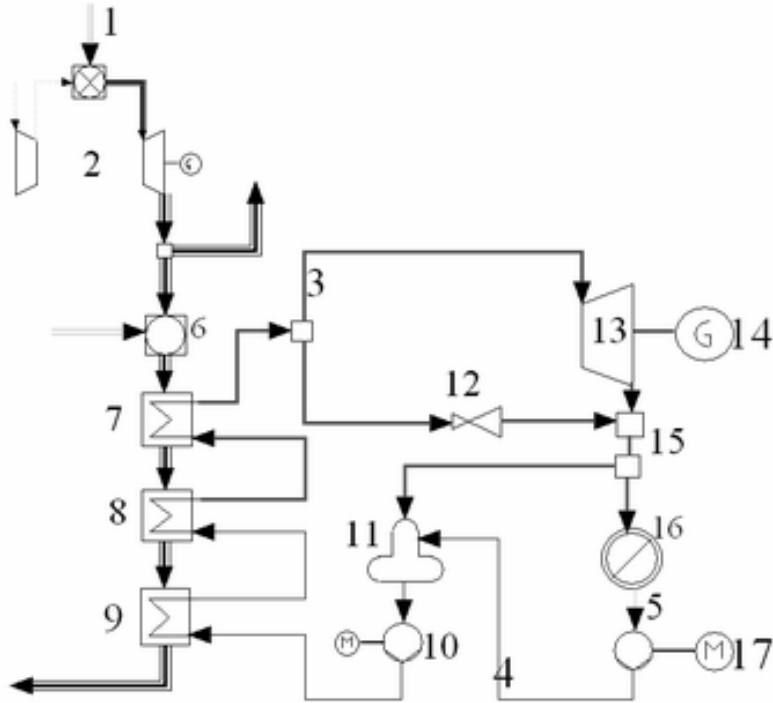- power plants coupled to seawater desalination plants.

Fig. 1. Diagram of the principle of a Combined Cycle plant used for cogeneration, 1 – Fuel line, 2 – Gas Turbine, 3 – Steam line, 4 – Water line, 5 – Condensate line, 6 – Supplementary firing, 7 –preheater, 8 – evaporator, 9 – economizer, 10 – pump, 11 – Deaerator / Feed water tank, 12 – Reducing station, 13 – Steam Turbine, 14 – Generator, 15 – flow mixer / divider, 16 – heat consumer, 17 - motor

2. Industrial Power Station

Wherever both electrical power and process steam are needed. It is thermodynamically and generally also economically better to produce both products in a single plant.

The number of possible solutions is large because each plant is a "special case." As an example, we will cite here a process with a single pressure level for the process steam. Often the cases involved are more complicated but the basic considerations remain unchanged. One important core parameter for cogeneration plants is the power coefficient, the ratio between the electrical power and the thermal energy produced [2].

One characteristic of the combined-cycle plant is its high minimum value for this power coefficient. It is therefore more likely to be suitable for processes where a relatively great amount power must be generated.

2.1. Example of a Combined-Cycle Industrial Power Plant

Just as we did for power generation alone, we will base further considerations here on one given example, specifically: a gas-burning plant with supplementary firing, equipped the same 70 MW gas turbine as our other examples, and a back pressure turbine (absolute backpressure 3.5 bar). Tab.1and Fig.1 contains the main technical data for this unit.

2.2. The Effect of the Most Important Design Conditions

As with combined-cycle plants used for generation of power alone, the air temperature is of particular importance here, too, for power output.

In industrial processes, the demand for power generally does not depend on the ambient temperature. As a result, one is often compelled to select the highest ambient temperature for design purposes.

The pressure level of the process steam and the power coefficient also are of importance for design, because the pressure of the process steam directly affects the enthalpy drop in the steam turbine. The higher the pressure, the less electricity is produced.

If this pressure is very high, the use a steam turbine becomes questionable since its pressure differential is then too small. In that case, the steam process reduces to a waste heat boiler.

Fuel	Natural Gas
Gas Turbine Power Output	69 100 kW
Backpressure Steam Turbine Power Output	44 700 kW
Station Service Power	1400 kW
Net power output of the Plant	112 400 kW
Heat input to the Gas Turbine	230 000 kW
Heat input to the supplementary firing	79 600
Process Steam Flow	65,3 kg.s^{-1}
Process Steam pressure	3,5 bar
Thermal Energy of Process steam	152 000 kW
Rate of fuel utilization	85,4 %
Power Coefficient	0,74
Electrical yield	36,8 %
Efficiency of power production	79,9 %

Tab. 1. Main Technical Data of the Combined Cycle industrial Power Plant

The power coefficient of the plant is affected mainly by three parameters:
- the amount of fuel supplied directly to the boiler,
- the size of the condensing portion of an extraction /condensing turbine,
- the pressure level of the process steam.

Supplementary firing makes it possible to lower the power coefficient. However, this capability is limited because lowering it too much would reduce the thermodynamic advantages of the combined - cycle plant. Combined-cycle plants should be employed only where the power coefficient is high. That feature must not, however, be considered as a disadvantage since for industries which require low power coefficients it is often a better idea to obtain the power needed from the connected grid and to generate the steam in conventional steam generators.

An extraction/condensing turbine offers greater design and operating flexibility in the direction of higher power coefficients. The condensing portion of the turbine makes it possible to increase electrical power produced at the cost of process steam generation. However, this procedure works out unfavorably on the overall efficiency.

The backpressure turbine represents the optimum case for cogeneration. As soon as the power coefficient required changes, one moves away from that optimum. To the left of the maximum is the case with mixed process steam production: one portion of the process steam is being produced in the backpressure turbine and the remainder in a steam generator. Here, too, the efficiency of power production drops off rapidly.

2.3. Effect of the Most Important Parameters

When selecting the design data, it is necessary to distinguish between a fired and an unfired waste heat boiler. With supplementary firing, one should select live steam data similar to those for conventional steam power plants. Just as for plants used to generate electricity, the

feed water temperature must be as low as possible so as to attain a good utilization of the heat in the waste heat boiler. Without supplementary firing, the live steam data should be selected according to specific defined criteria for plant. The live steam pressure should, however, be higher to assure a reasonably high enthalpy drop between the live steam and the process steam. This is especially true if a relatively high pressure level is required for the process steam. Poorer heat utilization results, and this loss must be regained in a low pressure evaporator. Normally such low pressure systems are used only for the generating of process steam. Generally it is not worthwhile to introduce the low pressure steam into the turbine because of the slight pressure differential available between the low pressure and the process steam.

3. Conclusion

When designing a cogeneration power plant, the rule is always that for given economic conditions its design must always be simpler and less expensive than that for a power plant, which generates power alone. Thus, for example, the efficiency of the turbine can be a bit poorer because the losses in the machine are recovered energetically in the form of additional process heat.

References

[1] GUBSER, H.R.: *Combined Gas / Steam Turbine Power Station, Brown Boveri Review 65 1978, pp. 687 – 690.*

[2] KEHLHOFER, R.: *Comparison of Power Plants for Cogeneration of Heat and Electricity,* Brown Boweri Review 67, 1980, pp. 504 – 511.

[3] FRANTIŠEK BRUMERČÍK, MICHAL LUKÁČ, LUKÁŠ CIMPL, *Unconventional CVT transmissions*, 2007 In: TRANSCOM 2007 - S. 15-18.

[4] KOTRASOVÁ, K.: *Erdbebenwirkungen auf flüssigkeitsbehälter*, In: Proc. of the 5-th European Conference of Young Research and Science Workers in Transport and Telecommunications TRANSCOM 2003, Žilina, s. 133-136, ISBN 80-8070-086-9.

Selection of an Engine for Innovation of a Small Tractor

*Andrej Kovalčík, *Emil Toporcer

*University of Žilina in Žilina, Faculty of Mechanical Engineering, Department of Automotive Technology, Univerzitná 1, 01026 Žilina, Slovakia, {andrej.kovalcik, emil.toporcer}@fstroj.uniza.sk

Abstract. The contribution was created within the frame of a project from European Union – theme – operating program for Research and Development. The paper deals with a selection of an engine for the small tractor "AGZAT".

Keywords: engine, small tractor, AGZAT, engine BRIGGS & STRATTON.

1. Introduction

This contribution was created within the frame of a project under the name "Equipment of a wheel chassis of mobile working field machines by a caterpillar chassis". The project was submitted at the Department of Automotive Technology on February this year.

We can see the small tractor AGZAT with its original engine and chassis in Fig. 1 on the left. The small tractor with the caterpillar chassis is shown in Fig. 1 on the right.
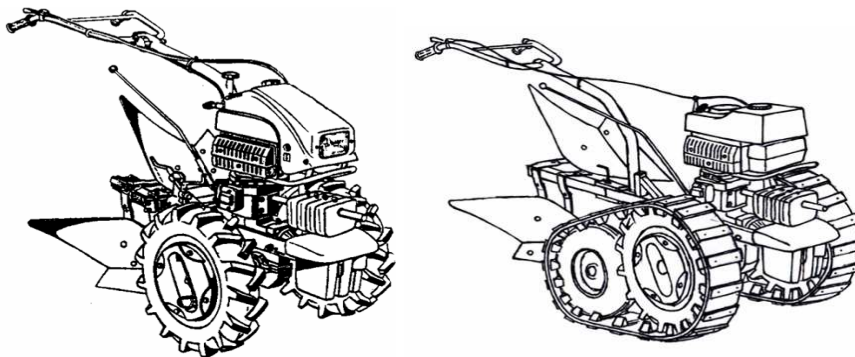
Fig. 1. Small tractor AGZAT.

2. Feasible solution

In this solution a combustion engine BRIGGS & STRATTON is selected. The main reason for the choosing of this engine was the increase of the engine power over the value of ten kilowatts together increase the engine life. The weight of small tractor is about 290 – 300 kg

Fig. 2 shows the speed-torque diagram of the original combustion engine AGZAT JM 4 – 002.
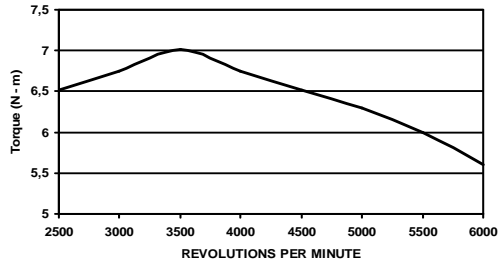
Fig. 2. Speed-torque diagram.

In the Figs. 3 and 4 we can see the speed-torque diagram and the view of the engine BRIGGS & STRATTON. The value of max. tourque is 35,3 Nm / 2600 r.p.m.
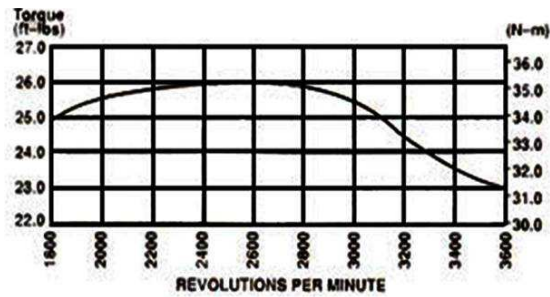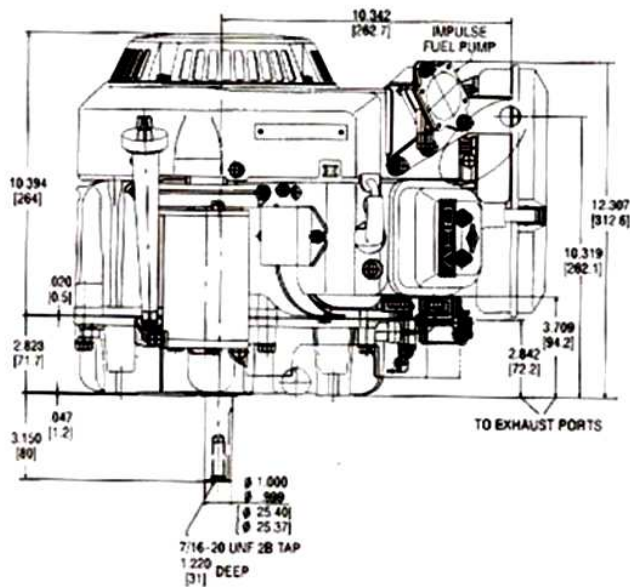

Fig. 3. Speed-torque diagram.

Fig. 4. Engine BRIGGS & STRATTON.

Equation (1) shows the calculation of the tractive force on the wheel:

$$F_h = \frac{M}{R} \cdot \frac{1}{i} \cdot \eta \quad \text{[N; Nm; m]} \tag{1}$$

52

where F_h – tractive force,
            M – torque,
            R – radius,
            i – gear ratio,
            η – efficiency.

Fig. 5 illustrates the dynamic characteristic of small tractor with the original engine and with engine BRIGGS & STRATTON

Dynamic characteristic
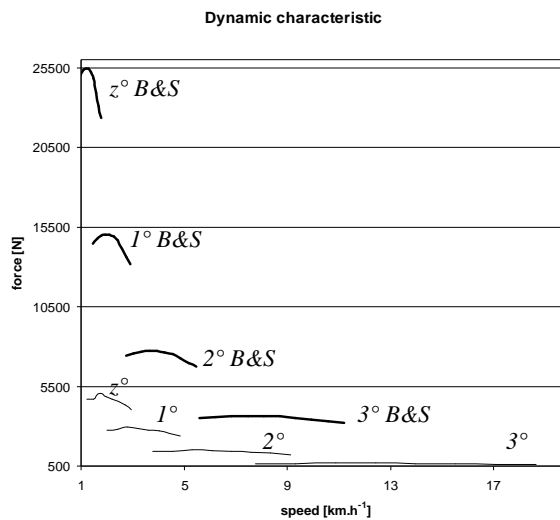
Fig. 5. Dynamic characteristic.

From the dynamic characteristic results that the max. speed of small tractor with engine B & S and original gear box is 11,2 km.h^{-1} on 3rd speed gear. The max. value of the tractive force is 15,1 kN on 1st speed gear, 7,7 kN on 2nd speed gear, 3,6 kN on 3rd speed gear and 25,5 kN on z° speed gear.

The Tab. 1 shows the technical parameters of the original gear box on the small tractor.

	gear ratio	efficiency	
i_1	125,112	η_1	0,91
i_2	66,395	η_2	0,88
i_3	32,434	η_3	0,85
i_z	205,2	η_z	0,94

Tab. 1. Technical parameters.

3. Conclusion

BRIGGS & STRATTON engine can be used as a replacement of the original engine AGZAT JM4 – 002 on the original small tractor. This engine is a construction with a vertical crankshaft and with air cooling. We will need a next gear box between the engine and the original gear box because of the different revolutions per minute of the mentioned engines, and think ahead with a slower machine run of the small tractor. The second solution of choosing engine is using an engine with engine cooling by water.

References

[1]   AGZAT. *Firm publications.*

[2]   BRIGGS & STRATTON. *Firm publications.*

[3]   KRAL M. *Project design of the European Union, "Equipment of wheels chassis of mobile, working, field machines by the caterpillar chassis",* University of Zilina, Faculty of Mechanical Engineering, Department of Automotive Technology 2009.

Difficulties with Funicular Laying Mechanism
of Scissor-Shaped Mobile Bridge

Jan Kroulík

University of Defence, Faculty of Military Technology, Department of Engineer Technology,
Kounicova 65, 662 10 Brno, Czech Republic, jan.kroulik@unob.cz

Abstract. Within the context of the AM70 truck-launched bridge development by company VOP-026 Šternberk Czech Republic, on the base of brief description of scissor-shaped mobile bridge and its laying operation, this article outlines requirements on new hydraulic drive of funicular laying mechanism.

Keywords: armored vehicle-launched bridge (AVLB), funicular actuation, hydraulic drive, laying and loading operation, parallelogram mechanism.

1.   Introduction

Military mobile bridges take place in crisis management also in peace. They are well-proven means especially during such disasters as floods. Engineer corps of the Army of the Czech Republic are equipped with armored vehicle-launched bridges (AVLBs) of different types, among others with AM-50 truck-launched bridge. Nowadays a new AM70 truck-launched bridge is being developed. However, the new AM70 keeps some disadvantages of the outmoded AM-50 conception. Further, thanks to different gravity axis layout, AM70 deals with even more difficulties given by funicular actuation of the scissor-shaped bridge.

2.   Laying Operation

The run of laying and loading operations of the AM-50 truck-launched bridge is shown at Figure 1. The bridge laying mechanism is mounted on the back side of the truck. There are two actuating ropes at laying mechanism, these two ropes are connected singularly to both parts of scissor-shaped bridge, see Figure 2.
- Winch rope
- Opening rope

The ropes obviously can only pull the bridge parts. Then, for pushing the bridge parts and for supporting the ropes, there are two mechanisms installed, see Figure 2 and Figure 3:
- Bolster
- Mast

AM-50 crews experience troubles with actuating ropes within all the bridge laying operation and vice-versa during the loading operation along similar trajectories [1]. Difficulties with actuating ropes cause unwanted delays, which decreases tactical and operational capability of the mobile bridge. The ropes require proper leading, especially in the phases when approaching or leaving particular pulleys. In these phases the laying and loading operations must be interrupted often from different reasons:
- Manual corrections of the rope positions in pulleys and winch drum
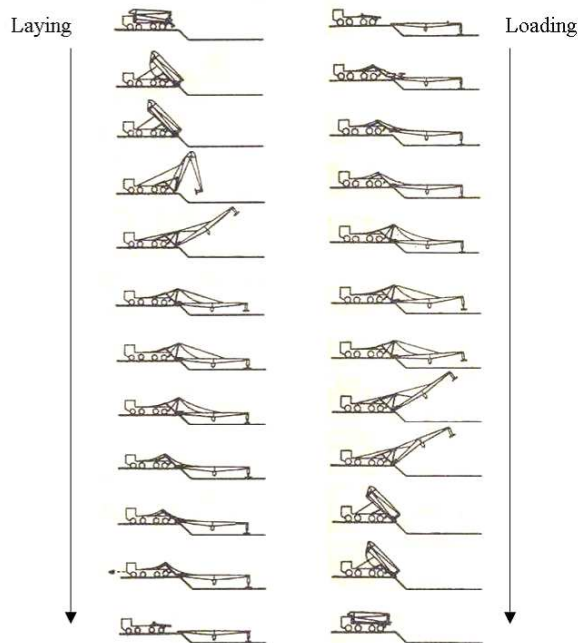- Elimination of unwanted oscillation of the bridge and truck

Fig. 1. Run of the laying and loading operations of the AM-50 truck-launched bridge.

2.1. Bolster-Ropes Cooperation

After the AM-50 or AM70 truck-launched bridge is established in the starting position for laying operation, the bolster tilt can begin.
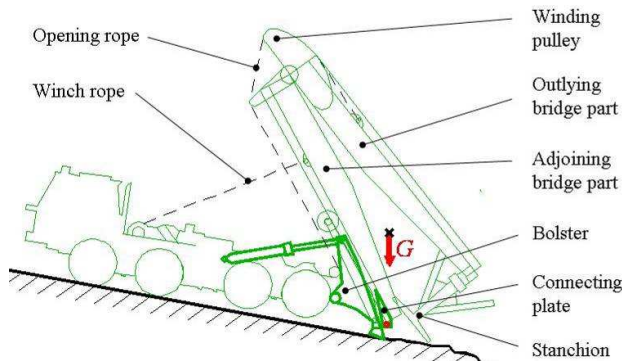

Fig. 2. Main parts and possible bridge gravity axis layout at the end of bolster tilt.

The bolster, actuated by a pair of hydraulic pistons, lifts the bridge up from the truck. At the end of the bolster tilt – see Figure 2 – the bolster bottom touches the ground to provide a stabilization support for next bridge operations above the obstacle.

The opening rope should slacken in this phase, to keep the bridge closed.

The winch rope unreeling must be coordinated with bolster tilt, because the winch has two antagonistic roles here:

- At the start of the bolster tilt – winch pull unwanted – to let the bolster to lift the bridge. The winch also must not rip the bridge out from the connecting plate. To avoid ripping the bridge from the connecting plate, there is an interlock at the new AM70.

▪ At the end of the bolster tilt – winch pull needed – to keep the bridge leaned on the bolster. In the case of slacken winch rope, the bridge could fall from the bolster to the obstacle (and twitch the slacken winch rope) either because of wind, or because of its gravity forces layout, see Figure 2. This effect is highlighted at AM70 with much heavier bridge stanchion than at AM-50.

2.2. Mast-Ropes Cooperation

After the bolster bottom touches the ground to provide a stabilazation, the opening rope must tighten and then the mast-winch cooperation can begin.
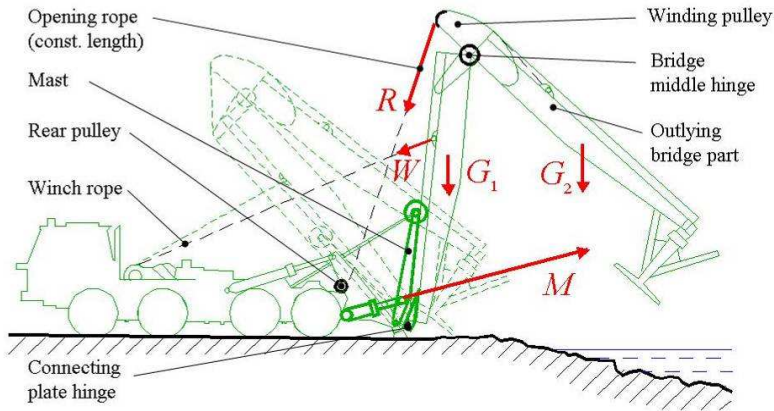
Fig. 3. Main parts, bridge self-opening parallelogram and forces layout within the mast raise.

The mast, actuated by a hydraulic piston, pushes the bridge from the bolster to the position above the obstacle, see Figure 3.

The opening rope actuator is stopped in this phase, but the parallelogram kinematics cause the bridge self-opening and it keeps approximately constant slope of the outlying bridge part during the mast raise. [2] Force R in the opening rope is given by the balance at the bridge middle hinge axis – mostly by the gravity of outlying bridge part with stanchion G_2. Due to opening parallelogram, the force R increases the needed force M in the mast piston. This effect is highlighted at AM70, because its stanchion "got weight" more than bridge parts, comparing AM-50.

The winch rope unreeling follow the mast raise, to avoid the bridge fall into the obstacle. So, there is need of a „tug-of-war" between the mast and both ropes (balance at the connecting plate hinge axis), even when the bridge gravity axis is positioned above the obstacle. This „tug-of-war" causes excessive stress of mast and winch. This problem is highlighted at AM-50 by needless mast overbrake and overheats of the hydraulic fluid, because there is no remote control of secondary pressure relief valve in the AM-50 mast circuit.

2.3. Ropes Cooperation

After the mast is raised at its full range, see Figure 3, the opening rope and winch rope cooperation starts. The bridge parts just hang on both ropes in this phase, without push of any other mechanism, see Figure 4.

The opening rope starts reeling, in order to open fully the bridge. Force R in the opening rope is given by the balance at the bridge middle hinge axis – mostly by the gravity of outlying bridge part with stanchion.

The winch continues unreeling, in order to lower the bridge. Force W in the winch rope is given by the balance at the connecting plate hinge.
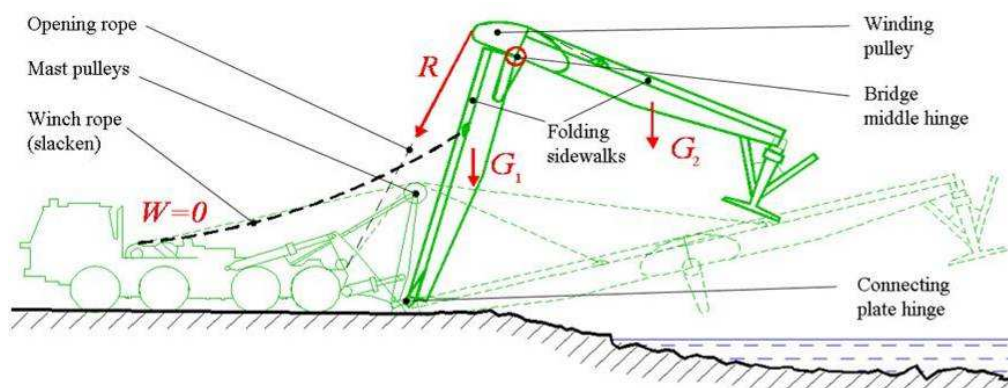
Fig. 4. Main parts and trouble with the winch rope slacken within cooperation with the opening rope.

Due to opening parallelogram, the force W in the winch rope is decreased by the force R in the opening rope. This effect can even cause the winch rope slacken; see Figure 4, which is unwanted but often at AM-50. [2] In such situation the bridge become uncontrollable, because continued reeling of opening rope causes not intended lowering and opening (around the bridge middle hinge), but just unwanted lift of the bridge (around the connecting plate hinge). Then the operator has to reverse – unreel the opening rope, to get sufficient force W in the winch rope, and finish the bridge manipulation with lower stanchion trajectory above the obstacle. This unwanted effect is highlighted at AM-50 with mechanical self-folding sidewalks, which raise passive resistance against the bridge opening and closing as well.

Both the winch rope and opening rope are approaching their supporting mast pulleys subsequently in this phase, and the opening rope leaves its winding pulley in the bridge, see Figure 4. Ropes approaching and leaving pulleys cause significant dynamic effects, even oscillation of whole machine including the truck on the bolster bottom. These troubles are highlighted at AM-50 with simple on-off control of the hydraulic actuation.

3.   Conclusion

Most of described difficulties during laying and loading operations are caused by funicular actuation of both parts of the scissor-shaped mobile bridge. When keeping this outmoded AM-50 conception, the new AM70 hydraulic drive should deal with these inherited disadvantages. Then, there is need for sophisticated master-slave control of hydraulic pressure and flow rates in partial circuits of the cooperating mechanisms. Utilization of modern proportional valves and advanced electronics give a good chance.

Acknowledgement

References

[1] KROULÍK, J. *Innovation suggestion at fluid-powered engineer machinery. 1st International Scientific and Technological Conference Special Technology*, Slovak Republic, 2006, p. 274-279. ISBN 80-8075-128-5.

[2] KROULÍK, J. *Gravity forces compensation on the engineer vehicles. Proceedings of the International Scientific Conference on Ground Forces Weaponry and Equipment*. Slovak Republic, 2004, p. 130-135. ISBN 80-8040-248-5.

Hydraulic Control System with a Pressure Transmitter

*Kulpa Jakub

*University of Technology, Faculty of Center for Laser Technologies of metals 25-314 Kielce, Poland,
jakub-kulpa@wp.pl

Abstract. This paper presents the results of a project focused on building a special laboratory stand presenting capabilities and tasks which can be realized by a hydro-electric pressure switch.

The first stage of the project aimed at designing the system. First of all, a didactic stand was provisionally planned and several project calculations were done in order to select appropriate elements and their parameters. Then, a simulation was performed with the use of FluidSim Hydraulics programme by Festo. This application allowed to check the assumed conception of the system's operation.

The second stage of the project was connected with making the didactic stand. In the first place the process of controlling the system by the control panel was checked. This way of controlling is easy and convenient for the operator. Next, the pressure transmitter was added to the system. With the appropriate adjustment of the switching pressure, the return stroke of the cylinder was realized automatically.

The research shows that it is possible to control actuator pressure by hydro-electric switch pressure.

Keywords: switch; hydraulics, pressure.

1. Introduction

1.1. Working rules of hydro-electric transmitter

The main task of pressure transmitter is to switch on and off the electric circuit by micro-switch. It is done by pressure change in the hydraulic circuit depending on inputted value of the pressure of the switch. Pressure transmitters are mostly used to control valve or the process for example: emergency stop (engine emer. Stop). These pressure transmitters can signalize the state of connection through optical (LED diode) or acoustics (bell) signals.
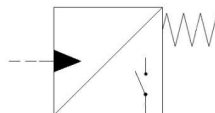

Fig. 1.   Symbol of the hydro-electric pressure switch.

1.2. Construction of hydro-electric pressure switch

Piston pressure switch

Hydro-electric pressure switch showed in Fig. 2, is a piston pressure switch. If the pressure to be monitored is lower than the set value, the micro-switch (5) is operated. The pressure to be monitored is applied via orifice (7) to piston (2). Piston (2) is supported on spring plate (6) and acts against the infinitely variable force of compression spring (3). Spring

plate (6) transmits the movement of piston (2) to micro-switch (5) and releases the latter when the set pressure is reached. This switches the electrical circuit on or off depending on the circuitry.

The mechanical limit stop of spring plate (6) protects micro-switch (5) against mechanical destruction in the event of a sudden pressure drop and, in the event of overpressure, prevents compression spring (3) from hitting the block.
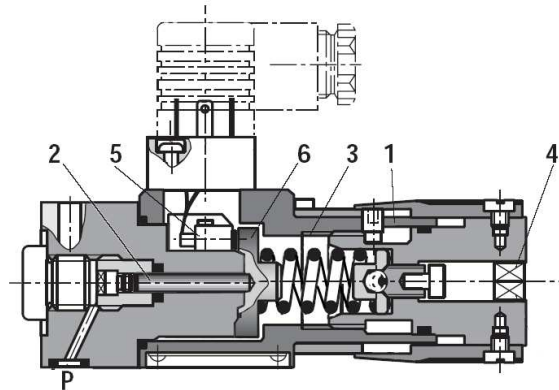

Fig. 2. Hydro-electric pressure switch of type HED8.1 – housing; 2 – piston; 3 – compression spring; 4 –adjustment element; 5 – micro-switch; 6 – spring plate; [1]

Transmitters with a spring tube

There is a transmitter with spring tube in fig.3. Increasing pressure which flows through a damping tube connected by **a** quick coupling (4) sealed by a gasket (8) works on the spring tube (2) making its strain. When the pressure reaches the adjusted value, the spring tube initiates the lever of the micro-switch.
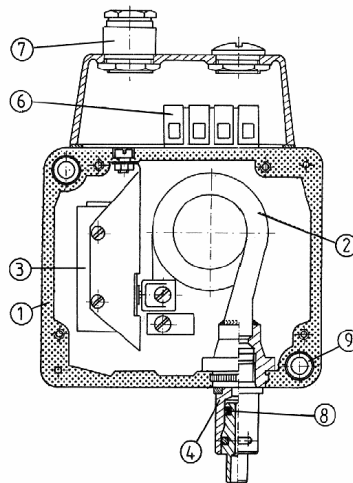
Fig.3. Hydro-electric pressure switch of type HED 2: 1 – housing; 2 – bourdon tube; 3 – micro-switch; 4 – quick coupling; 6 – terminal board; 8 –gasket; 9 – absorber; [2]

2. Analysis and results investigation

In the first part of the research a circuit with actuator controlled by steering desk was checked. This steering process was done by a proper adjustment of directional valve. In the initial position of that valve, oil is pumped to the right chamber of the actuator (the piston is blocked). After turning on the electrical circuit, the valve's solenoid is provided with voltage, which causes switching a directional valve. The valve will go back to its initial position when there is no voltage on the solenoid.

In the second part the pressure transmitter was added. This transmitter controls the return of the actuator in the pressure function. There are three different states which depend on the switching pressure adjusted to the transmitter:

1. When the switching pressure on the transmitter is set on a minimal value, the piston of the actuator is not moving, because the pressure value in the source chamber of the actuator has reached the adjusted value on the transmitter. This pressure was created by a friction of piston needed to start moving.

2. When the switching pressure on the transmitter is set on nearly the same value of the pressure, the piston of the actuator will go back to its initial position automatically. The piston will only return when it reaches its final position, because mechanical limits of expansion makes the pressure in the source chamber of the actuator reaches the pressure value of the source.

3. When the pressure value on the transmitter is larger than the pressure of the source, the piston does not return automatically, because the pressure in the source chamber of the actuator is lower than the switching pressure value set on the transmitter.
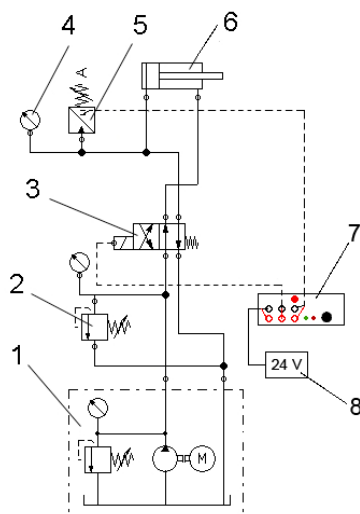

Fig.4. Circuit diagram: 1 – pump unit; 2 –pressure relief valve; 3 – directional valve; 4 - manometer ; 5 – pressure transmitter; 6 - actuator; 7 – steering desk; 8 –power supply adapter 24V
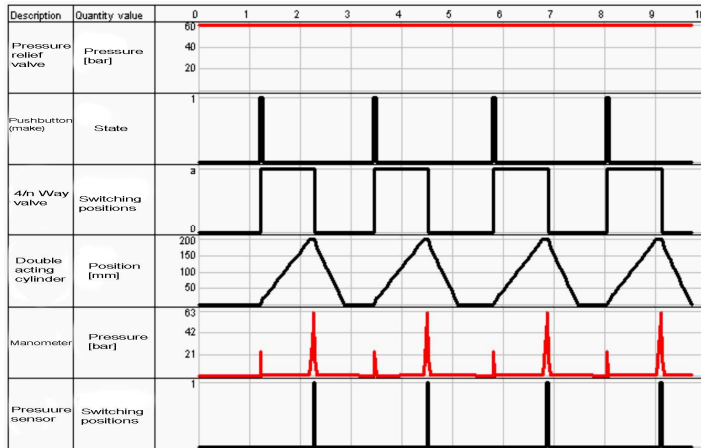
The state diagram of the circuit is presented in fig. 5.

Fig.5. State diagram.

3. Conclusion

Transmitters may be applied in hydraulic circuits in many ways. They can be used to control circuits, regulate forces, or as emergency switches. Regulating forces of the surface pressure may be done by adjusting the switching pressure on the transmitter. This force depends not only the pressure value of the source but also on the switching value of the pressure set on the transmitter.

References

[1]   MANNESMANN REXROTH. *Projektowanie i konstruowanie układów hydraulicznych . C*ompany catalogue

[2]   PONAR WADOWICE. Company catalogue

[3]   DINDORF R.. *Modelowanie i symulacja nieliniowych układów regulacji napędów płynowych*. 1st ed. Kielce: Politechnika Świętokrzyska, 2004. ISSN 0239-4979

[4]   KULPA J. *Projekt i wykonanie hydraulicznego układu sterowania z przekaźnikiem ciśnienia.* Uniw. masters thesis, head: Ryszard Dindorf

The Influence of Friction on Results of the Impact Four-Point Bend Tests

Paweł Łabędzki

Kielce University of Technology, Faculty of Mechatronics and Machine Building, Chair of Machine Design Basics, Al. Tysiąclecia Państwa Polskiego 7, 25-314 Kielce, Poland, pawlab@tu.kielce.pl

Abstract. Finite element analysis was used to investigate the influence of the Coulomb friction on the results of the impact four-point bend tests. A simple formula for quasi-static part of the dynamic stress intensity factor (DSIF) was derived taking into account the friction. It was shown that friction leads to increasing of forces on strikers and on supports, their quasi-static components behaved similarly. Opposite conclusion was drawn for DSIF and its quasi-static component, which decreased with friction.

Keywords: the impact four-point bend test, friction, dynamic stress intensity factor.

1. Introduction

Friction practically does not influence the results of quasi-static four point bend (4PB) tests, because specimen slides along the rolling strikers, supports. The strikers and supports are fixed during an impact 4PB test, so the friction could have much influence on the test results in this case. The influence of friction on the results of impact three-point bend (3PB) tests was investigated by Rokach [1]. The 4PB case is slightly different, at least because there is also some friction between the strikers and specimen. In this study influence of friction on results of the impact 4PB test is investigated in similar way. First, formula for quasi-static component of the dynamic stress intensity factor (DSIF) is derived taking into account friction, then there are presented results of finite element (FE) simulations of impact 4PB tests conducted for various specimens and various coefficients of friction (CoF).

2. Quasi-static part of the dynamic stress intensity factor

After some transition period the quasi-static component of DSIF become dominant. When crack starts to grow sufficiently late, quasi-static methods of the dynamic fracture toughness evaluation could be used. This makes computation of the quasi-static part of DSIF an important task.

When the force on striker F increase monotonically, the strikers slides along the specimen surface in the direction of the center section of the specimen, for monotonically increasing force on support R, the supports slides along the specimen surface in the direction of the specimen ends, so, for monotonically increasing forces F, R, the friction forces F_t, R_t act as it is shown in Figure 1a. The quasi-static 4PB test with friction in zones strikers/specimen and supports/specimen could be decomposed into three simple cases of loading: frictionless 4PB and two cases of loading presented in Figure 1. c,d.

The supports and strikers spans, considered in this paper, were the same as in experiment reported by Böhme [2]: $S_R=4W$, $S_F=W$, where W is specimen width (see Figure 1a). Formulas presented in this section were derived for such spans.
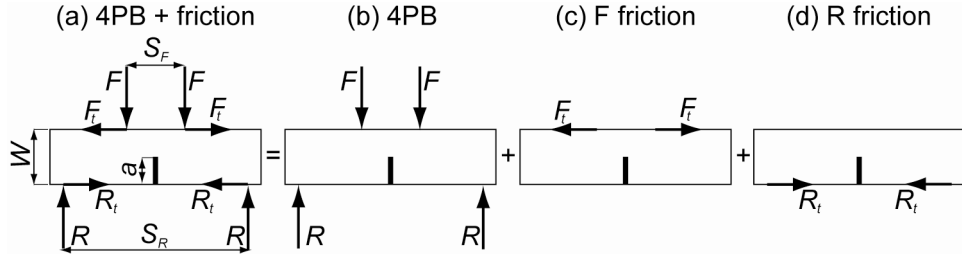
Fig. 1. The decomposition of the quasi-static 4PB test with friction in zones specimen/strikers and specimen/supports into simple cases of loading.

A standard formula for the stress intensity factor (SIF) for 4PB from [3] was used. The formulas for SIF for loading cases presented in Figure 1c,d were obtained by fitting of the results of FE analysis. They had the same form:

$$K_I^i = \frac{P}{B\sqrt{W}} Z_i(\lambda), \ i = F, R, \tag{1}$$

where $\lambda = a/W$ is the relative crack length, Z_F, Z_R are dimensionless functions:

$$Z_F(\lambda) = 1.145 + 0.313\lambda + 2.701\lambda^2, \tag{2}$$

$$Z_R(\lambda) = 18.391 - 152.973\lambda + 584.965\lambda^2 - 925.102\lambda^3 + 586.643\lambda^4. \tag{3}$$

The accuracy of formulas (1) for $0.3 \leq \lambda \leq 0.7$ is better than *1%*.

The influence of friction on SIF for increasing friction forces F, R is obvious: additional loads F_t, R_t try to close the crack, so the SIF would be smaller than in frictionless case. If F and R decrease, the influence of friction is opposite. The above could by written as one formula using *sign* function (f – CoF):

$$K_I = K_I^{4PB} - f \cdot \left(sign(\dot{F})K_I^R + sign(\dot{F})K_I^F\right), \tag{4}$$

where the dots denoted the derivatives with respect to time, equilibrium condition $R=F$ was used.

For the displacement-controlled test forces have to done more work to achieve the same displacement as in the frictionless test. Therefore, force on striker F_f is greater than in frictionless test F (see also Fig. 2 and Fig. 3). The correction factor could be evaluated using virtual displacement principle in similar way as it was done in [1]:

$$F_f = \frac{F}{1 - f(\alpha + \beta)}, \tag{5}$$

where $\alpha = \delta_F/\delta$, $\beta = \delta_R/\delta$, δ, δ_F are the normal and tangent displacements of the point on specimen surface where striker hit, δ_R is the tangent displacement of the point on specimen surface where the specimen touch the support. The approximation for $\varphi = \alpha + \beta$ was found by fitting of the results of the FE analysis:

$$\phi(\lambda) = 0.474 + 0.183\lambda + 0.057\lambda^2, \tag{6}$$

the accuracy of this formula is better than 1%. The formula (4) with force (5) allow to compute SIF for 4PB with friction for given load level.

3. The results of FE simulations of impact 4PB tests

The interaction between the specimen and supports, strikers is more complex during impact 4PB tests. Forces on the striker and on support $F(t)$, $R(t)$ vary quite fast, so there are frequent changes in the directions of friction forces, in addition there are also periods when the strikers and/or supports are stuck to the specimen.

Direct FE simulations were conducted for impact and quasi-static 4PB tests, commercial FE software ADINA 8.4.1 was used. The following set of parameters was considered: $L/W=4.1, 4.2, …, 6$, $a/W=0.3, 0.4, …, 0.7$, $f =0, 0.1, …, 0.8$. Other test parameters, used in simulations, were the same as in experiment reported in [2]. The plots, presented here, are in dimensionless scales with dimensionless time: $\tau=t(E\rho)^{1/2}/W$ (E, ρ are the Young modulus and density of specimen material, respectively, v is an impact velocity without unit, B is the specimen thickness).
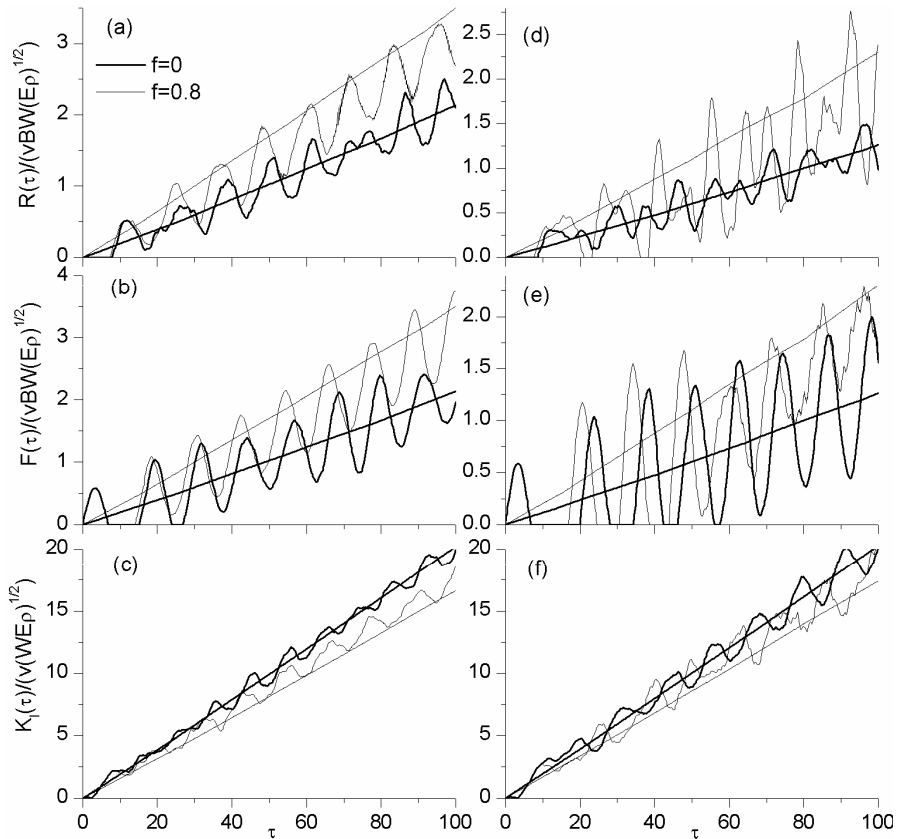
Fig. 2. The results of quasi-static and impact 4PB tests for *L/W=4.1* and *a/W=0.3* (a)-(c), *a/W=0.5* (d)-(f) (straight lines represent results of quasi-static FE simulations).

It was noted that the proportionality between friction and normal forces is violated frequently due to the sticking between specimen and strikers, supports and changes of the direction of friction forces. This affect the values of forces on strikers and supports, which oscillate around values less than their quasi-static components (see Figs. 2, 3).

It was observed that friction between strikers and specimen does not influence much test results. The Figs. 2, 3 shown that friction increase the quasi-static components and amplitude of loads and decrease DSIF and its quasi-static component.
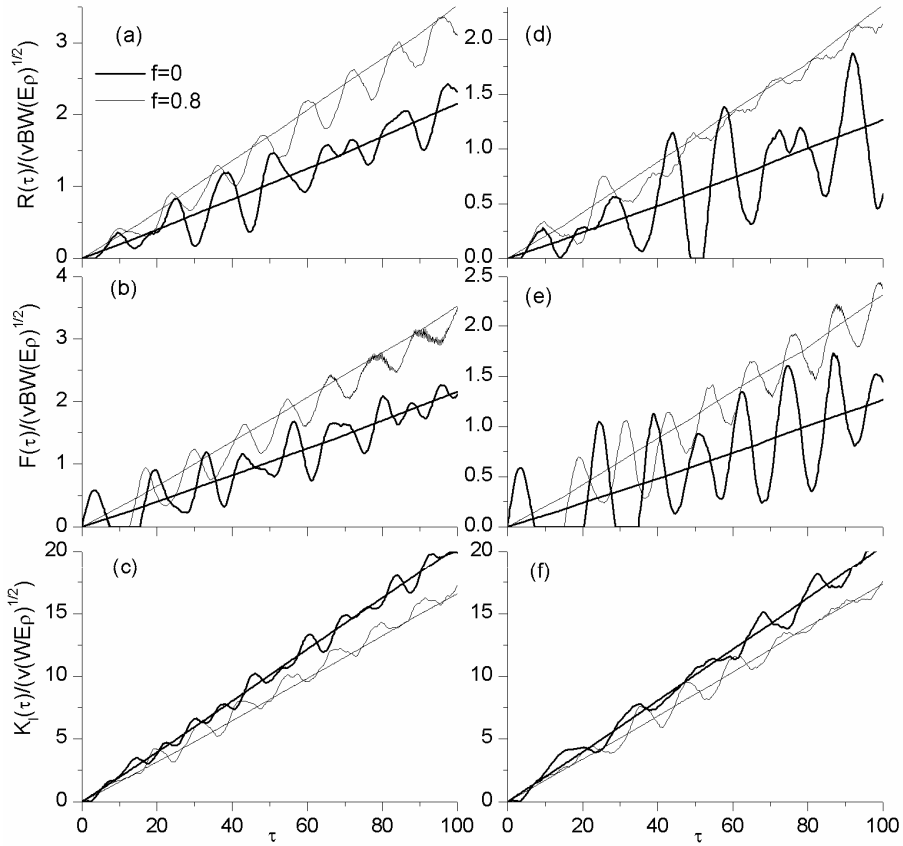
Fig. 3. The results of quasi-static and impact 4PB tests for *L/W=5.5* and *a/W=0.3* (a)-(c), *a/W=0.5* (d)-(f) (straight lines represent results of quasi-static FE simulations).

It was also noted that formula (4) agree well with the result of the FE simulations of the quasi-static 4PB test.

4. Conclusions

Friction between specimen and strikers, supports increase the forces on strikers and supports and decrease the DSIF. Simple formula for quasi-static part of DSIF for impact 4PB test with friction was derived and good accuracy with FE was achieved was achieved.

References

[1] ROKACH, I.V. *Influence of friction on results of an impact fracture test*, Archive of Mechanical Engineering, 51(3):377-389, 2004

[2] BÖHME, W. *Experimentelle Untersuchungen zum invertierten Kerbschlagbiegeversuch und fur dynamischen Wechselwirkung von Mehrfachrissen*, Wissenschaftlicher Bericht W 1, 1987

[3] MURAKAMI, Y. *Stress Intensity factors handbook*, Pergamon Press, 1986

Combustion of Alternative Fuels

[*]Ján Lábaj, [*]Marek Patsch, [**]Dalibor Bárta
[*]University of Žilina, Faculty of Mechanical Engineering, Department of Power Engineering,
Univerzitna 2, 01026 Žilina, Slovakia
[**]University of Žilina, Faculty of Mechanical Engineering, Department of Automotive Technology,
Univerzitna 2, 010 26 Žilina, Slovakia

Abstract. In this contribution there are analyses of the course of the pressure curves, which were measured in the diesel engine MD UR IV. The results of the analyses confront the properties and quality of fuels. The measuring was realized with a constant rotation speed of the engine and by using different fuels. The fuels were diesel fuels with additives of hydrogenate RO, FAME, and ethanol.

Keywords: Pressure curves, FFT analyses of pressure data, diesel fuel, hydrogenate RO, FAME, and ethanol

1. Introduction

Most useful information about the diesel combustion process can be obtained by the measurement and analysis of the cylinder pressure. Specifically, the indicated mean effective pressure and the apparent heat release rate can be computed. Other quantities such as the peak pressure and the peak rate of the pressure rise are also useful as the indicators of the overall stress and noise levels, respectively.

A crucial factor for pressure measurement in the engine during combustion is the sensor position within the combustion chamber. The pressure sensor type is of secondary importance; at most, the cavities between the combustion chamber and the sensor may influence the measuring signal.

A central measuring position in the combustion chamber is ideal for the pressure measurement because it does not register any adverse effects on the pressure signal. Therefore it is recommended for an accurate measurement of the combustion cycle.

Cylinder pressure data usually require smoothing before they can be used for analyses. This smoothing can be accomplished by averaging a large number of consecutive cycles, polynomial smoothing, curved line smoothing, or digital filtering.

2. Analysis of cylinder pressure data

Indicator diagram of combustion engine

We can know the real work cycle of the combustion engine only by the measurement of the course of the pressure in the combustion chamber. The process is called engine's indication. The result of the measurement is an indicator diagram in p - V co-ordinates. The indicator diagram will be shown in a rolled out form, dependent on the pressure and angle of the crank shaft.

Ignition delay

The ignition delay is defined as the time period between the start of fuel injection and the start of combustion (it is found from changes of tendency curve $p - \alpha$ diagram, or from curve of heat release rate, eventually by using luminescent detector). As described earlier, the fuel must vaporize, mix with air, and undergo preflame reactions before auto-ignition occurs.

The ignition delay shows itself by a mild fall of the pressure in $p - \alpha$ diagram, which is due to the evaporation of the injected fuel. The size of the ignition delay affects markedly the peak rate of the pressure rise. The bigger the ignition delay is, the higher the peak rate of the pressure rise (that means the slope of the pressure increase in the combustion chamber) the engine has, so we try to use fuels with a short ignition delay. The fuel chemical structure is also important because the cetane number is a property of the fuel that indicates the fuel's readiness to autoignite. Fuels with high cetane numbers have short ignition delays. The time period depends on the cetane number of the fuel but also on the temperature of the compressed air because it accelerates the vaporization and the radical-forming preflame reactions.

The peak rate of the pressure rise

The peak rate of the pressure rise is defined as the pressure rise in the engine's cylinder per one degree of crankshaft rotation $dp/d\alpha$. Its value changes during combustion depending on the heat release rate.
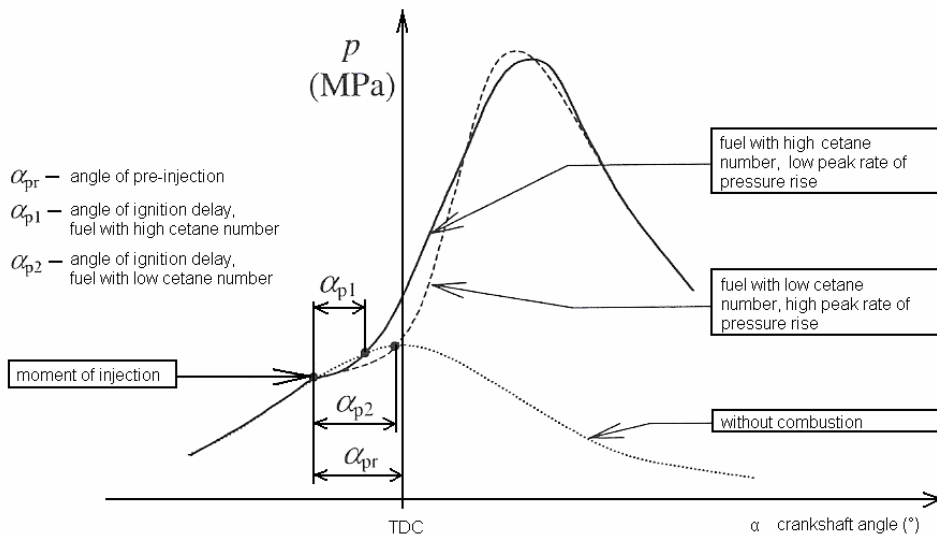
Fig.1. Effect of cetane number of diesel fuel (TDC – top dead center)

The figure 1 shows the course of the combustion pressure p vs. crankshaft angle, the influence of the cetane number on the peak rate of the pressure rise and on the ignition delay.

3. Used measurement technique

The accurate measurement of the cylinder pressure requires three things:
- a pressure transducer that can survive the engine environment,
- means for synchronizing the pressure measurements with the engine,
- means for recording the pressure measurements.

Cylinder pressure sensor

Modern pressure transducers are piezoelectric devices that use quartz crystals (silicon dioxide - SiO_2) to produce electric charges when mechanically loaded.

The piezoelectric pressure sensor **Kistler type 6302A** was used for the measurement of the combustion pressure**.** It is a small cylinder pressure sensor in the probe configuration; it is designed for a permanent operation in combustion engines where there is a minimum amount of space available.

This type of sensor requires the use of a protecting case for its installation. The protecting case has a connecting bore between the combustion chamber and the membrane of the sensor. The case of the sensor has to separate the sensor and water space in the cylinder head, and protect the membrane of the sensor.

Charge amplifier

We had to use a charge amplifier because the electric charge produced by the pressure sensor was rather faint. We used a series-connected charge amplifier **Kistler type 5029A.**

Crank angle encoder

Crank angle encoder allows synchronizing of the pressure measurements with the engine; it is directly coupled to the engine crankshaft.

We used the crankshaft position sensor **Kistler type 2613B** for the measurement. It consists of a crank angle encoder, signal conditioner, and line terminator. This device contains a precision marker disk with a trigger mark, and 360 angle marks which are scanned by a transmission photoelectric cell. Their light intensity is regulated in order to compensate for any soiling. The disk and the photoelectric cell are encased in dustproof housing.

Recording device

We used the charge meter **Kistler type 5015A** for the measurement. It is a universal charge meter with an LCD display; it is suitable for measurements in an industrial environment. It can display instantaneous, peak and average values as well as reference deviations.
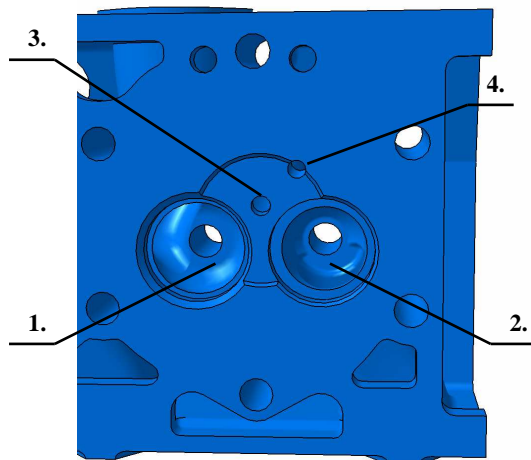
Diesel engine

We used the diesel engine **MD UR IV 8004.000** for the measurement of the combustion pressure. It is a four-stroke, turbocharged four-cylinder-in-line engine with an OHV actuating gear and direct fuel injection. The engine has liquid cooling and it is turbocharged without the intercooler of compressed air. The engine was loaded by the dynamometer MEZ Vsetin DS 1002-4/V.

Fig.2. The final solution of the pressure sensor mounting
1. Inlet
2. Outlet
3. Hole for fuel injector
4. Hole for pressure sensor

Measurement scheme

The first cylinder was chosen for the measurement of the combustion pressure because its environment offered enough space for mounting of the sensor.

The most useful placement of the sensor, its installation into the central position in the combustion chamber, was not possible because cylinder head did not offer enough space in this position. Therefore, we had to find another placement which was as close as possible to the ideal position so that the connecting bore of protecting case would eventuate into the toroid combustion chamber in the engine's piston. The second requirement was as little impairment of the resistance of the cylinder head construction as possible. Figure 2 shows the final solution of the mounting.

The protecting case and water space in the cylinder head were sealed with engine silicone. The crank angle encoder was mounted onto the crankshaft pulley, which was on the free end of the crankshaft. The measurement scheme and connection of the measurement technique are shown in figure 3.
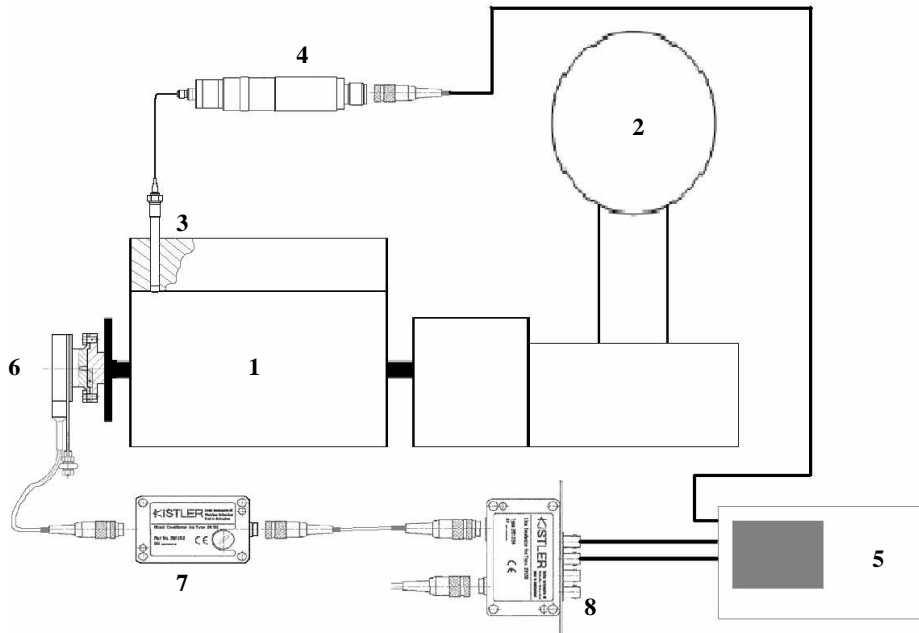
Fig. 3.   Measurement scheme
1. Diesel engine MD UR IV 8004.000
2. Dynamometer MEZ Vsetin DS 1002-4/V
3. Pressure sensor Kistler type 6302A
4. Charge amplifier Kistler type 5029A
5. Recording device Kistler type 5015A
Crank angle encoder:
6. Crank angle encoder with 6-hole flange
7. Signal conditioner
8. Line terminator

4.   Measurement results and interpretation

Measuring was realized in the diesel engine MD UR IV with the constant rotation speed 2200 min^{-1}, at the same time we measured the engine power characteristics and exhaust gas

composition, which was not the object of this thesis. In the first evaluation of the measuring, we observed the slope of the pressure curve and an ignition delay when we used different fuels. We did not use smoothing; subsequently we had to use running average to smooth the signal. An example of the measured data is shown in figure 4 for fuel 1. More advanced methods of analyses contain Fourier transformation of signal (FFT) which converts signal into phase and frequency spectrum. There are specific areas and different types of combustion processes in this spectrum:

1. Frequencies 30 to 1000 Hz describe the peak rate of the pressure rise. The bigger the decrease of the curve in db/octave is in this area, the softer the peak rate of the pressure rise is.
2. Frequencies 1 kHz to 6 kHz describe proper oscillations of the combustion chamber and combustion noise, which are the images of the character of the combustion process. Abnormal combustion shows itself in this area. High-level frequencies 3 kHz to 6 kHz present knock combustion at engines with applied ignition. Very hard combustion can show in frequencies 1 kHz to 3 kHz, we call it dieseling at engines with applied ignition and rumbling at diesel engines.

The frequency spectrum is shown in logarithmic co-ordinates of signal proportions in dB mV, not as the energy density. There was zero as the reference level of the pressure; it was 220 dB, in graphs of FFT analyses for transfer into dB of the acoustic pressure.

Tested fuels:

Fuel 1: Diesel fuel NM-3HD820-1335
Fuel 2: 95 % of diesel fuel NM-3HD820-1335 + 5 % of Hydrogenate RO
Fuel 3: 94 % of diesel fuel NM-3HD820-1335 + 1 % of Hydrogenate RO + 5 % FAME
Fuel 4: 93 % of diesel fuel NM-3HD820-1335 + 2 % of Ethanol + 5 % of FAME
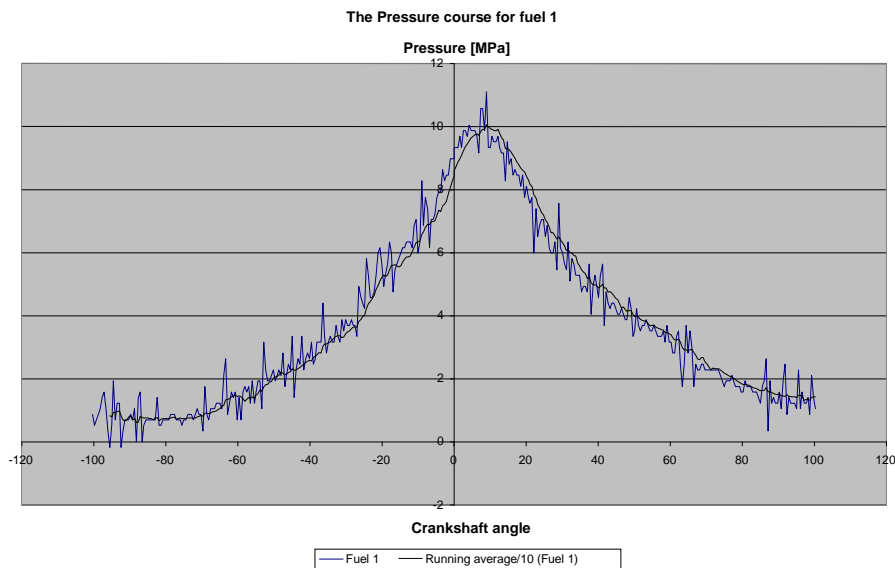Fuel 5: 90 % of diesel fuel NM-3HD820-1335 + 3 % of Ethanol + 7 % of FAME

Fig. 4 The pressure course in dependence on the crankshaft angle and smoothing curve for fuel 1.

Fuel 1: The fuel was a classic diesel fuel with the cetane number 50. It was used as the reference fuel. Figure 5 shows the time behavior of the signal. The engine had a sizable peak rate of the pressure rise with this fuel, which is shown in the slope of the curve in figure 6.

Oscillations of the combustion chamber were shown in the area from 1 kHz to higher frequencies. The unfiltered signal is shown in figure 5.
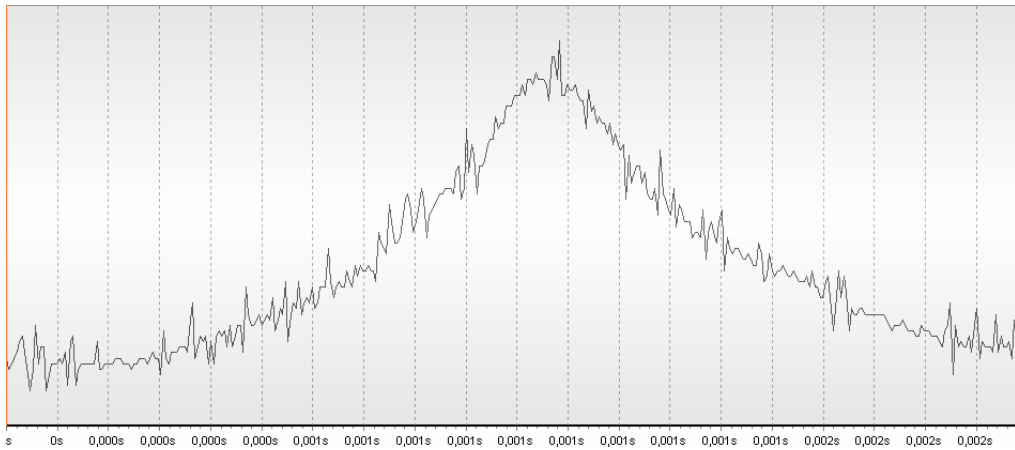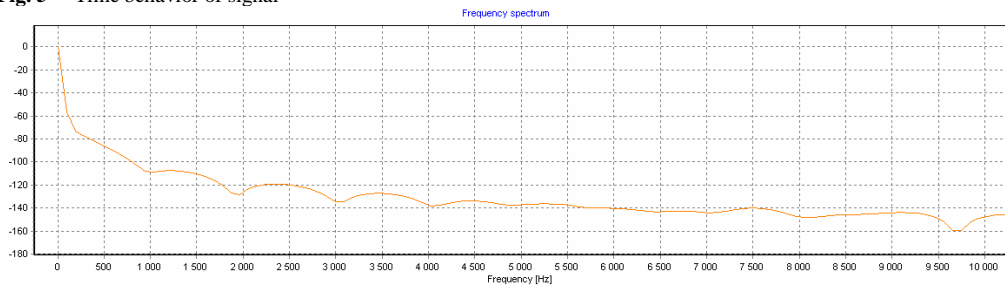

Fig. 5 Time behavior of signal

Fig. 6 FFT analysis of signal

<u>Fuel 2:</u> The engine was running very softly with this fuel. It is apparent from the sudden fall of the curve in figure 8. The combustion process was not much vibrant. It caused a quiet combustion noise and a silent running of the engine. This fuel was the best of all the tested fuels.
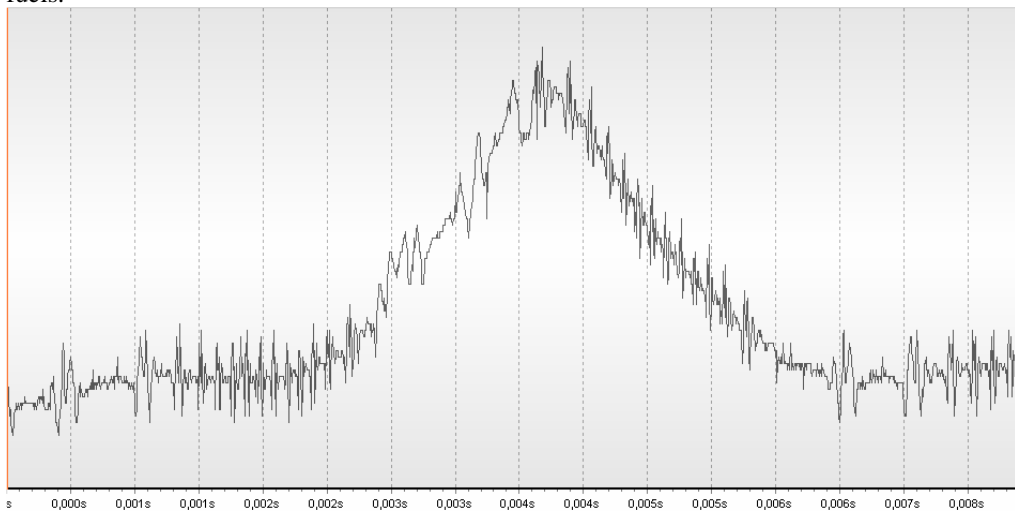
Fig. 7 Time behavior of signal

72
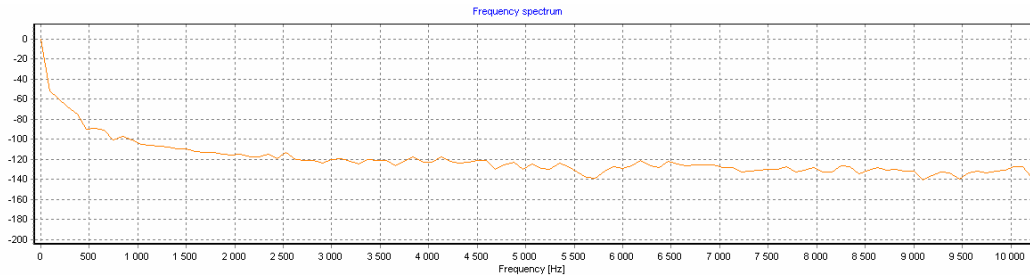
Fig. 8 FFT analysis of signal

Fuel 3: With this fuel, the engine had a similar peak rate of the pressure rise like with fuel 1, but it had a vibrant course of the combustion process throughout the monitored area. It caused a noisier engine running with bigger combustion beats.
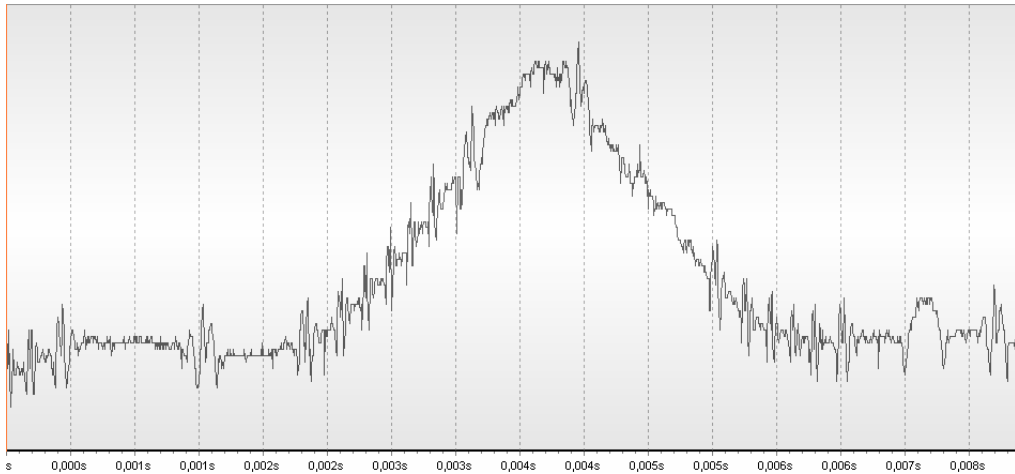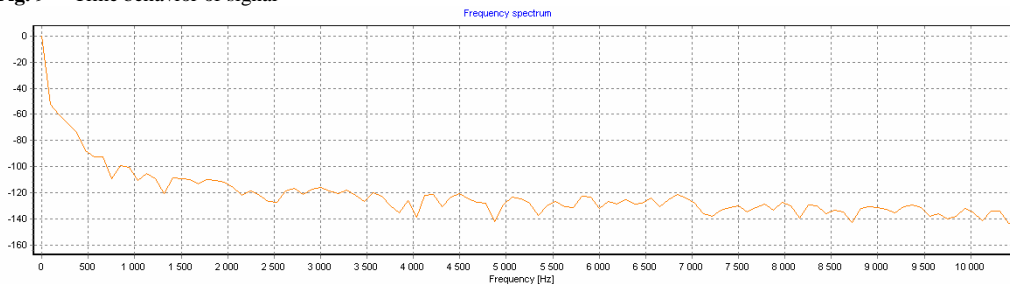

Fig. 9 Time behavior of signal

Fig. 10 FFT analysis of signal

Fuel 4: With this fuel, the engine running had a similar course like with fuel 3, but it showed a very expressive oscillation character of the combustion process which was observed in figure 12 as an expressive unsteadiness of the curve course in the full frequency area from 1 kHz.
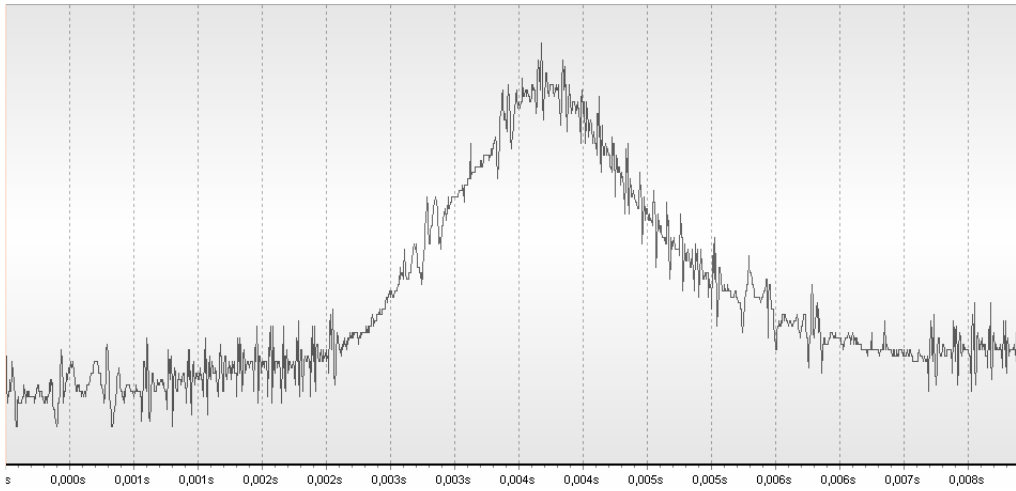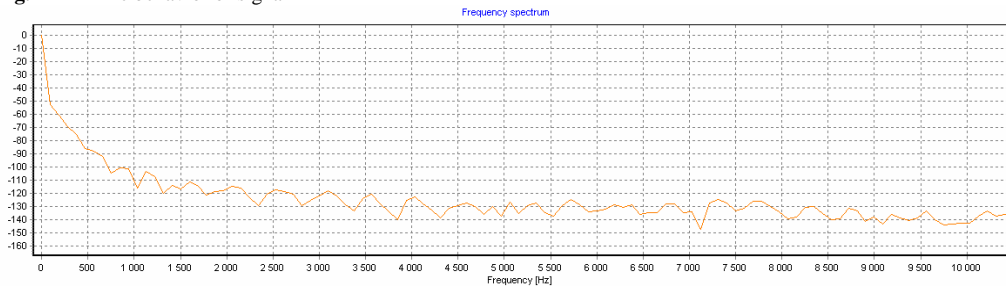
73

Fig. 11 Time behavior of signal

Fig. 12 FFT analysis of signal

Fuel 5: The engine had a hard running with this fuel. It had a stabilized course of combustion. It was caused by adding ethanol into the diesel fuel. Ethanol evaporates quickly and it burns with a kinetic flame with a quick combustion process. A stabilized course stresses the engine less.
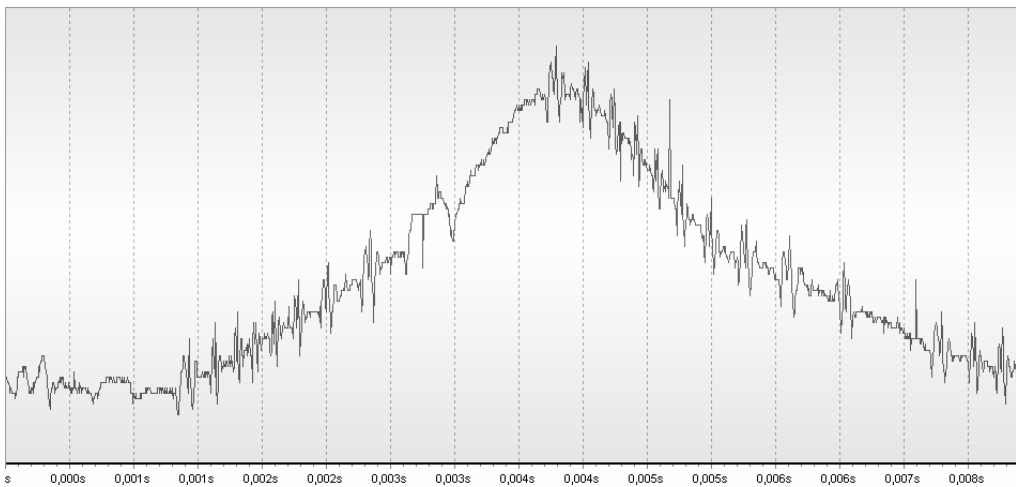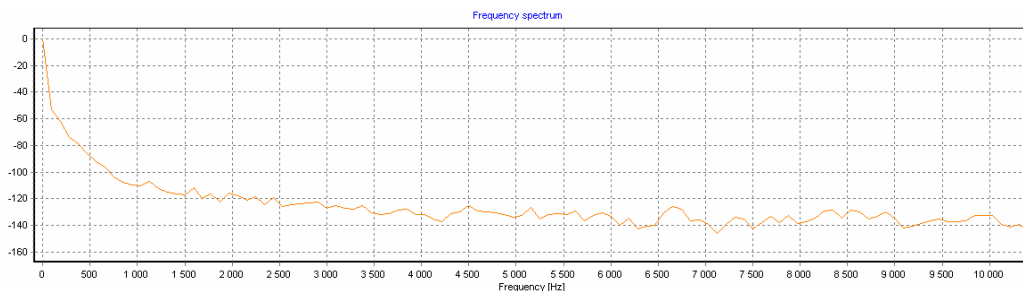

Fig. 13 Time behavior of signal

Fig. 14   FFT analysis of signal

Conclusions

The most favourable fuel is fuel 2 as resulted from the measurement. A very soft and silent running of the engine was secured by adding hydrogenate RO into the diesel fuel. Adding other components into the fuel changed the combustion process, which resulted in the unsteadiness of the course of the pressure curves.

Acknowledgement

References

[1]   MARTIN DIESEL, a.s.: *Technická dokumentácia motora MD UR IV 8004.000*.

[2]   KALINČÁK, D., GERLICI, J., KUKUČA, P., LÁBAJ, J., LACK, T., POLÁCH, O., SÁGA, M.: *Dopravný prostriedok výpočtové metódy*, Žilinská univerzita v Žiline, EDIS, 2005.

[3]   ISTENÍK, R., LABUDA, R., HLAVŇA, V., KUKUČA, P., SOJČÁK, D., BARTA, D., LÁBAJ, J.: *Spaľovacie motory riešené príklady*, Žilinská univerzita v Žiline, EDIS, 2005.

[4]   CHALLEN, B., BARANESCU, R.: *Diesel Engine Reference Book*, Second edition, Butterwort Heinemann, Oxford, 1999.

[5]   KISTLER INSTRUMENTE AG: *Pressure Indication during Knocking Conditions*, Kistler Instrumente AG, Winterthur, Switzerland, 2006.

[6]   KISTLER INSTRUMENTE AG: *Application of an Improved Model for the Determination of Acoustic Resonances in Indicator Passages for Combustion Pressure Measurements in Large Bore Gas Engines*, Kistler Instrumente AG, Winterthur, Switzerland, 2007.

[7]   GROSSWEILER, CH., WILLSON, B., WALTER, T.: *Application of an Improved Indicator Passage Correction Model for Combustion Pressure Measurement*, Aachen, 2006.

[8]   HLAVŇA, V., KUKUČA, P., ISTENÍK, R., LABUDA, R., LIŠČÁK, Š.: *Dopravný prostriedok jeho motor*, Žilinská univerzita v Žiline, EDIS, 2007.

[9]   HEYWOOD, J. B.: *Internal Combustion Engine Fundamentals*, McGraw-Hill, Inc., New York, 1988

[10] LÁBAJ, J.: *Spaľovanie a plameň*, Knižné centrum v Žiline pre Vedeckotechnickú spoločnosť pri Žilinskej univerzite, 2002.

[11] MATĚJOVSKÝ, V.: *Automobilová paliva*, Grada Publishing, a.s., Praha, 2005.

[12] KOŽOUŠEK, J.: *Výpočet a konstrukce spalovacích motorů I*, SNTL – Nakladatelství technické literatury, Praha, 1978.

[13] TRNKA, J., URBAN, J.: *Spaľovacie motory*, Vydavateľstvo Alfa, Bratislava, 1992.

[14] KISTLER INSTRUMENTE AG: *Technical documentation of pressure sensor, type 6302A*.

[15] KISTLER INSTRUMENTE AG: *Technical documentation of charge amplifier, type 5029A*.

[16] KISTLER INSTRUMENTE AG: *Technical documentation of charge meter, type 5015A*.

[17] KISTLER INSTRUMENTE AG: *Technical documentation of crank angle encoder, type 2613B*.

Numerical Modeling of Passive Roof Cooling Convectors

[*]Richard Lenhard, [*]Jozef Jandačka

[*] University of Zilina, Mechanical engineering, Department of power engineering, Univerzitná 8215/1, 010 26 Žilina ; {richard.lenhard, jozef.jandacka}@fstroj.uniza.sk.

Abstract: The article describes mathematic model of boundary conductance with natural convection by the passive cooling convectors. It is determinable criterion equations. Mathematic model was used for simulation of these convectors kinds with change his geometric proportion and CFD model was make simulation of these convectors kinds and subsequent alteration was comparator from mathematic model. Mathematic methods sets on final volume (CFD method) showed like very acceptable on optimalization passive cooling convectors.

Keywords: CFD model, passive cooling convectors

1.   Introduction

Passive roof convector for cooling characterized in that unused for cooling active part for inlet air on difference from active roof convectors. For this reason passive roof convector for cooling are characterized would-be „quiet cooling". They don't generate secondary space flowing.

Fig.1.0 Passive roof cooling convector

1.1.   Method of operation passive roof cooling convector

The passive roof cooling convector is actually a ribs pipe heat exchanger in which cooling water runs. The convector is set under the roof but a minimum length must be half of width of the convector. A warm air in the top part of the convector is being cooled, it is being fell naturally.

2. Mathematics simulations

In mathematical simulations was changed only geometric proportion passive roof cooling convector and it ribs distance, tube diameter for stabilize input conditions $t_{11}=16°C$, $t_{21}=26°C$ from change water mass flow when was stabilized head drop on 16/19°C for find out maximal power.

A. Simulation with change rib distance s_r:

For stabilized heat drop on 16/19°C with change rib distance and change water mass flow achieved maximum power 675,505 W form rib distance 3,5 mm.

s_r [mm]	m_v [kg.s^{-1}]	Q [kW]	t_{12} [°C]	t_{22} [°C]	v_{vz} [m.s^{-1}]
3,5	0,053	0,675	19,004	23,36	0,253
4,5	0,041	0,525	19,003	23,673	0,223
5,5	0,033	0,429	19,004	23,897	0,202
6,5	0,028	0,362	19,006	24,067	0,185
7,5	0,025	0,314	19,009	24,202	0,172

Tab. 1.
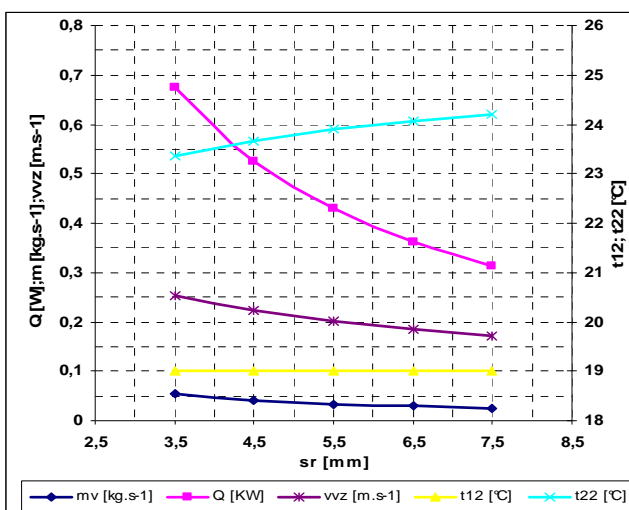

Fig. 1.

B. Simulation with change pipe diameter d_1:

For stabilized heat drop on 16/19°C with change rib distance and change water mass flow achieved maximum power 447,33 W for used pipe diameter 12 mm.

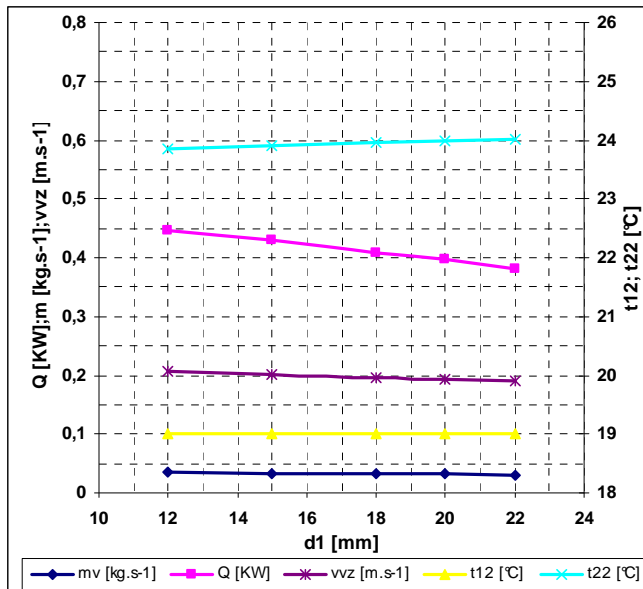| d_1 [mm]	m_v [kg.s^{-1}]	Q [kW]	t_{12} [°C]	t_{22} [°C]	v_{vz} [m.s^{-1}]
12	0,035	0,448	19,02	23,853	0,206
15	0,034	0,429	19,004	23,897	0,202
18	0,032	0,409	19,007	23,946	0,197
20	0,031	0,396	18,996	23,979	0,194
22	0,030	0,382	19,003	24,015	0,190

Tab. 2.

Fig. 2.

In simulations A and B was change (rib distance, pipe diameter), where for each one geometric changes was found out heat drop 16/19°C from change water mass flow when was stabilized head drop on 16/19°C for find out maximal power. Maximum power achieved 675,505 W form rib distance 3,5 mm.

3. CFD simulation

Flow modeling in passive roof cooling convector was made in program Fluent and Gambit which sets boundary condition which are first good step for correct calculation.

3.1. CFD model passive roof cooling convector (with cover)

On pic.3.1-3.2 is 5 ribs CFD – model passive roof cooling convector (with cover) on which was made simulations and results with this model was compared with mathematical model.

Input conditions:
For input condition are sets real geometric sizes except for his length regardless of on performance used computer where for 5 ribs model is number of cells more than 1,7 millions. The whole model without space would have 100 millions cells considering on performance used computer can not to be computed.

- Turbulent model: k - ε;
- Input: velocity - inlet;
- Output: pressure - outlet;
- Aluminium rib: solid;
- Water in pipe: wall with sets temperature;
- Cuprum tube convector: thickness wall and shell conduction;
- Gravitational acceleration 9,81 m.s^{-1}.

On fig. 3.1-3.2 is CFD – model (with cover) in cut. Calculation was solving method final volume: space, fluid flow cross, is separate on final parts small volume. For each volume is calculate transport mass, momentum and energy where can see velocity air flow, which range around 0,22 m.s⁻¹.

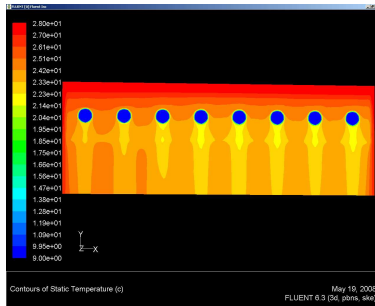## 3.2. CFD model passive roof cooling convector (with cover)in space

Fig. 3.1 CFD – model passive roof cooling convector, temperature profile.
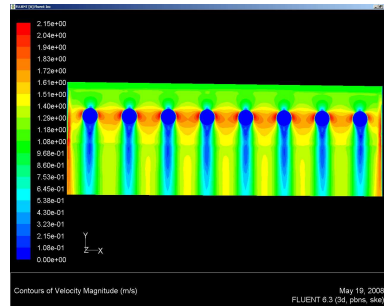

Fig. 3.2 CFD – model passive roof cooling convector, velocity profile.

Input conditions:

For input condition are sets real geometric sizes except for his length regardless of on performance used computer where for 5 ribs model is number of cells 3,5 millions (1000 iterations – 24 hours). The whole model would have 200 millions cells considering on performance used computer can not to be computed.

- Turbulent model k - ε - RNG;
- Input and output to do convector is interior;
- Aluminium rib: solid;
- Water in pipe: wall with sets temperature;
- Cuprum tube convector: thickness wall and shell conduction;
- Gravitational acceleration 9,81 m.s⁻¹.

On fig. 3.3 - 3.8 is see cut CFD – model with cover and add volume in determinate steps calculation where can watch flow air what can't watch in to model without space. Result are velocity and temperature profile.
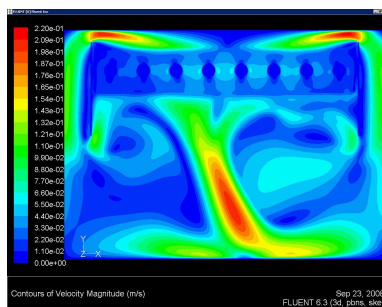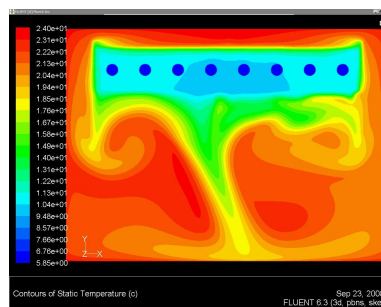

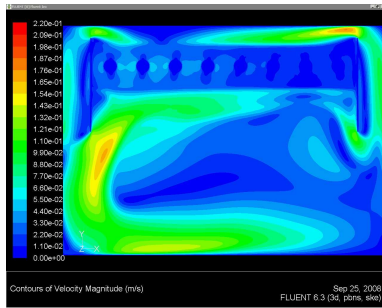**Fig. 3.3** CFD – model 12100 iteration

Fig. 3.4 CFD – model 12100 iteration

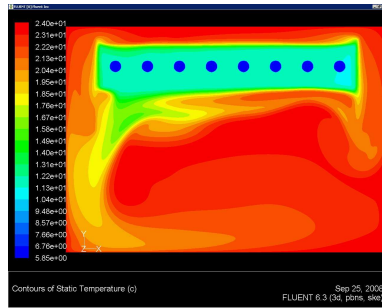**Fig. 3.5** CFD – model 31500 iteration   **Fig. 3.6** CFD – model 31500 iteration
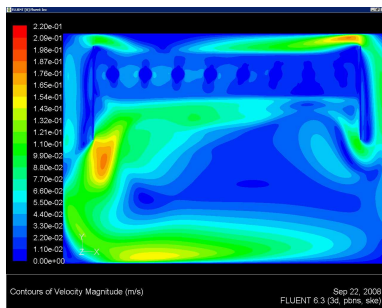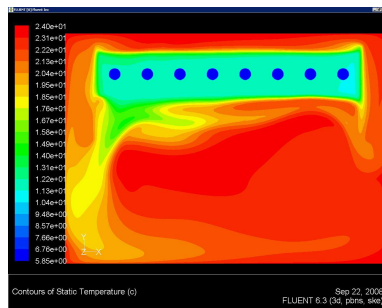

Fig. 3.7 CFD – model 50100 iteration   **Fig. 3.8** CFD – model 50100 iteration

On fig. 3.5 - 3.8 is seen not come up in large changes movement flowing base on this result is possible state are model is stable and can be consider for calculate to the end.

4. Evaluate results

Comparison real device with model crated in Excel on base origin geometric size for reason find out correct mathematic model. In tab. 3 are data measured and computed value for comparison accuracy.

For verifying a result from mathematic model is necessary makes numerical simulation if given results are in the equality and if this mathematic model is consider for correct.

Type model	$\dot{m}_V$ [kg.s^{-1}]	Q [kW]	t_{11}[°C]	t_{12}[°C]	t_{21}[°C]	t_{22}[°C]	$\dot{m}_{VZ}$ [kg.s^{-1}]
Fluent	0	0,0191	9	9	28	27	0,018
Fluent/Excel	0,0044	0,0193	9	10,044	28	26,865	0,017
Type model	$\dot{m}_V$ [kg.s^{-1}]	Q [kW]	t_{11}[°C]	t_{12}[°C]	t_{21}[°C]	t_{22}[°C]	$\dot{m}_{VZ}$ [kg.s^{-1}]
Real	0,037	0,3675	16	18,1	25,1	24	0,5-2,2
Real/Excel	0,036	0,3676	16	18,44	25	23,99	0,361

Tab. 3.

By simulations was determinate power passive roof cooling convector and on the base given results can make optimization this devices for achieve increase power.

Comparison results from models we can use criteria equation for modeling this type of convector.

Acknowledgement

References

[1] LENHARD, R., JANDAČKA, J., ČAJA, A.: *Matematické simulácie pri zmene geometrických rozmerov u pasívneho stropného chladiaceho konvektora.* XVI. Medzinárodná vedecká konferencia - Aplikácia experimentálnych a numerických metód v mechanike tekutín. Žilina 2008, ISBN 978-80-8070-826-9

[2] LENHARD, R., JANDAČKA, J.: *Numerické modelovanie pasívneho stropného chladiaceho konvektora*, Colloquium FLUID DYNAMICS 2008 Institute of Thermomechanics AS CR, v.v.i., Prague 2008, ISBN 978-80-87012-14-7

[3] JANDAČKA, J., MALCHO, M. A KOL:. *Meranie a vyhodnotenie chladiacich výkonov pasívnych chladiacich konvektorov*. Žilina 2006

Monitoring of Vehicle Parameters by CMMS

[*] Jana Lorincová, [*]Roman Poprocký, [*]Vladimír Stuchlý

[*]University of Žilina, Faculty of Mechanical Engineering, Department of Transport and Handling Technology, Univerzitná 1, 01026 Žilina, Slovakia, {jana.lorincova, roman.poprocky,vladimir.stuchly}@fstroj.uniza.sk

Abstract. The article offers an overview of the changes of monitoring parameters for a traction vehicle (TV) with the help of CMMS, specifically with the help of the information system (IS) datastream 7i. The single parts contain the description of the implementation of the system of the TV's repairs into the IS, the system of preventive maintenance and the definition of predictive maintenance – on an example of measuring the height of a roadband on a TV – the change of a parameter is defined and evaluated.

Keywords: maintenance, information system, traction vehicle, maintenance system.

1. Introduction

In the present time a broad scale of software products for operation support and maintenance planning exist and is used in the world.

A CMMS software package maintains a computer database of information about an organization's maintenance operations. This information is intended to help maintenance workers do their jobs more effectively (for example, determining which storerooms contain the spare parts they need) and to help management make informed decisions (for example, calculating the cost of maintenance for each piece of equipment used by the organization, possibly leading to better allocation of resources).

I will use the IS datastream 7i for the monitoring of the vehicle's parameters.

1.1. Implementation of the TV's repairs system into the IS

An essential part of the implementation of the TV's repairs system into the information system is the creation of a structure from the input data – the definition of the device's structure, employees, professions and changes. Every single from these parts must have – for the transparency and simplification of the work – its own code and description, yet contains more additional information.

As an example I will present the TV series 162, on which I will monitor the parameters that are needed for the reference of preventive maintenance and also parameters for predictive maintenance. Fig. 1 shows a part of a hierarchy structure created with the help of the IQ-Fmea software and a part of a structure created in the IS d7i Fig. 2.
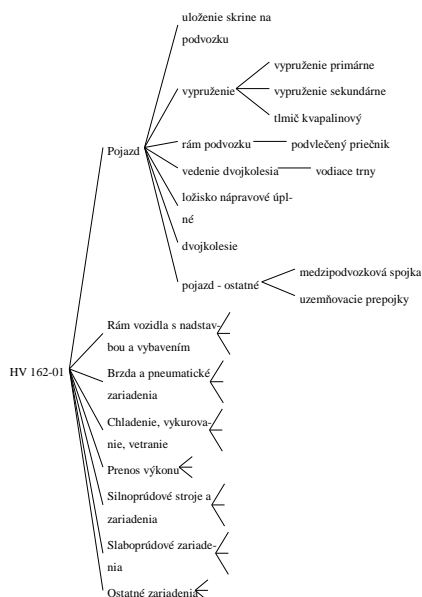
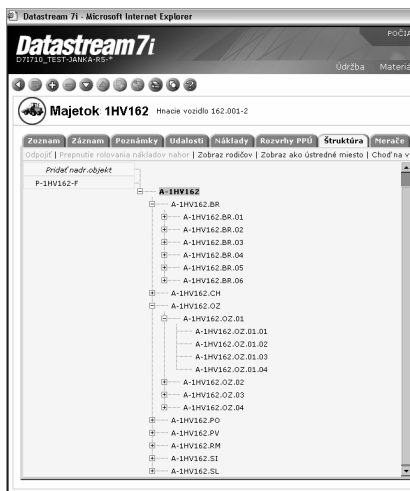**Fig. 1.** Part of the hierarchy structure created in IQ-Fmea software.

Fig. 2. Structure created in the IS d7i.

1.2. Preventive maintenance system

The technical eligibility of TVs in operation is secured through maintenance. TVs have defined a preventive maintenance system.

The determining index is the cycle of repairs defined as maintenance cycle. A TV has the maintenance cycle determined by mileage run, which is monitored with the help of a logical meter, that is installed for each device (every object individually).

If a TV achieves the limit of the mileage (for the TV series 162 it's 4.500 km that are necessary for carrying-out the service), the IS will warn of released jobs that contain activities which are necessary to carry-out within the scope of preventive maintenance.

The scope and content of the activities for the TV series 162 is defined in the work standard almanac. In the d7i system it contains a database of all maintenance interventions that

are carried-out when servicing the TV whereby every activity has a number of employees assigned which are divided according to their qualification grade and professions.
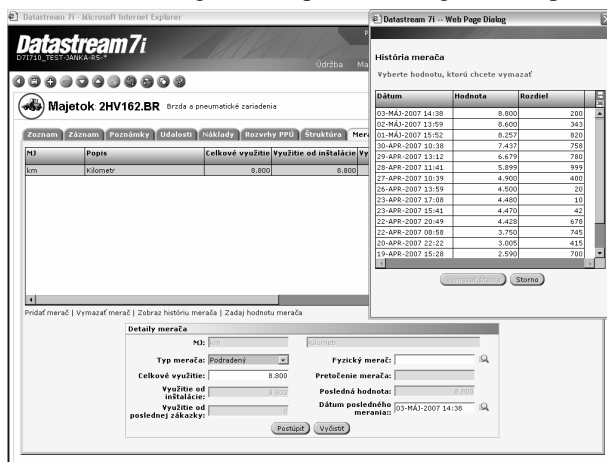

Fig. 3. Surveyors.

After planning and carrying-out the job an hours-per-employee entry is done and the job is closed.

1.3. Definition of predictive maintenance

In this case the maintenance action is carried-out after determining the real technical condition of the object by any of the technical diagnostics method and calculation of the time during which the object will probably without a breakdown.

We will have a closer look on this system of maintenance on the example of wearing out the roadband of the TV series 162. On the roadband is a check carried-out during which the height, thickness and the steepness are measured as shown on Fig. 4 the spots for the check are identical and on every wheel the measurement is carried-out once.
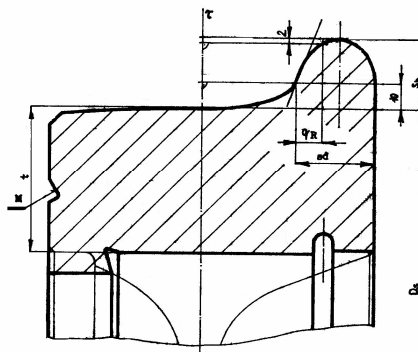

Fig. 4. Measured values on the rim's profile.

The check monitors and records the technical shape of the object and consists of the following steps:
- release of the job for PPM depending on the surveyor or another value:
  - carrying-out the PPM – for every object,
  - determining of the inspection procedure,
  - defining the spots of the check;

- carrying-out the check and recording values,
- generating of the job if a limit has been exceeded,
- standard job – contains activities necessary to recover the original condition.

Every object on which the check is carried out has defined its nominal value, maximal extreme and maximal criticalness in Fig. 5. It is also possible to show the content of the measurements and approximate a time estimate to the next check with a connection to a standard job that contains activities for removing the unwanted condition.

Fig. 5. Defining values.

Based on the excess of the value from the surveyor a PPM job that contains a check will be generated. This job contains activities necessary for carrying-out the inspection and the planned evaluation time. After these activities are done, the results of the measurement will be recorded and the job will be assigned as finished.

In case, that the measured value exceeds the maximum criticalness or reaches maximal extreme, a job based on the standard job will be automatically generated (contains activities necessary for removing the unwanted condition and the following return to the nominal values).

2.   Conclusion

If a MIS is used for operation support, it has to be capable to record all the necessary data about machines and equipment but also provide records for operative maintenance control and system analysis. The right choice and application of an appropriate maintenance information system supports the effectiveness of the maintenance which means optimization of the maintenance costs, cutting loses from drop-outs, failures and breakdowns of equipment as well as optimization of stock levels and purchase management and in the end affects the economy of the enterprise.

References

[1]   DATASTREAM 7i, *Documentation for users*.

[2]   LORINCOVÁ J., *Information system and effective maintenance (In Slovak: Informačný systém a efektívna údržba,* diploma work, Žilina, 2007

Development of the Autonomous Mobile 3D Laser Scanning System

*Milan Magdech, *Milan Gregor
*University of Žilina, Faculty of Mechanical Engineering, Department of Industrial Engineering, Univerzitná 1, 01026 Žilina, Slovakia, {Milan.Magdech, Milan.Gregor}@fstroj.uniza.sk

Abstract. This article deals with the autonomous mobile 3D laser scanning system and dividing by the scanning mode. It is here named the key problem of such a system faces in its activities and the subsequent processing of data. In the third section describes the elements of a mobile 3D Laser Scanning System and their properties with the reasons why they are necessary in the autonomous mobile 3D laser scanning system.

Keywords: 3D laser scanning, mobile robot, autonomous mobile system.

1. Introduction

In our work of the digitization we use a static laser scanner, which has wide application. We have learned through it's acquire and process data for 3D models. Now we would like to make this process of digitization has become effective, whether in cash or time. Means that we would like to achieve is the development of autonomous mobile 3D Laser Scanning System.

2. Mobile 3D laser scanning system

Uses the technology of laser scanning where the scanner is located on the mobile device, which receives from the area of 3D points. A key problem of such a system is the harmonization of spatial data with the position and orientation system. In order to create the right environment, 3D model, it is necessary that the different scans were merged into a single coordinate system. This process is called registration. If the scans have a different coordinate system leads to error. As a byproduct, successful registration of 3-D scans relocalizes the robot in 6D by providing the transformation to be applied to the robot pose estimation at the recent scan point.

Autonomous mobile 3D scanning systems can be divided into two groups. And according to the mode in which scanning takes place:

a, scanning mode "stop - scan - go"
b, mode scanning "go - scan"

3. Elements of 3D laser scanning system

The system consists of the essential elements of a mobile device, a laser scanner and the supporting technology, which record the position and orientation of the whole system such as ERSP Navigation, ERSP Vision, GPS and IMU.

3.1. Autonomous mobile device.

Autonomous mobile vehicle must be able to fulfill a specific set of demands. It moves in specified environment, gains information about it's current position and environment, processes this information and modifies it's behavior accordingly.

For the purpose of developing an autonomous mobile 3D scanning system, we decided to use the Evolution Robotics ER1 platform. ER1 is a set of features that use of technologies that are needed. Patented solutions ERSP Vision and ERSP Navigation giving robots the possibility to move independently and the ability to recognize images and objects situations.

ERSP Navigation

Allows the robot or device to be fully autonomous, move in their environment with knowledge of the location, create a map to plan an effective route to the destination point.

Main features:
- vSLAM (Visual Simultanous Localization and Mapping) is a set of navigation features that allow localization and mapping using camera and roller encoders as sensors. The system itself generates a map, which consists landmarks, which generates the robot during exploration environment. Each point is composed of identifiable images recorded from each position. One of the most important skills vSLAM allows the robot to recover after the transferred to another location,
- path planning, this module allows the user to select a target position and request a list of items, which have brought the robot safely,
- voiding obstacles, allows the robot to detect obstacles and continuously develop local routes to avoid them, which ensures the safe movement of robots,
- the survey, property survey allows the robot to move safely in an unknown environment,
- grid deployment represents two-dimensional map of the robot environment using precision grid, which model the occupied and empty space environment[12].

ERSP Vision

It allows the robot or device to identify 2D and 3D objects in real terms, the lighting and the location of the object is not checked. Vision functions provide access to extremely efficient algorithms of computer vision. These algorithms able to analyze images from the camera and know how to extract information from them, which can be used for different tasks.

Evolution Robotics ER1 platform is compiled from available parts in different ways. We have chosen to compile in the form of the chassis, as can be seen in the figure[12].

Fig. 1. Chassis Evolution robotics platform ER1.

In coincidence developing a tracked chassis. Tracks are better suited for uneven terrain The vehicle can be used both outdoors and indoors. Smaller front tracks were added in order to give the vehicle stairway climbing ability. This can be crucial in some applications.

Platform is driven by two electric motors. They are powerful enough to move it in 45 degree climb. This is useful when a movement through some natural or artificial barriers is required. The negatives of track based approach are higher power drain and less precise movement [11].

Fig. 2. Chassis Tracked chassis.

Another type of mobile device that you can use the car. In our case, a car Wolksvagen Touareg, this mobile platform 3D Scanning system need to be supplemented by additional devices, and GPS IMU.

3.2. Laser scanner

We can use two types of scanners, 2D and 3D.
- 2D are optimized to meet the requirements for high speed scanning. The sensor mechanism is based on the rapidly rotating polygonal mirror, which creates a complete one and parallel lines. The sensor is the maximum angle of 180 °.
- 3D broadcast laser beam is made using a rotating mirror with 360 ° visual slash. There thus creating any gaps[7].

It is possible to use one or more scanners when scanning. The number of scanners is dependent on environmental conditions and Scanning.

3.3. Additional equipment

Additional equipment, namely GPS and IMU are needed especially when they are using a mobile device, which has not technology to identify the location and orientation. Such mobile devices may be a car.

GPS
Global Positioning System (GPS) can be used to determine the exact location and provide a highly accurate reference almost anywhere on Earth. Accuracy of a single GPS signal is about 5 meter. Through Differential GPS (DGPS) deviation from the true value at a radius of 10 km is centimeters and radius of 400 km is meters. Measurement of position using DGPS is a bit more complicated than in the GPS, there is a need for at least two GPS receivers. One receiver is placed at a known fixed position, which was established Geodetic measurement. This receiver is called the RS - a reference station. This station continuously take measurements of all visible satellites, pseudorange compared with the measured value (data on its location) and their differences sends its own separate channel to all users of DGPS. The DGPS receivers calculate deviations to apply the correction to the correction of the measurements.

IMU
IMU (Inertial Measurement Unit) is a major component of inertial guidance systems used in aviation, space shuttle, ships and missiles. IMU senses movement, including the type

of course and direction of movement with the assistance of the accelerometers and gyroscope. IMU detects current speed, acceleration as well as rotation and swing out. This data is then computer processed to calculate the current speed and position of the input values of speed and position. IMU system is error prone, so it is good to be combined with the already mentioned GPS.

The presence and alignment of elements of GPS and IMU is given their function in the mobile scanning system is important. Additional elements of the system are software combine geometric scanning profiles obtained with the position and orientation data and digital camera, which extends the visualization.

4. Conclusion

The aim of the article is to highlight how it is possible to increase the efficiency of the digitization process using autonomous mobile 3D Laser Scanning System. The article named the key problem, which is associated with autonomous mobile 3D laser scanning system, and also means that the problem can be solved.

Acknowledgement

References

[1] ĎURAJOVÁ, M., MAČÚŠ, P., GREGOR, M., MEDVECKÝ, Š. *Objects Digitization Using 3D Laser Scanning.* Research study, No. 008-UKaI-06.

[2] GREGOR, M., BUDZEĽ, F., ŠTEFÁNIK, A., PLINTA, D. *3D Laser scanning in Digitization of current production systems.* In: 9th IFAC Workshop on Intelligent Manufacturing Systems, Szczecin, 2008, p.137 – 144.

[3] HUNTER, G., COX, C., KREMER, J. *Development of a commercial laser scanning mobile mapping system – Streemapper.* Geomatic World, 2008.

[4] HAALA, N.,   PETERA, M., KREMERB, J., HUNTER, G. *Mobile lidar mapping for 3D point cloud collection in urban areas – a performance test.* Geomatic World, 2008.

[5] BARBER, D. M., MILLS, J.P. *Vehicle based waveform laser scanning in a coastal environment. International Archives of Photogrammetry, Remote Sensing and Spatial Information Sciences,* 6 pages. Newcastle University, UK, 2007.

[6] NUCHTER, A., LINGEMANN, K., HERTZBERG, J. *Kurt 3D a mobile robot for 3D mapping of environments.* Universität Osnabruck, 2008.

[7] RIEGL Laser Measurement Systems GmbH. Technical data, at: www.riegl.com, 2009

[8] FARO Laser Systems. Technical data, at: www.faro.com, 2009.

[9] RAJA, V., FERNANDES, K. J., *Reverse Engineering - An Industrial Perspective.* Springer-Verlag London Limited 2008.

[10] FURMANN, R., BUDZEĽ, F. *Digitalizácia výrobných hál pomocou technológie reverzného inžinierstva.* In: produktivita a Inovácie č.2, 2008, s. 11-12, ISSN 1335-5961.

[11] GREGOR, M., MAGDECH, M., MICHULEK, T. *Development of the autonomous mobile system for 3D laser scanning of large objects. In: Metody i techniki zazadzania,* Bielsko Biala 2009, pp. 109-116, ISBN978-83-60714-64-5.

[12] EVOLUTION ROBOTICS, Inc. *Getting started guide ERSP 3.0 robotic development platform.* Evolution Robotics part number MC6125, Pasadena USA, 2004.

[13] KARLSSON, N., Di BERNARDO, E., OSTROWSKI, J., GONCALVES, L., PIRJANIAN, P., MUNICH, E. M. *The vSLAM algorithm for robust localiyation and mapping.* Publishe in Proc. Of Int. Conf. on robotics and automation (ICRA) 2005.

Finite Element Method Simulation of Equal Channel Angular Pressing

[*]Richard Melicher
[*]University of Žilina, Faculty of Mechanical Engineering, Department of Applied Mechanics,
Univerzitná 1, 010 26 Žilina, Slovakia, richard.melicher@fstroj.uniza.sk

Abstract. The objective of this paper is to evaluate the accumulative effective plastic strain and effective stress induced by equal channel angular pressing (ECAP) in the aluminium workpiece. Another analyzed quantity is the pressing force acting on the workpiece after five passes in route C at room temperature using the finite element method (FEM). For this purpose two-dimensional model was developed using a plane strain condition. Created model was assumed as isothermal with frictionless condition during constant pressing speed. In one variant was also study the influence of friction condition. The deformation behaviour was studied using the commercial finite element software ADINA.

Keywords: equal channel angular pressing, finite element method, accumulative effective plastic strain, effective stress, pressing force.

1. Introduction

In recent years, bulk nanostructured materials (NSM) processed by methods of severe plastic deformation (SPD) have attracted the growing interest of specialists in material science. This interest is conditioned not only by unique physical and mechanical properties inherent to various nanostructured materials, e.g. processed by gas condensation or high energy ball milling (HEBM) with subsequent consolidation but also by several advantages of SPD materials as compared to other NSM.

Segal and co-workers developed the method of ECA pressing realizing deformation of massive billets via pure shear in the beginning of 80s. Its goal was to introduce intense plastic strain into materials without changing the cross-section area of billets. Due to that, their repeat deformation is possible. In the early 90s the method was further developed and applied as an (SPD) method for processing of structures with submicron and nanometric grain sizes.

2. Fundamental parameters in ECAP

2.1. Styles Slip systems for the different processing routes

During ECA pressing a billet is multiple pressed through a special die using an ECA facility in which the angle of intersection of two channels is usually 90°. If necessary, in the case of a hard-to-deform material, ECAP is conducted at elevated temperatures.

Since the cross-sectional area remains unchanged, the same sample may be pressed repetitively to attain exceptionally high strain. For example, the use of repetitive pressings provides an opportunity to invoke different slip systems on each consecutive pass by simply rotating the samples in different ways between the various passes.

In practice, many of the investigations of ECAP involve the use of bars with square cross-sections and dies having square channels. For these samples, it is convenient to develop processing routes in which the billets are rotated by increments of 90° between each separate pass. The same processing routes are also easily applied when the samples are in the form of rods with the circular cross-sections. During ECAP the direction and number of billet passes through the channels are very important for microstructure refinement. In papers and books the following routes of billets were considered (see Fig. 1.) [1-4]:

- route A where the sample is pressed repetitively without any rotation,
- route B_A where the sample is rotated by 90° in alternate directions between consecutive passes,
- route B_C where the sample is rotated in the same sense by 90° between each pass,
- route C where the sample is rotated by 180° between passes.

The given routes are distinguished in their shear directions at repeat passes of a billet through intersecting channels. Due to that, during ECAP a change in a spherical cell within a billet body occurs.
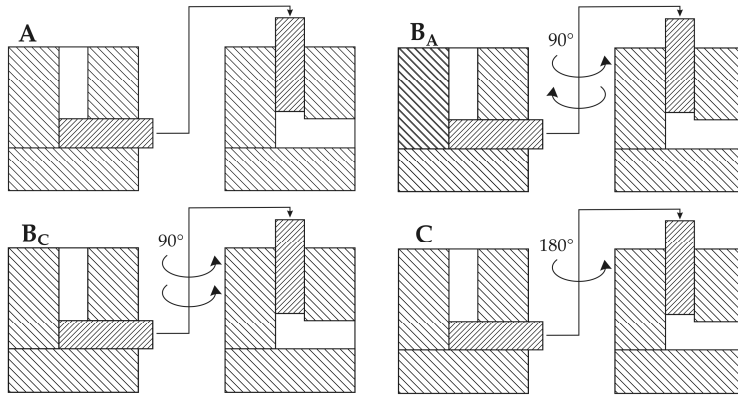

Fig. 1. The four fundamental processing routes in ECAP.

2.2. Analytical solution of the effective plastic strain

Since the same strain is accumulated in each passage through the die, the effective strain after N passes ε_N may be expressed in a general form by the relationship

$$\varepsilon_N = \frac{N}{\sqrt{3}} \left[2\cot\left(\frac{\phi}{2} + \frac{\psi}{2}\right) + \psi\,\mathrm{cosec}\left(\frac{\phi}{2} + \frac{\psi}{2}\right) \right]. \tag{1}$$

Thus, the strain may be estimated from equation (1) for any pressing condition provided the angles ϕ (value of the angle within the die between the two parts of the channel) and ψ (value of the angle at the outer arc of curvature where the channels intersect.) are known.

3. FEM simulation

Nowadays finite element method is used for simulation of technological processes increasingly. FEM simulations are helpful to estimate some correct parameters of ECAP device and pressing process such as geometry parameters, the pressing speed of the ram, pressing temperature or load displacement curve [4].

3.1. General assumptions in simulation

The FEM is used because it can provide us direct information on the evolution of plastic deformation during the ECAP and enable us to simulate the deformation of materials subjected to single or multi-pass ECAP.

In the simulation, the following assumptions are made [4]:

- First, the material is isotropic and homogeneous.
- Second, the material is elastoplastic with strain-hardening exponent being zero in order to consider the effect of elastic deformation on the morphological change of the extruded billet.
- Third, the system is isothermal.
- Fourth, the von Mises flow rule is used to construct the constitutive relation for the simulation.
- Fifth, there is no friction between the surface of the material and the die wall due to the use of lubricant in the ECAP.

4. Used FE model and simulation parameters

FEM simulation was carried out with the same geometry of workpiece. This fact led to creation of the same mesh of points that were analyzed and compared with each other. These points were chosen with respect to given workpiece geometry. Each workpiece contained 24 points with the same co-ordinates as shown in Fig. 2. Moreover, all points were organized into the four cutting planes and six levels together. These cutting planes and levels can be also seen in Fig. 2 [4].
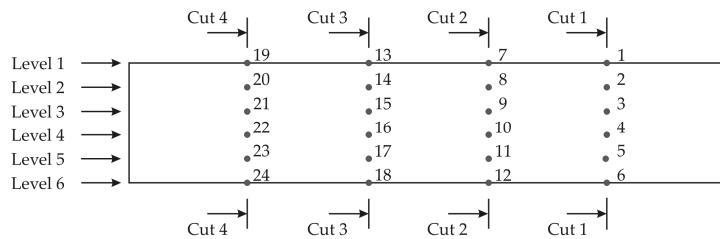

Fig. 2. Analyzed points, cut planes and levels in the workpiece
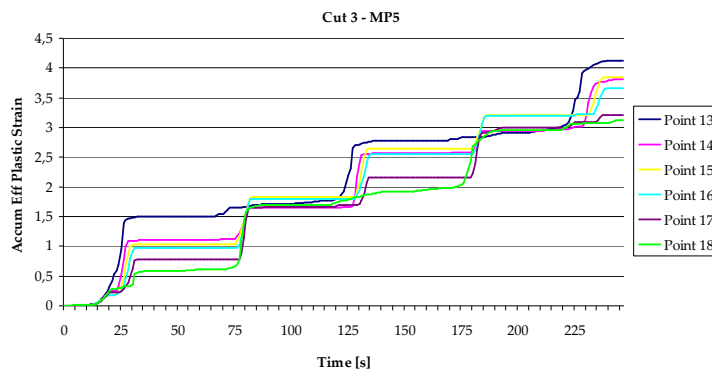
5. Results

Fig. 3. Course of accumulative effective plastic strain changes in points belong to cutting plane 3
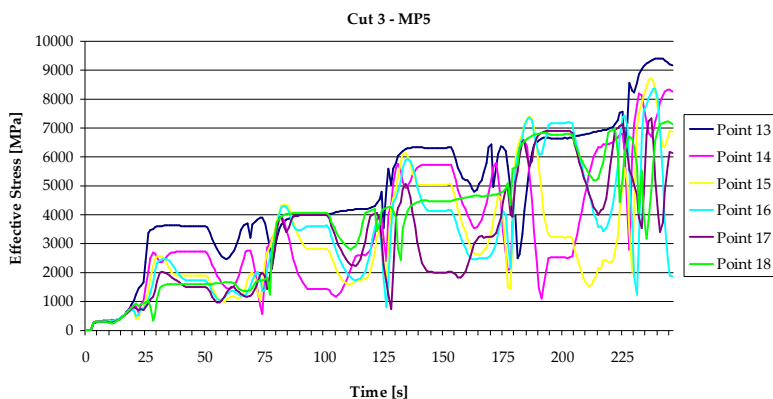
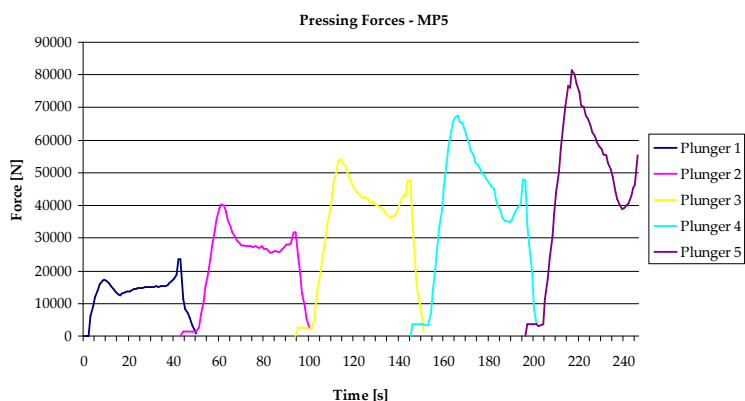**Fig. 4.** Course of effective stress changes in points belong to cutting plane 3.

Fig. 5. Pressing forces acting on the workpiece.

6. Conclusion

The precision of obtained results can be influenced by contact and its weak formulation. Another fact that can influence the results may be the discretization of solution on the finite elements. Obtained results are in good agreement with the experimental data.

References

[1] MELICHER, R., HANDRIK, M. *Analýza parametrov tvaru nástroja pre technológiu ECAP.* Optimalizácia mechanických sústav a zariadení,, Acta Mechanica Slovaca 3-C/2008, Košice, 2008, pp. 273-284, ISSN 1335-2393.

[2] MELICHER, R. *Konečnoprvková analýza plastickej deformácie hliníkovej vzorky pomocou ECAP procesu.* Nekonvenčné technológie 2008, 21/235 (2008) pp. 1-12.

[3] MELICHER, R. *Mechanické modelovanie intenzívnych objemových plastických deformácií v technológiách ECAP a ECAR.* Písomná časť dizertačnej práce, Žilina 2007.

[4] MELICHER, R. *Numerical simulation of bulk nanostructured materials processed by the method of equal channel angular pressing.* Dizertačná práca, Žilina 2008.

Emissions from the Combustion of Fast-Growing Sallow

[*] Jana Mičicová, Peter Pilát
[*] University of Žilina, Faculty of Mechanical Engineering, Department of Power Engineering,
Univerzitna 2, 01026 Žilina, Slovakia, {jana.micicova, peter.pilat}@fstroj.uniza.sk

Abstract. The article deals with emissions from the incineration of fast-growing sallow. Home is devoted to the burning wood, the fast-growing trees are discussed generally and specifically three types of sallow. Article describes the boiler for which the measurement is effected, as well as an accurate measurement procedure. At the end of the evaluation is the form of graphs.

Keywords: burning, emissions, sallow.

1. Introduction

Burning is a chemical process of rapid oxidation, which releases the chemical energy bound in the combustion of fuel for thermal energy. Chemically bound energy in the fuel is transformed into heat and the combustion additional products (combustion gas and ash). This is concerned the simplest method for the thermal conversion of organic fuels for thermal energy. Takes place in when there is a particular point in time present fuel, oxidizing agent (oxygen) and flash point. The fuel and combustion air will get heat, by which parallel combustion takes place without the energy supply of the tied environment. Combustion of wood is accompanied by the production of undesirable accompanying substances, emissions, consisting of:

- carbon monoxide
- nitrogen oxides (NOx, NO, NO2)
- particular matter (fly ash and soot)
- organic matter

Fuel quality depends on fuel moisture.

2. Sallow

Sallows are one of the fast-growing plants that are grown specifically for biomass production. The period between planting and harvest is between 2 to 5 years. They are very specific in a great variability of shapes and growth, from small shrubs through the bushes up to massive trees. These are plants with deciduous leaves, very numerous species. In Slovakia there are about 20 known species of the world total number of species from this genus is estimated about 300 to 600th.

For these purposes have been used three varieties of sallows and ULV, ORM, and Rapp, which were bred at the Research Institute for Agriculture in the Swale in Sweden.

Characteristic of varieties:

RAPP – it has got specific red-brown colour of bark one year old branches and green-brown two-year old and older branches. Wood has a denser structure with good flexibility. The bark is smooth and glossy. Osiers of this type has got good elasticity.

ORM – is a smaller increase and is characterized by leaner shape. One year old branches are beige or even orange, two-year old and older branches are yellow-green. The bark is smooth. It is suitable for the manufacture of wicker products.

ULV - the colour of the bark in one year old branches is dark red to russet, two-year old and older branches are coloured in sage-green. In the top part is more branching. In contrast the previous species, it is less flexible - it is not suitable for the production of wicker products.

3. Measurement

The measurement was made on the boiler EKOS 10-30. It is a warm-water gasification boiler for combustion of dry wood from sawdust, wood briquettes and across chips to logs. Internal boiler room consists of filling tank, where the fuel is dried and gasificated. Wooden gas then passes through nozzle into the combustion chamber, where it burns by the aid of secondary air. Combustion gases pass in to the heat exchanger. The measuring device consists of a boiler and cooling circuits, which are separated by heat exchanger.

3.1. Measurement Procedure

We made measurements at various settings of primary and secondary air regulator. Primary air was flowing into the gasification area. Secondary air is fed into the combustion chamber through the internal cross section jokls grid, where the air is pre-heated. A very small proportion of secondary air is fed into the gasification area. Setting of primary and secondary air can be in the range 0 - 15mm. The measurement procedure for individual settings, the supply of primary and secondary air was as follows:
1. Creation of the basic layer of fuel
2. Setting the supply of primary and secondary air
3. Recording the weight before loading the fuel boiler.
4. Weighting the timber,
5. Loading the weighted fuel.
6. During the measurement interval of 60 seconds we have recorded: time, chimney flow, relative humidity, ambient temperature, stack temperature, the temperature in the combustion chamber, the temperature under the exchanger, reverse temperature, inlet temperature, mass flow of heating water, heating power, the weight of the boiler with the loading of fuel emissions.

Completion of the measurement was made at the moment when the weight of the boiler with heating up fuel stabilizes the initial weight prior to loading.

3.2. Measurement results

We have evaluated several sallow samples, at each other with different settings of primary and secondary air. Moisture content of wood was determined in the device for measuring the moisture content of fuel type WPS 50 SX.

Sample No. 1 contains 14,3 kg of bleached tree moisture 19,87%. Primary and secondary air was open to a maximum which is 15 mm. Results in this table are averages of the 37 minute measurement period.

Sample No. 2 contains 14,2 kg tree bleached with 19,87% moisture. Primary air was open for 10 mm and the secondary to the maximum (15 mm). Results in this table are averages of the 67 minute measurement period.

Sample No. 3 contains 14,5 kg of tree bark, the primary air was set to a maximum (15 mm), and secondary air supply was opened to 10 mm. Results in this table are average values for the 82 minute measurement period.

Furthermore, we have evaluated 4 samples of different sallow species, while settings of the primary and secondary air were the same in all cases: the primary air has been open for 10 mm, secondary to the maximum - which is 15 mm. Weight of the samples was 13,9; 13,3; 10,5; 11,5 kg and moisture was 6,76%; 30%; 37,69%; 39,59%.

	room chimn.	stack temp	stack move	power boiler	status meter	status meter	status meter	status meter
	t_0	t_k	p_k	Q	CO_2	NO_X	CH_X	O_2
	[°C]	[°C]	[Pa]	[kW]	[%]	[ppm]	[ppm]	[%]
1.sample	19,3	185,8	12,1	14,4	9,5	115,8	3,4	10,6
2.sample	19,8	228,3	11,7	19,1	8,7	70,9	1,7	11,6
3.sample	20,2	186,6	12,0	13,0	6,3	54,2	1,2	14,2
4.sample	20,3	231,4	12,3	18,7	7,6	97,2	1,7	12,7
5.sample	19,3	212,9	12,2	16,0	5,1	57,4	0,9	15,5
6.sample	18,8	226,1	12,3	15,5	4,5	56,1	0,7	16,1
7.sample	18,8	160,5	12,1	11,9	2,7	35,3	0,8	18,0

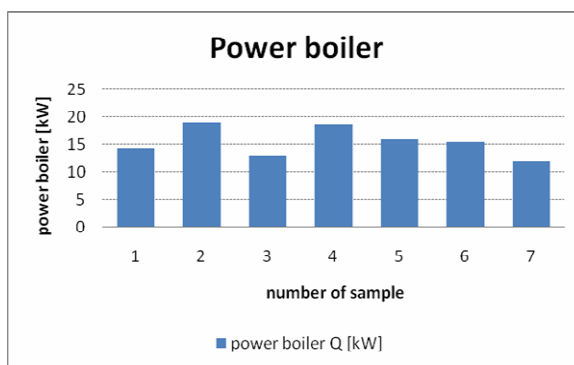**Tab. 1.** Measurement results

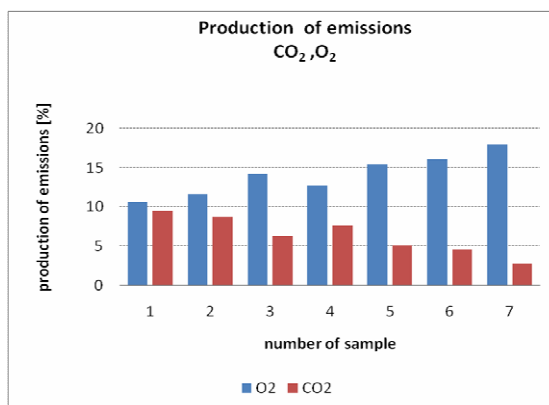

Fig. 1. Power boiler

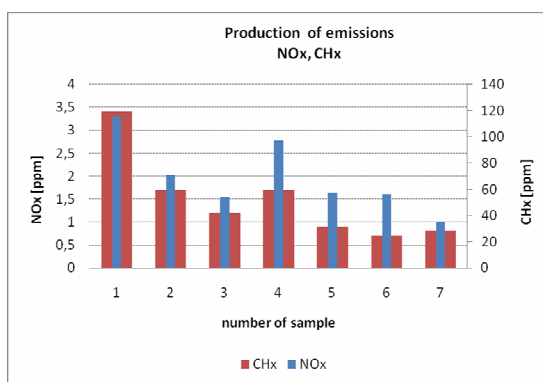**Fig. 2.**   Production of emissions CO_2, O_2

Fig. 3.   Production of emissions NOx, CHx

4.   Conclusion

Moisture content of wood is of great importance in the burning wood. By burning of wet wood combustion temperature decreases, what leads to errors in oxidation of all combustible components, there is a smokiness, choking smoke pipe reduction of the of the boiler life. Moisture in wood is released to the boiler and at the expense of heating. By proper combustion, and with proper moisture wood burns virtually smoke-free, is easily ignited, does not smudge during handling.

Acknowledgement

References

[1]   JANDAČKA, J., MALCHO, M., MIKULIK, M.: Ekologické aspekty zámeny fosílnych palív za biomasu, Žilina 2008, ISBN 978-80-969595-5-6

[2]   JANDAČKA, J., MALCHO, M., MIKULIK, M.: Biomasa ako zdroj energie, potenciál, Žilina 2006, ISBN 978-80-969161-3-9

Experiences with the Stator Reaction Measurement using Strain-Gauge Load Cells

*Ľubomír Miklánek

*Czech Technical University in Prague, Faculty of Mechanical Engineering, Josef Božek Research Center, Technická 4, 166 07 Praha, Czech Republic, {lubomir.miklanek}@fs.cvut.cz

Abstract. This contribution deals with the experiences with the measurement of the stator reaction of the dynamometer. Stator reaction was measured using a strain-gauge load cell on the known moment arm of the force within framework of research. Two various types of load cells were applied. During a calibration, a hysteresis in voltage output of the both applied load cells was observed. The maximal value of the hysteresis was about 0.5 % of the measured range. Moreover, a certain (pseudo)plasticity of the both load cells was occurred.

Keywords: Strain-gauge, load cell, hysteresis, dynamometer, torque.

1. Introduction

A precise measurement of the torque of the engine (ICE) is very important in research especially in case of the low load. An older type of electric dynamometer [1] is applied in author's laboratory. Originally, torque of the engine (stator reaction) was measured using an old balance mechanism.
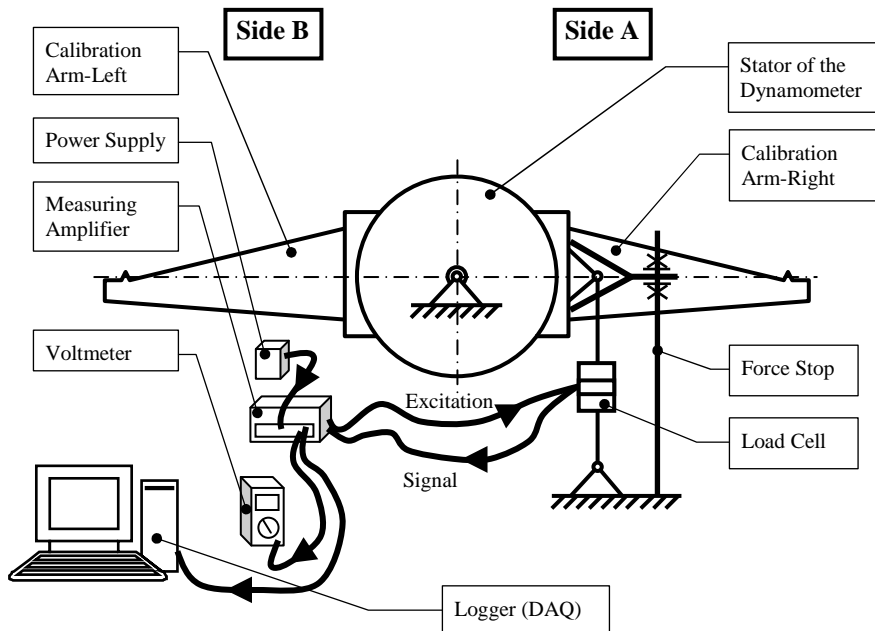

Fig. 1. Scheme of the measurement of the stator reaction using the load cell.

Because an increase of the measurement accuracy was required, the balance mechanism was replaced by a commercial strain-gauge load cell, see Fig. 1. A measuring amplifier [2] was used both as source for Wheatstone bridge excitation voltage and for output signal conditioning. Load cell output signal was converted by the measuring amplifier to the unified voltage output signal (±10V). This voltage output depends on the load (measured torque) and can be evaluated by the voltmeter or by the appropriate inputs of the Data AcQuisition System (DAQ).

To protect the applied load cell against the excessive values of load, a protection (Force Stop) was designed [3] and installed near the load cell, as it is visible in Fig. 1.

2. Performed Measurements

Within the framework of research and development activities in the author's laboratory, the measurement of the torque (Mt) of an engine S 781 NG (max. value of Mt = 90 Nm) was performed. To solve this task, the load cell with these parameters was applied: (Max. loading: 490 N; K-factor: 1.8553 mV/V; Input impedance: 415 Ω; Material: Anodized aluminum; 6-wire technique with two sensor lines), [4].

The properties of the applied load cells were found out during the calibration. The calibration of the load cell applied for the measurement of the torque of the engine S 781 NG, was performed for the both sides A and B, see Fig. 1. Measured plots are presented in Fig. 2 and Fig. 3. Used marking in Figures: **Mtcalibration** is calibration torque; **Mt** is measured torque using the load cell.

Over that, the measurement of the torque of another engine using other type of the load cell was performed. However, due to constraints with article length only the plots of the load cell described above will be given.

2.1. Calibration on the Side B

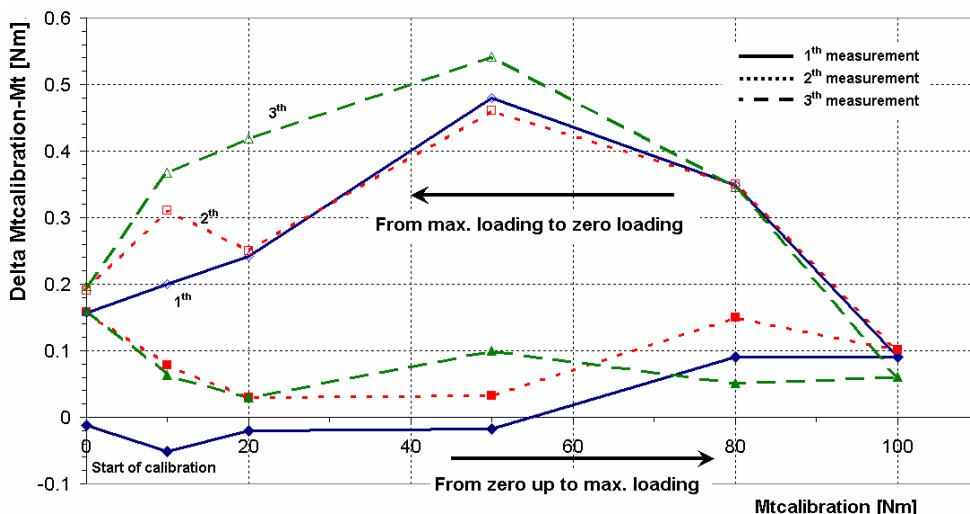The calibration began on the side B. The load cell was under no loading a few hours before the calibration process.

Fig. 2. Measured plots during the calibration of the applied load cell on the side B.

The calibration was performed from zero loading up to the maximal loading (tension) and back to the zero loading. This calibration process was repeated three times, see Fig. 2. As it is visible in Fig. 2, a hysteresis was occurred between the both increasing and decreasing loading. Its maximal value is about 0.5 % of the measured range during the calibration. Moreover, certain (pseudo)plasticity was occurred, as it is visible in Fig. 2. This plasticity caused a certain offset in measuring amplifier voltage output at zero loading of the load cell.

2.2. Calibration on the Side A

After calibration on the side B, the calibration on the side A (compression) was performed. Measured plots are presented in Fig. 3. As in previous case, three calibration measurements were performed consecutively. The hysteresis and the certain (pseudo)plasticity were occurred as well. Moreover, the plasticity from the calibration on the side B was not eliminated, but it was changed to the direction of load, see Fig. 3.

Nevertheless, it was observed that the mentioned plasticity (on the side A and B) disappeared by itself after a few hours of no loading of the load cell.
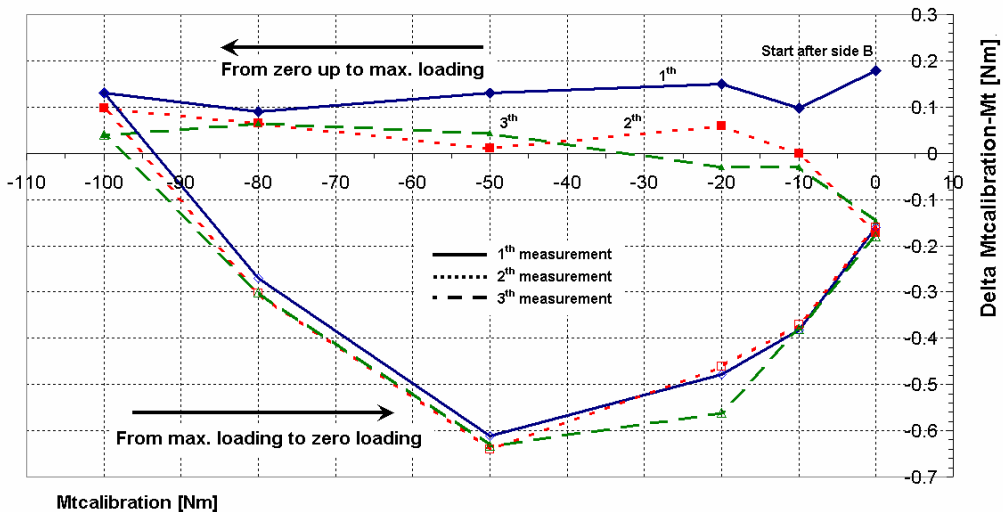

Fig. 3.   Measured plots during the calibration of the applied load cell on the side A.

2.3. Activation of the load cell protection

Design of the load cell protection (force stop) makes possible the adjustment of its activation, see Fig. 4. When the loading of the tension-compression load cell is less than the preset value, the force stop is not active. However, when the loading of the load cell is larger than the preset value, the force stop is active. Once the force stop is activating, the load is splitted into both the load cell and the force stop. This splitting causes the change in measured plot of loading of applied load cell.

The change in measured plot of the applied load cell loading before and after force stop activating is presented in Fig. 4. It is visible after the force stop activating, the loading of the load cell increases only slightly compared to the loading increasing without the force stop. Note, the maximum safe static overload of this type of load cell is about 150 % of the rated loading (490 N). The force stop should be activated at latest on the rated loading.
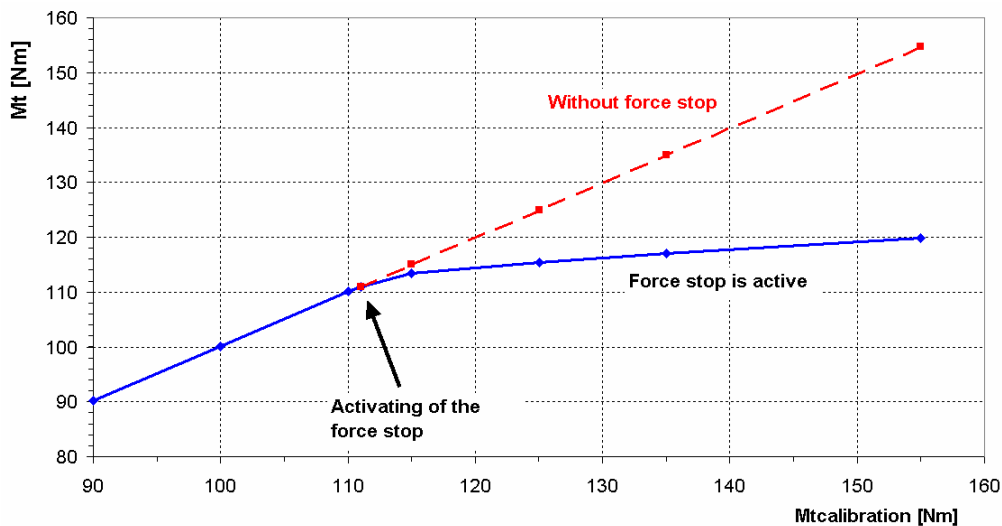
Fig. 4. Measured plots of the load cell loading before and after force stop activating.

3.   Conclusion

Properties of the applied load cell (Max. loading: 490 N, Material: anodized aluminum, 6-wire technique with two sensor lines) was observed during the calibration in both directions of stress – tensile stress (side B) and compression stress (side A). During the calibration, the hysteresis in voltage output signal was observed (about 0.5 % of the measured range). Moreover, certain (pseudo)plasticity of the load cell (about 0.17 % of the measured range) was occurred. This plasticity caused the small offset in output voltage especially in zero loading.

Upon the author's opinion, these observed properties of applied load cell have no significant effect on the required accuracy of measurements compared to the measured range.

Over that, the other load cell (Max. loading: 1962 N, Material: stainless steel, 6-wire technique with two sensor lines) was calibrated for another engine torque measurement. The similar properties of this load cell to the previous load cell were observed.

Acknowledgement

References

[1]   MIKLÁNEK, Ľ. *Utilization of automation test process in transient engine operating state*. Mecca, No. 3, Vol. I, p. 42-48, ISSN 1214-0821, 2003.

[2]   HOTTINGER BALDWIN MESSTECHNIK GMBH. *Clip electronic*. Operating Manual, 2008.

[3]   MIKLÁNEK, Ľ. *Strain-gauge load cell*. Patent application, No. 2007-433, Industrial Property Office, Praha 2007.

[4]   TEDEA-HUNTLEIGH ELECTRONICS. CO.LTD. *Load Cell Test Data Sheet-Model 614, 50kg*. 2008.

Influence Heat Transfer Limitations of Heat Pipes on their Cooling Power

*Patrik Nemec

*University of Žilina, Faculty of Mechanical engineering, Department of Power, Univerzitna 1, 01026 Žilina, Slovakia, patrik.nemec@fstroj.uniza.sk

Abstract. Article describes principle of operation wick heat pipes and processes heat transmission by the different working temperatures. Deal operating limits on basic used types of wick water heat pipes. Calculations various wick heat pipes with water as a working fluid are illustrated in graphic dependence limiting performances on the working temperatures. In conclusion are reviews influence working limits on cooling power of the heat pipes.

Keywords: heat pipe, heat transfer limitations, wick structure.

1. Introduction

The heat pipe is a vapor-liquid phase-change device that transfers heat from a hot reservoir to a cold reservoir using capillary forces generated by a wick or porous material and a working fluid. Figure 1 shows a schematic of a heat pipe aligned at angle y relative to the vertical axis (gravity vector). The heat pipe is composed of a container lined with a wick that is filled with liquid near its saturation temperature. The vapor-liquid interface, usually found near the inner edge of the wick, separates the liquid in the wick from an open vapor core. Heat flowing into the evaporator is transferred through the container to the liquid-filled wicking material, causing the liquid to evaporate and vapor to flow into the open core portion of the evaporator. The capillary forces generated by the evaporating interface increase the pressure difference between the vapor and liquid. The vapor in the open core flows out of the evaporator through the adiabatic region and into the condenser. The vapor then condenses, generating capillary forces similar, although much less in magnitude, to those in the evaporator. The heat released in the condenser passes through the wet wicking material and container out into the cold reservoir. The condensed liquid is then pumped, by the liquid pressure difference due to the net capillary force between the evaporator and condenser, out of the condenser back into the evaporator. Proper selection and design of the pipe container, working fluid, and wick structure are essential to the successful operation of a heat pipe. The heat transfer limitations, effective thermal conductivity, and axial temperature difference define the operational characteristics of the heat pipe.
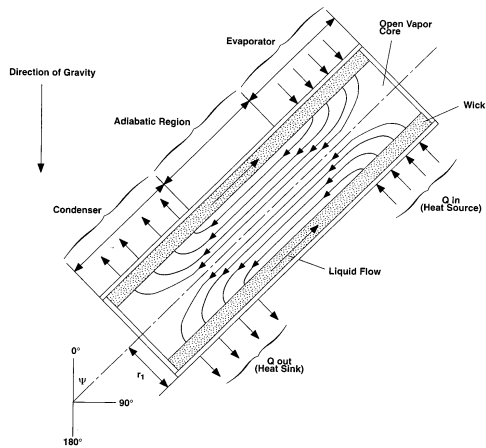
Fig. 1. Wick heat pipe

2. Heat Pipe container

The material and geometry of the heat pipe container also must have a high burst strength, low weight, high thermal conductivity, and low porosity. The most commonly constructional materials of heat pipes are steels, copper and glass.

2.1. Working Fluid

Using the proper working fluid for a given application is another critical element of proper heat pipe operation. The working fluid must have good thermal stability properties at the specified operational temperature and pressure. The operational temperature range of the working fluid has to lie between its triple point and its critical point for liquid to exist in the wicking material. The wettability of the working fluid contributes to its capillary pumping and priming capability. High-surface-tension fluids are commonly used in heat pipes because they provide the capillary pumping and wetting characteristics necessary for proper operation. Other desirable thermo-physical properties include a high liquid thermal conductivity, high latent heat of vaporization, low liquid viscosity, and a low vapor viscosity .

2.2. Wick Structures

The wick structure and working fluid generate the capillary forces required to pump liquid from the condenser to the evaporator and keep liquid evenly distributed in the wicking material. Heat pipe wicks can be classified as either homogeneous wicks or composite wicks. Homogeneous wicks are composed of a single material and configuration. The most common types of homogeneous wicks include wrapped screen, sintered metal, axial groove, annular, crescent, and arterial. Composite wicks are composed of two or more materials and configurations. The most common types of composite wicks include variable screen mesh, screen-covered groove, screen slab with grooves, and screen tunnel with grooves. Regardless of the wick configuration, the desired material properties and structural characteristics of heat pipe wick structures are a high thermal conductivity, high wick porosity, small capillary radius, and high wick permeability.

Temperature (°C)	Latent Heat (kJ/kg)	Liquid Density (kg/m³)	Vapor Density (kg/m³)	Liquid Thermal Conductivity (W/m°C)	Liquid Viscosity (cP)	Vapor Viscosity (cP,X 10^2)	Vapor Pressure (bars)	Vapor Specific Heat (kJ/kg°C)	Liquid Surface Tension (N/m X 10^2)
Water									
20	2448	998.0	0.02	0.603	1.00	0.96	0.02	1.81	7.28
40	2402	992.1	0.05	0.630	0.65	1.04	0.07	1.89	7.00
60	2359	983.3	0.13	0.649	0.47	1.12	0.20	1.91	6.66
80	2309	972.0	0.29	0.668	0.36	1.19	0.47	1.95	6.26
100	2258	958.0	0.60	0.680	0.28	1.27	1.01	2.01	5.89
120	2200	945.0	1.12	0.682	0.23	1.34	2.02	2.09	5.50
140	2139	928.0	1.99	0.683	0.20	1.41	3.90	2.21	5.06
160	2074	909.0	3.27	0.679	0.17	1.49	6.44	2.38	4.66
180	2003	888.0	5.16	0.669	0.15	1.57	10.04	2.62	4.29
200	1967	865.0	7.87	0.659	0.14	1.65	16.19	2.91	3.89

Tab. 1. Thermo-physical properties of water for wide operating temperature range.

3. Heat Transfer Limitations

Heat pipes undergo various heat transfer limitations depending on the working fluid, the wick structure, the dimensions of the heat pipe, and the heat pipe operational temperature. The next episodes qualitative description of the various heat transfer limitations, which include vapor-pressure, sonic, entrainment, capillary, and boiling limitations. Graphic dependencies show that as the operational temperature increases, the maximum heat transfer rate of the heat pipe is limited by different physical phenomena. As long as the operational heat transfer rate falls within the shaded region, the heat pipe will function properly.

3.1. Vapor-pressure limitation

The vapor-pressure limitation (or viscous limitation) in heat pipes develops when the pressure drop in the vapor core reaches the same order of magnitude as the vapor pressure in the evaporator. Under these conditions, the pressure drop due to flow through the vapor core creates an extremely low vapor pressure in the condenser preventing vapor from flowing in the condenser. A general expression for the vapor-pressure limitation is (Dunn and Reay, 1982)

$$Q_{vp} = \frac{\pi . r_v^4 . h_{fg} . \rho_{v,e} . P_{v,e}}{12 . \mu_{v,e} . l_{eff}} .$$ (1)

3.2. Sonic limitation

The sonic limitation also can occur in heat pipes during start-up at low temperatures. The low temperature produces a low vapor density, thereby reducing the speed of sound in the vapor core. Thus, a sufficiently high mass flow rate in the vapor core can cause sonic flow conditions and generate a shock wave that chokes the flow and restricts the pipes ability to transfer heat to the condenser. Dunn and Reay (1982) give an expression for the sonic limitation that agrees very well with experimental data,

$$Q_s = 0{,}474 . A_v . h_{fg} . \left(\rho_v . P_v \right)^{0,5} .$$ (2)

3.3. Entrainment limitation

The entrainment limitation in heat pipes develops when the vapor mass flow rate is large enough to shear droplets of liquid off the wick surface causing dry-out in the evaporator. A conservative estimate of the maximum heat transfer rate due to entrainment of liquid droplets has been given by Dunn and Reay (1982) as,

$$Q_e = A_v . h_{fg} . \left(\frac{\rho_v . \delta_l}{2 . r_{c,ave}} \right)^{0.5} . \tag{3}$$

3.4. Capillary limitation

The capillary limitation in heat pipes occurs when the net capillary forces generated by the vapor-liquid interfaces in the evaporator and condenser are not large enough to overcome the frictional pressure losses due to fluid motion. This causes the heat pipe evaporator to dry out and shuts down the transfer of heat from the evaporator to the condenser. For most heat pipes, the maximum heat transfer rate due to the capillary limitation can be expressed as (Chi, 1976).

$$\dot{Q}_c = \frac{\sigma_l . \rho_l . h_{fg}}{\mu_l} . \frac{K . A_v}{l_{ef}} . \left(\frac{2}{r_{c,e}} - \frac{\rho_l . g . l_t . \cos \Psi}{\sigma_l} \right) . \tag{4}$$

3.5. Boiling limitation

The boiling limitation in heat pipes occurs when the degree of liquid superheat in the evaporator is large enough to cause the nucleation of vapor bubbles on the surface of the wick or the container. Boiling is usually undesirable in heat pipes because local hot spots can develop in the wick, obstructing the flow of liquid in the evaporator. An expression for the boiling limitation is (Chi, 1976)

$$\dot{Q}_b = \frac{4\pi . l_{eff} . \lambda_{ef} . T_v . \sigma_v}{h_{fg} . \rho_v . \ln \frac{r_i}{r_e}} . \left(\frac{1}{r_n} - \frac{1}{r_{c,e}} \right) . \tag{5}$$

4. Experiment

Experiment was developed at 3 types of wick structure water heat pipes to transport of waste heat from an electronics component. Solutions operating limits of heat pipes are solved in excel by expression in previous paragraph. Graphic dependencies operating performances from working temperatures some chosen wick structures of heat pipes are design by excel too. Parameters of heat pipe and wick structure are in next tables.

evaporator length	l_e	0.1	[m]
adiabatic length	l_{ad}	0.1	[m]
condenser length	l_c	0.1	[m]
total length	l_t	0.3	[m]
effective length	l_{ef}	0.2	[m]

inner radius	r_i	0.0075	[m]
cross - sectional area	A	0.000176	[m^2]
axial angle	Ψ	90	[°]
thermal conductivity	$λ_m$	393	[W.m^{-1}.K^{-1}]
cross - sectional area of wick structure	A_k	0.00000439	[m^2]
vapor core radius	r_v	0.0065	[m]

Tab. 2. Heat pipe parameters.

grooves wick structure	groove high	h	0.0004	[m]
	groove width	b	0.0004	[m]
	groove pitch	e	0.0004	[m]
	permeability	K	0.0000000114	[m^2]
	effective radius wick structure	r_{ef}	0.0004	[m]
	effective thermal conductivity	$λ_{ef}$	2.066	[W.m^{-1}.K^{-1}]
Screen wick structure	wire diameter	d	0.0001	[m]
	wire width	a	0.00015	[m]
	porosity	e	0.67	[m]
	permeability	K	0.000000000226	[m^2]
	effective radius wick structure	r_{ef}	0.000125	[m]
	effective thermal conductivity	$λ_{ef}$	1.287	[W.m^{-1}.K^{-1}]
Sintered wick structure	sphere diameter	d	0.0005	[m]
	porosity	e	0.5	[m]
	permeability	K	0.000000000833	[m^2]
	effective radius wick structure	r_{ef}	0.64375	[m]
	effective thermal conductivity	$λ_{ef}$	2.589	[W.m^{-1}.K^{-1}]

Tab. 3. Wick structure parameters.
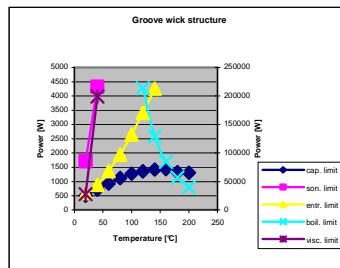
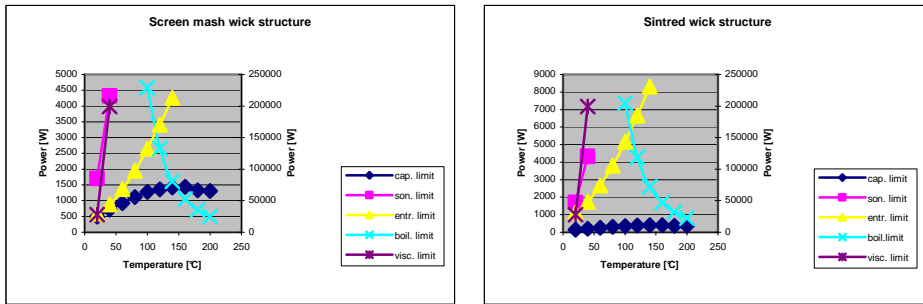**Fig. 2.** Heat pipe with groove wick structure heat transfer limitations

Fig. 3. Heat pipe with screen mash wick structure transfer limitation; heat pipe with sintered wick structure.

5. Conclusion

Graphic dependencies expressly define, who limiting performance influencing total cooling performance of heat pipe. Generaly limit values depend to heat pipes parameters, wick structure parameters and thermophysical properties of working fluid. The most highly values reach viscous limitation and sonic limitation. These limitations reach so high values, that are not important for influence total heat pipe performance, because is not possible to get so high total cooling performance by heat pipe. Critical values influencing to heat pipe performance are values entrainment limitation and capillary limitation. While thermophysical properties of working fluid influencing entrainment limitation, wick structure influencing capillary limitation, therefore wick structures and dimensions of heat pipes are design so that factor N_G was maximum. N_G factor involves all main diameters and parameters of heat pipes and wick structure. However we have to be careful because increase permeability and increase pores dimensions decrease capillary pressure, which is biggest influencing for circulation of the working fluid. Generally, the capillary limit is the primary maximum heat transport limitation of heat pipe.

References

[1] Chi, S.W.: *Heat Pipe Theory and Practice, Hemisphere Publishing*, Washington, D.C., 1976.

[2] Dunn, P.D. and Reay, D.A.: *Heat Pipes, 3rd ed*., Pergamon Press, Oxford, U.K., 1982.

[3] Gaugler, R.S.: *Heat Transfer Device. U.S. Patent No. 2350348*, 1944.

[4] Grover, G.M.: *Evaporation-Condensation Heat Transfer Device. U.S. Patent No. 3229759*, 1963.

[5] Peterson, G.P.: *An Introduction to Heat Pipes Modeling, Testing, and Applications*, John Wiley & Sons, New York, 1994.

[6] Swanson L. W.: *Heat pipe, Heat and Mass Transfer, Mechanical Engineering Handbook,* Ed. Frank Kreith Boca Raton: CRC Press LLC, 1999.

Railway Vehicle Computational Model Dynamic Analysis

[*]Zuzana Ondrová, [*]Juraj Gerlici, [*]Tomáš Lack
[*]University of Žilina, Faculty of Mechanical Engineering, Department of Transport and Handling Technology, Univerzitná 1, 01026 Žilina, Slovakia, {Zuzana.Ondrova, Juraj.Gerlici, Tomas.Lack}@fstroj.uniza.sk

Abstract. The paper is aimed at the dynamic simulation of the rail vehicle running on an actual track. The practical computations performance, contact forces, derailment indexes assessment under various rail head profiles and rails inclinations computational conditions were executed with the help of MSC.ADAMS /Rail programme package. The vehicle parameters correspond to the four-axle two - bogies coach wagon that is known as ERRI Wagon. The railway wheel tread profile data are of a theoretic ground. The dynamic analysis of vehicle properties was executed with the help of the programme MSC.ADAMS. The track model as the input parameters was set on the ground of actual railway stock section in Slovakia.

Keywords: railway vehicle model, multibody system analysis, safety against derailment, simulation programme package, real track definition.

1. Introduction

The article focuses on dynamic simulations of rail vehicle running on an actual track. This topic binds the solution of rail vehicles properties evaluation and special-purpose utilization of computational technology and specialized programmes in order to reach desired results – the prediction of dynamic phenomena which control the vehicle behaviour on an actual track. The purpose of simulation computations is to acquire values, or possibly time or track dependences of physical quantities which, after a modification, enter mathematical relations in order to compute proportional quantities which might be considered as directive and it is possible to compare them mutually in order to acquire the information about the advantages or disadvantages of their utilization in the given running mode on a track.

2. Computational model

The computational model consists of a vehicle model, a track model and a wheel/rail contact module model. The dynamic vehicle model should be as simple as possible but it should grasp dynamic properties of real mechanic vehicle system in a sufficient amount.

2.1. Wheel / rail interaction

The contact couple wheel/rail has an important influence on kinematical and dynamical vehicle behaviour on a track. The couple is represented by a running wheel profile and a rail head profile. The geometrical relation of the wheelset and the rail is characterised by geometrical characteristics which are primarily defined in [8].

2.2. Rail vehicle model

From the point of view of a model system type and specification of its parameters, we deal with a double bogie coach wagon which is known under the name "ERRI Wagon" for the purpose of the evaluation of dynamic analysis results and for the evaluation of computational systems in order to analyse dynamics of material systems.
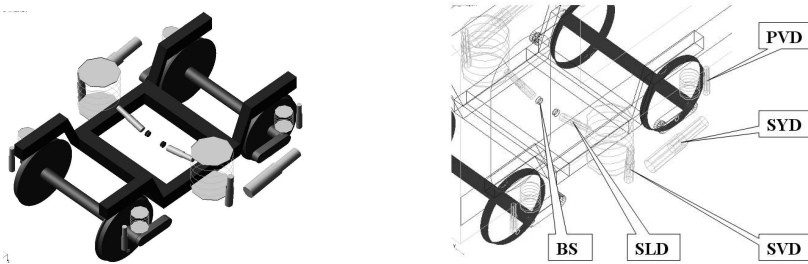

Fig. 1. The scheme of a bogie design – PVD is a primary vertical damper, SYD is a secondary longitudinal damper, SVD is a secondary lateral damper and BS stands for a bump stop.

The carriage model is equipped with springs and dampers with non-linear characteristics. Geometrical, weight parameters and flexible joints parameters are identical with vehicle parameters which are accessible in the verification model MSC.ADAMS/Rail. The coach wagon has a primary damper as well as secondary one. The wheelset wheels have the wheel tread surface profile S1002.
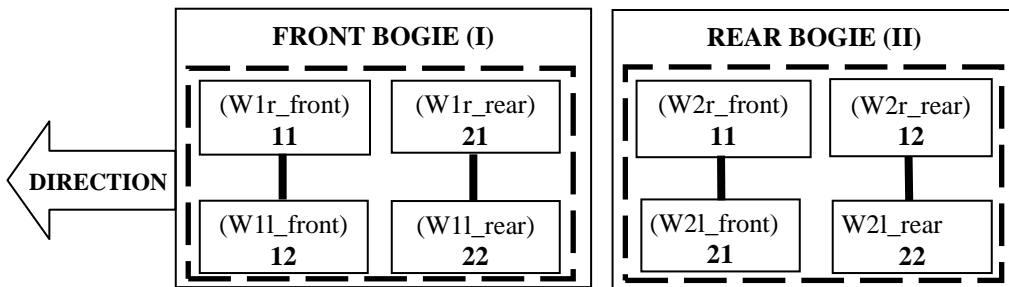
Fig. 2. Distribution of positions in a vehicle.

In Fig. 2 there are markings of separate places on the carriage bogies in accordance with the marking of output signals which one can acquire when depicting output data after the execution of simulation computations. The ride direction in marked mainly from the reason of transparency when setting arcs orientations and subsequent results evaluation.

2.3. Track model

The rail profile is UIC60, the standard rail slope is 1:40. For the purpose of analyses, the rail profile was supplemented by S49 which is on the base of records used when building the track Šurany-Úľany nad Žitavou (See Fig. 3). The tracking of the track was used as a real rail when analyzing safety against derailment. All accessible data which concern arcs radii, installed rail cant and track levelling were put into the computational system. The maximum speed is 60 km/h on the track. All the calculations are executed at this speed. Safety against derailment (BPV) was analysed for the rail profile UIC60/1:40, S49/1:40 a S49/1:20.

Comparing calculations were realized for the installed rails slope 1:20 which represent the least favourable case from the point of view of profiles and slopes combinations. The results given in Fig. 4 represent force courses in the wheel/rail contact.
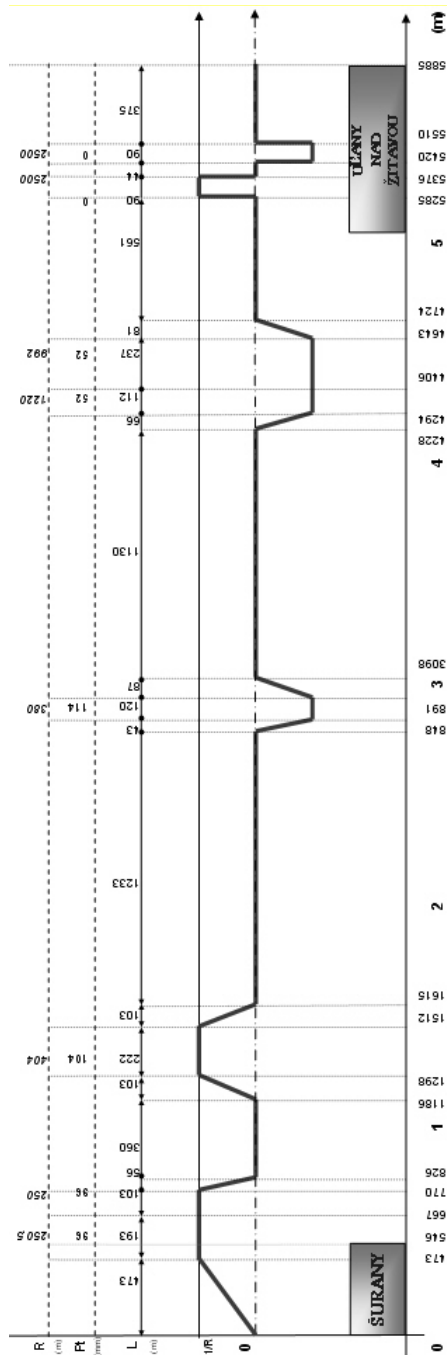
3. Safety against derailment

Safety against derailment is defined as the guiding and wheel force ratio. The results given in Fig. 4 represent the force courses in the wheel/rail contact. For the simplicity of orientation in the pictures we can specify the following. The track geometry is depicted in the lower graph.

- The vertical axis branded on the left side gives the overturned value of arcs radii; the vertical axis on the right side gives the outer rail cant.

- The upper half and positive radii values are valid for right arcs, the lower part and negative values of arcs coordinate are valid for left arcs.

- The vertical distance is numbered from the bottom in ascending order from zero.

- In the upper graph, there is a safety against derailment (BPV) coefficient course which represents a dimensionless quantity [-].

4. Conclusion

It is clear from Fig. 4 that the leading wheel of the first wheelset of the first bogie is the most loaded wheel when traversing an arc curve. The formation and transmission of the biggest right guiding force in the horizontal level appears at this place. The second wheel of the leading wheelset shows the wheel force as well as guiding force loss. At the straight track the wheel forces stabilized on their nominal values and the guiding forces approach zero. The forces course proved that the vehicle moves stably and the model communicate comprehensibly with the track via their mutual force action. In accordance with the track courses (shape), it is possible to gain orientation in sizes and directions of acting forces relatively quickly. The results of sizes and courses of wheel, guiding forces, as well as

Fig. 3. The scheme of track shape.

safety against derailment, are within the allowed limits, the most favourable ratio safety against derailment (BPV) on this section is for this contact couple configuration at about 0.5 what is less than 1.12 allowed for the ride profile S1002.
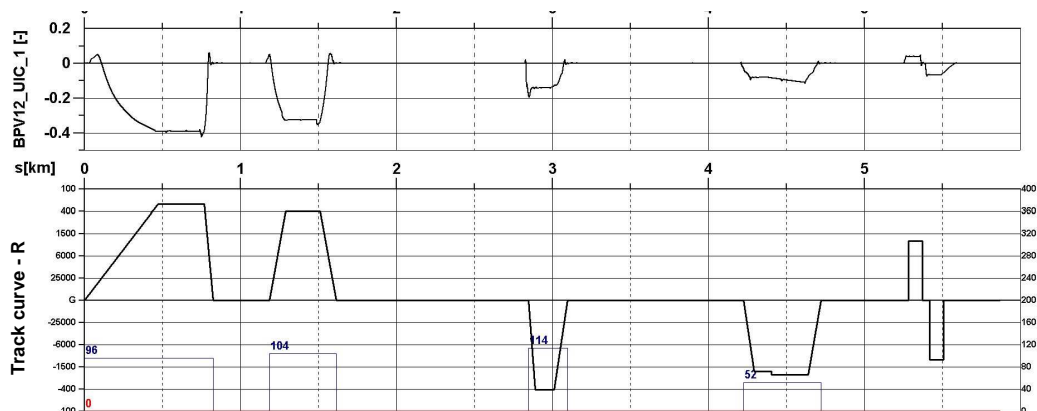

Fig. 4. The horizontal track geometry and safety against derailment index evaluation along the track.

The created model allows us to realize further analyses when changing separate vehicle parameters (flexible joint characteristics), it allows to analyze the acceleration size acting on the vehicle (passengers, load) and on the base of it, to evaluate passengers comfort and its change as a consequence of different vehicle parameters.

Acknowledgement

References

[1] DUKKIPATI., R., V., AMYOT, J., R. *Computer-aided simulation in railway dynamics*. Pp.423. ISBN 0-8247-7787-5. Marcel Dekker, New York, USA 1988.

[2] GERLICI, J., LACK, T., ONDROVÁ, Z. *Evaluation of comfort for passengers of railway vehicles*. Communications – Scientific papers of University of Žilina, 4/2007, Str. 44-49, ISSN 1335-4205, EDIS – Publishing house of University of Žilina 2007.

[3] KALKER, J., J. *Three-dimensional elastic bodies in rolling contact*. Kluwer academic publishers, Dordrecht, Netherlands, 1990.

[4] ONDROVÁ, Z., GERLICI, J., LACK, T. *Comfort for passengers of railway vehicle analysis. In: proceedings of international conference* "TRANSCOM 2007", ISBN 978-80-8070-696-8, proceedings, Section 7, pp.205-210. EDIS – Publishing house of University of Žilina 2007.

[5] ONDROVÁ, Z., GERLICI, J., LACK, T.: *Dynamics properties analysis of rail vehicle when moving*. (In Slovak) Proceedings of the 4-th international conference Dynamics of rigid and deformable bodies. Univerzity of J. E. Purkyně. ISBN 80-744-782-6. Pp. 155-162.Ústí nad Labem, 2006.

[6] POLÁCH, O.: *Railway vehicles dynamics analysis*. In: Kalinčák, D. at al.: Transport mean – computational methods. Pp. 165-200. Textbook. (*In Slovak*)University of Žilina. ISBN 80-8070-476-7, EDIS 2005.

[7] SÁGA, M., VAVRO, J., KOPECKÝ, M. *Computer analysis and synthesis of mechanical systems (In Slovak)*. ISBN 80-968605-4-2. Žilina, ZUSI, 2002.

[8] UIC CODE (2008): 518 OR *Testing and approval of railway vehicles from the point of view of their dynamic behaviour – Safety – Track fatigue – Running behaviour*. January 2008.

The Distribution of Stresses during the Process of Extruding the Hollow Torus

[*]Piotr Paszta

[*] Częstochowa University of Technology, Institute of Machines Technology and Production Automation, 42-200 Częstochowa, Al. Armii Krajowej 21, Poland, e-mail: paszta@itm.pcz.czest.pl

Abstract. The numerical computations carried out have enabled particular phases of forming torus pieces to be analyzed. The performed thermomechanical simulation of the process of extruding the torus piece has allowed the determination of values that characterize the state of strain, stress and temperature.

Keywords: Extrusion, torus, analysis of the state of stress.

1. Introduction

The distribution of stresses during the process of extruding the hollow torus is complex in character. During the extrusion process, the copper charge is deformed and is subject to the ram pressure force, friction forces and forces associated with die and sizing bar reactions. Part of these forces deforms the charge, and the other part attempt to block the movement of metal particle relative to each other and in relation to the die and bar surfaces. Under the effect of the above-mentioned active and reaction forces, the material remains in a state of stress. In the analyzed extrusion process, triaxial compression occurs in the plastic deformation region, owing to which the metal has the best plasticity in these conditions. A stress pattern exists here, which is the most advantageous in terms of plasticity, and which includes one tensile strain and two compressive strains. Conditions occur here, in which the copper under compressive stresses flows in the direction of the highest stress gradient from the surface of contact of the ram face with the metal, on which the average stresses reach the highest magnitude, to the ring-shaped die hole, where on the surface of flowing-out copper the normal stresses attain a zero value.
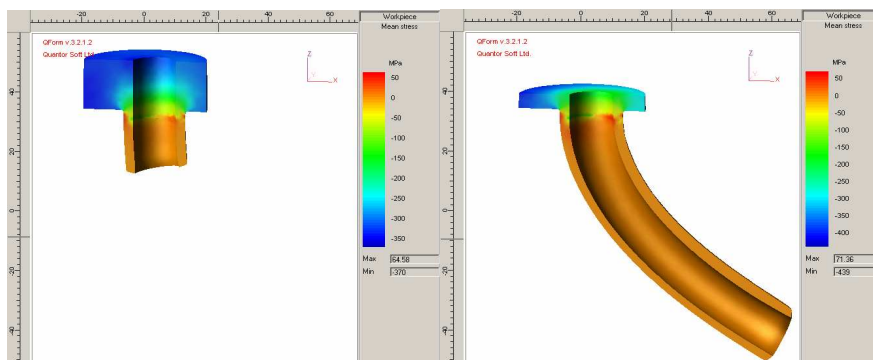

Fig. 1. The distribution of average stresses

1.1. Analysis of the state of stress

The distribution of average stresses is illustrated in Fig. 1. During the extrusion of a copper ring through the die ring-shaped hole compressive stresses occurs in the entire volume of the material being deformed, which vary in the extrusion direction in a continuous manner from about -450 MPa to 30 MPa. The value of 30 MPa can be explained by the effect of a large diameter reduction during extrusion, the occurrence of a dead zone, a particular effect of metal friction forces in the sizing gap, and, to a small extent, by an additional displacement of metal particles in the transverse direction; the equalization of particle movement velocities may give rise to tensile stresses. The average stress on the external surface amounts to approx. -400 MPa and is higher compared with the stress forming in the zone of contact of copper with the sizing bar, which is demonstrated in Fig. 2.
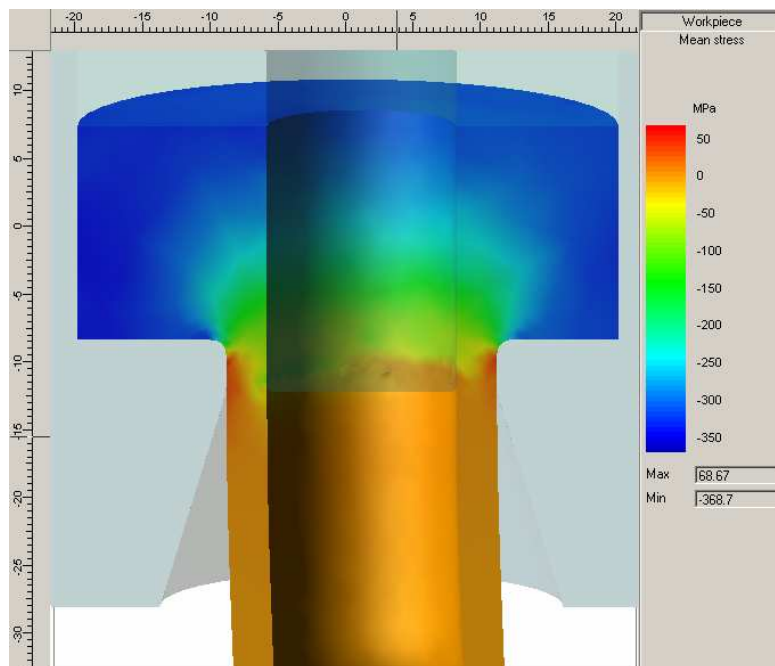
Fig. 2. The average stress on the external surface

1.2. Analysis of temperature distribution

The simulated extrusion process progressed relatively slowly, with good heat exchange with the environment. The charge temperature remained constant during the process, only slightly increasing by 4.8^{0} in the initial phase of extrusion. In this case, we can regard the process as isothermal.

The presented distribution of stresses can also be related to the changes of temperature within the die. In the deformation region within the die around the ram, where a slight increase in temperature is visible, the deformation resistance decreases and the average stress ranges from -100 to -200 MPa, whereas in the areas near the die surface, where practically no areas of temperature increase exist, the deformation resistance is higher and, at the same time, the stress amounts to approx. -440 MPa. In the free flow area the average stress takes on a negative value, which is advantageous in view of a possibility of closing possible material defects.

Maintaining the zero value of the average stress is fully sufficient for attaining plastic flow stability.

In the considered cases, as shown in the sections of internal stress map in Fig. 3, it is important to know the stresses in the finished extruded piece in order to assess its suitability for proper use. Based on the results of extrusion process simulation using the QForm 3D program, high usefulness of the obtained products can be found. A uniform stress distribution occurs within the extruded piece walls, which is close to zero.
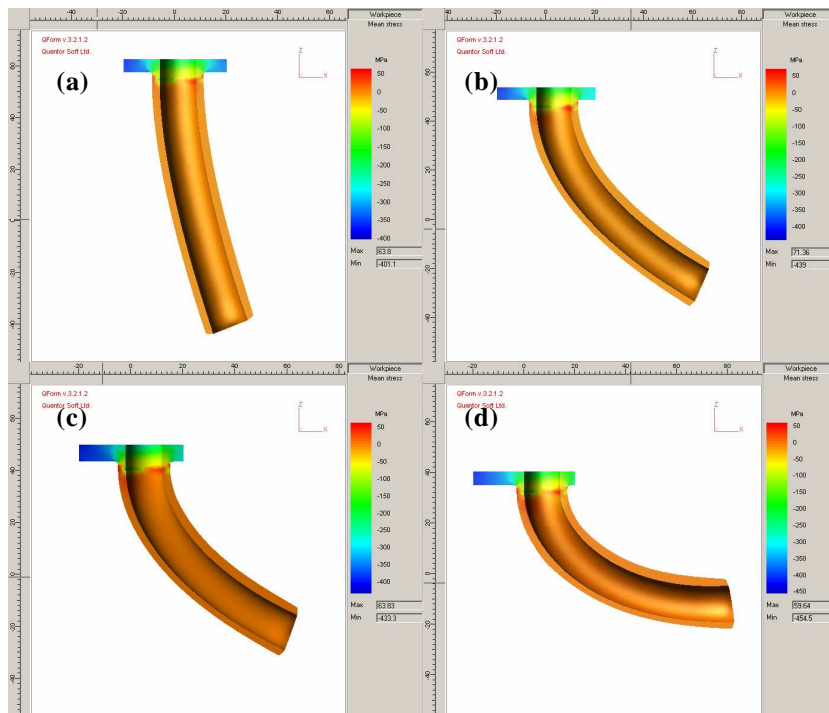
Fig. 3. Internal stress map 1mm, 3mm, 5mm, 7mm

The stability of plastic flow of copper during the formation of a hollow torus extruded piece is only possible in the case of using proper tool shapes providing the possibility of forming in the presence of all-side compressive stresses. It has been found based on the analysis of eccentric extrusion simulation results that these conditions are satisfied by the eccentric die which forces the metal flow with contribution of sufficiently high average compressive stress. Based on the simulation results it has been determined that the course of metal deformation is controlled by the die walls, bar and the ram.

1.3. Extrusion force

The variations of extrusion forces necessary for extruding toruses during the extrusion process, as determined by numerical computations, are presented in the diagram in Fig. 5.12 below.
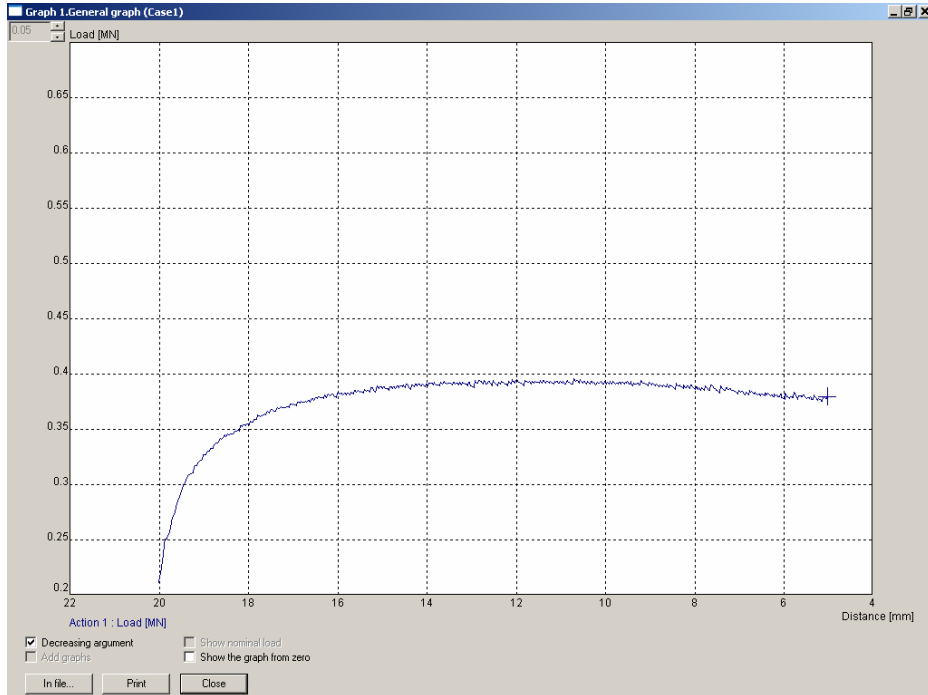

Fig. 4. Extrusion forces

2.   Conclusion

The obtained results confirm the correctness of the boundary conditions taken, and the obtained distributions of numerically computed parameters should be regarded as close to reality. In view of the above it can be stated that the computations carried out for copper are correct and will allow the technology of direct extrusion in dies with eccentrically shifted sizing holes to be further streamlined.

References

[1]   PASZTA, P. *Analiza montażu stempla z matrycą podczas procesu wyciskania drążonych torusów*. Technologia i Automatyzacja Montażu. Ogólnopolski Kwartalnik Naukowo-Techniczny Nr 2 (60) kwiecień – czerwiec 2008.

[2]   PASZTA, P. *Pomiary zarysów torusowych na maszynach współrzędnościowych.* Konferencja Naukowo – Techniczna Metrologia w Technikach Wytwarzania Maszyn Bielsko Biała 2002

[3]   JEZIERSKI, J., PASZTA P. *Pomiary zarysów torusowych na maszynie pomiarowej Renishaw Cyclone*. X Krajowa i Międzynarodowa Konferencja Naukowo-Techniczna Metrologia 2003. Kraków 25-27 września 2003

Utilization of Sorption Effect for Cooling Systems

[*]Peter Pilát, [*]Jana Micicova

[*]University of Zilina, Faculty of Mechanical engineering, Department of Power engineering, Univerzitna 8215/1, 01026 Zilina, Slovakia, { peter.pilat, jana.micicova}@fstroj.uniza.sk

Abstract. This article describes alternative feasibility of waste heat or sun energy utilization in cooling systems. Waste heat is product of power systems or industry, which is usually utilized in winter for heating systems of householders. The same problem is with energy from sun. Tri-generation is an answer how to use this heat in summer time and here is place for sorption cooling systems.

Keywords: adsorption, absorption, cooling system

1. Introduction

Advantage of sorption cooling systems is utilization of thermal energy abundance from the sun collectors in the summer months or waste heat from energetic systems. Consumption of energy on heating in the summer time is minimal, but still more often we meet houses, which are air-conditioned. And here is the consumption of energy not so negligible. Energy from sun is still for free or why not utilize waste heat.

2. Working principle of the sorption device

The basic process of cold generation is the compression of a refrigerant fluid, which causes evaporation of the liquid at low temperatures and pressures and condensation of the vapour at higher temperatures and pressures. Instead of mechanical compression like in electrical air-conditioners, thermal driven chillers use thermal energy for the compression of the fluid. The basic principle of the thermal compression is the ab- or adsorption of the refrigerant in a liquid or solid material. Whereas absorption chillers use the liquid lithium-bromide in adsorption chillers solid adsorbents like silica gel or zeolites are used. Both machine has to be operated at very low pressures in a vacuum tight containment [4].

Absorption systems are working with two liquids – coolant and absorbing agent. These devices are usually working continually. They have five basic parts: evaporator, absorber, generator (desorber), condenser. Thermal energy to generator is delivered from sun collectors or is utilized waste heat. Between evaporator and absorber is low pressure and between generator and condenser is high pressure. Low pressure and high pressure zone divide between condenser and evaporator throttle and between absorber and generator is inserted pump. Cool from the evaporator is delivered to air conditioning system. Consumption of electricity for pump is cca 5% of cumulative energy needed for this system. Coefficient of performance (COP) at this devices is between 0,3 – 0,7.
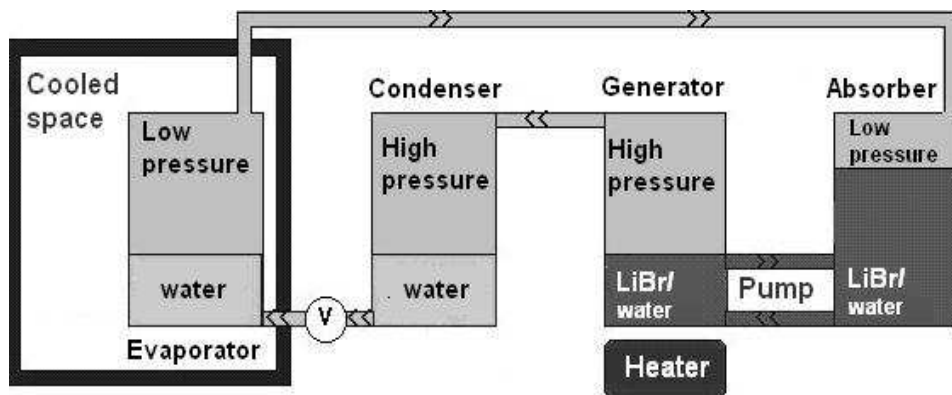
Fig.1. Absorption cooling system with working pair LiBr/water

Adsorption cooling device are simple construction systems. It is assembled from evaporator-condenser and absorber-generator. Because the adsorption device is not continually working, in 1st phase absorber (adsorbent is charged by water vapour) absorb the vapour from the evaporator is cooling and the cool we can sample to air conditioning system. In the 2nd phase we need the adsorbent discharge. In this case absorber become to generator and evaporator become to condenser. Discharge the adsorbent is possible by the heat and in our case by the solar thermal energy from collector or by the waste heat. By heating of generator is the adsorbent agent discharged and water vapour is condensed in condenser. If we need continual working adsorption cooling system, we have to use two adsorber/ desorber. The first one is charging – heating the adsorbent and desorbing the coolant and second one is discharging – adsorbing the vapours of coolant and cooling. When is the second one discharged, is necessary change their function. Then the first one is discharged – adsorbing and the second one charging by heat- de sorbing.
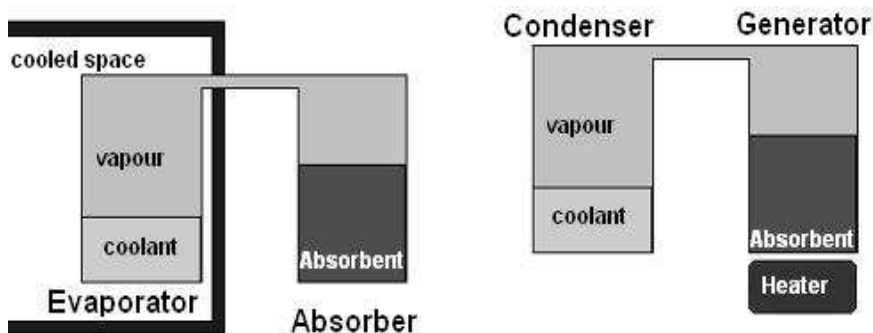
Fig.2. Adsorption cooling system

3. Types of sorption cooling systems

Typical cooling absorption systems are working with pair coolant/ absorbing agent H_2O/LiBr or NH_3/H_2O. In system H_2O/LiBr is H_2O coolant and LiBr is absorbing agent. In systems NH_3/H_2O is H_2O absorbing agent and NH_3 is coolant.

One of the most known pairs are zeolits used like adsorbent and some liquid coolant H_2O, methanol, ethanol). Advantage of this pair is price and accessibility. We know the zeolit like a rock occurred in nature. Cleanness of this zeolit is around 70 %. But 100% zeolit is not

problem to buy, because is made synthetically. Synthetic zeolit is not only one type [3], zeolits are used like molecular sieves. Is possible to specify, which one is the best for particular job. Big advantage of zeolit is using in innumerable cycles and his structure is still the same. Only for desorption is not good use the temperatures higher than 300°C. [1]

Desorption temperatures are between 160 – 200°C. This temperature is problem at using in solar cooling systems with conventional solar collector. We have to use concentric or vacuum collectors. COP at this system is between 0,1- 0,3.

Pair active carbon/methanol is known as well. With system utilizing this pair are used for ice making, because achieve temperature under zero is not problem. Active carbon is made synthetically and is not too expensive. Desorption temperatures are between 90°C – 100°C, what is advantage of this pair, because is not necessary to use some special sun collector, the usual flat collector is good for this system. But COP of this system is not too high, only around 0,1.

In this time the most popular adsorbent is silicagel at using with water like coolant. Silicagel has good properties for the adsorption cooling systems. Desorption temperatures are around 100°C. Silicagel is neutral to environment and is easy to use it. We no need any special sun collector and COP is between 0,4 – 0,7.

4.   Conclusion

Efficiency of sorption cooling systems is not comparable with compressor cooling systems, but advantage of sorption systems is utilization of waste heat or sun heat, what can be used in tri-generation systems.

We know lot of other pairs adsorbent/ coolant, but these are best for the using in cooling systems. In present time we are still looking for some new and the better pair.

References

[1]   MASARYK, M. (1997): Využitie zeolitových technológií v klimatizačnej technike, Zpravodaj českého zväzu chladiacej techniky 6/97 (ČR), str. 14-18.

[2]   http://www.solarserver.de/index-e.html.

[3]   www.vurup.sk.

[4]   JAKOB, U., MITTELBACH, W.: *Development and investigation of compact silica gel/ water adsorption chiller integrated in solar cooling systems*, VII Minsk International Seminar "Heat Pipes, Heat Pumps, Refrigerators, Power Sources", Minsk, Belarus, September 8-11, 2008.

Obtainment of Diagnostic Signals Based on Emission NO$_x$ in Light of Monitoring of Catalytic Converter

[*]Marcin Rychter

[*]Motor Transport Institute, Diagnostic and Servicing Proccess Department, PL-03-301 Warsaw, 80 Jagiellońska St., Poland, rychter@poczta.fm

Abstract. The paper presents basic roles of emission limits for PC and PDV vehicles with CI engine. Furthermore, catalytic converter supports and basic characteristic parameters have been shown. Propose methods of catalytic converter monitoring methods have been described. In the main part of the paper a new concept of catalytic converter monitoring has been presented and results of tested engine with experimental catalyticall converter with 200 cpsi support.

Keywords: temperature, monitor, OBD II, catalytic converter

1. Introduction

The OBD system (On Board Diagnostic system; known in the United States as the OBD II system and in Europe as the EOBD one) is a set of diagnostic tests and calculation and decisive procedures which are performed in a real time and are intended as a measure for evaluation of the emission efficiency and the efficiency of elements responsible for the passive and active safety of a vehicle.

2. Analyses of tested catalytic converter with 200 cpsi

In order to determine the effectiveness of the applied catalytic converter for the reduction of the NO$_x$ emission according to the obligatory official certification test ESC some preliminary examinations of its efficiency under the engine test bend conditions were performed. Taking the operation nature (character) into consideration the NO$_x$ emission in each phase of the test was analysed [1].

To determine the reduction in the NO$_x$ emission the emission measurements were taken after each catalytic block. The presented results are referred to the NO$_x$ concentration values before the catalytic converter**.**

Due to the diversified parameters characterising the catalytic converters, which are being built with the use of the catalytic carriers with different cell densities, the examinations were performed for the catalytic blocks based on the carriers with a cell density typical for the compression-ignition engines of 200 cpsi. The application of the catalytic carriers with higher cell densities was considered inadvisable because of a high resistance of flow of exhaust gases intensified by the PM emission.

The operation performance of the catalytic converter with the 200 cpsi carrier is similar in each phase of the test (fig. 1).

In phases II-XIII the catalytic converter was characterized by an effectiveness of the reduction in the NO$_x$ emission of 15%. The analysis of the measuring points shows that from the point c3 on the reduction in the NO$_x$ emission level was constant. That means that the

catalytic reactor volume is sufficient with reference to the assumed amount of the active layer deposited on each catalytic block. The ratio of that volume to the engine displacement volume was 0.76. The analysis of the bibliographic data shows that this ratio values are in the 0.75 - 1.3.range.
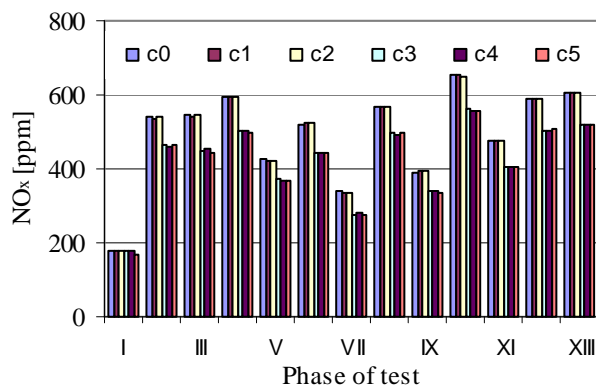

Fig. 1. Value of NO_x concentration during ESC test of catalytically converter with 200 cpsi [1].

The emission measurements in points $c6$–$c8$ are considered close to the emission measured in the point $c5$. For the discussed points the difference in the NO_x concentration was at the indication error level of the measuring exhaust gas analyser.

The performed analysis shows that the catalytic converter with the 200 cpsi carrier allows to obtain a satisfactory difference in the voltage signals basing on the NO_x concentration after the third catalytic block. However, it should be noted that the obtained effectiveness of the catalytic converter for the NO_x reduction is unsatisfactory. The average percentage effectiveness of the discussed catalytic converter in the measuring point c5 was 14%.

The obtained values of the voltages signals (fig. 2) present the levels of nitric oxides concentrations for the individual test phases. In the whole test the differences in signals from the examined sensors were found after the third catalytic block at the points U3, U4, U5.

At those points, which were considered as the measuring points after the catalytic converter, the level of voltage signals was constant. Assuming that the preset working temperature of the sensors is being maintained this means that the obtained differences in pressure at the discussed measuring points do not significantly affect the possibility of obtaining the voltage signals.

It was found that the voltage differences at the points U3–U5 of the discussed catalytic system with a 200 cpsi carrier are of negligible importance. In the following analysis the average voltage values for each phase of the test at those points are assumed.

The values of the generated voltage signals in the tested system were in the range from 0.76 to 2.72 mV. The maximum value was found in phase X and the minimum one in phase VII. The signal values above 2 mV were obtained were obtained for those test phases which were characterized by loads from the range of 75 to 100% of the maximum torque. Those values were obtained from the sensor placed before the catalytic converter for phases II, IV, VIII, X, and XIII and they were of 2.06, 2.27, 2.1, m2.72, 2.06, and 2.09 respectively. It means that in case of a large volume of the gas reactants in the measuring probe, and thereby at a higher probability of collisions of particles, an ability of de-pumping the oxygen from the areas 1 and 2 is high and it results in a high efficiency of initialising the electro-catalytic decomposition on a rhodium electrode. It can be concluded that for such engine parameters the

system sensitivity is highest. It can be confirmed by the difference in the voltage signals generated under such same working conditions of the engine (fig. 3).
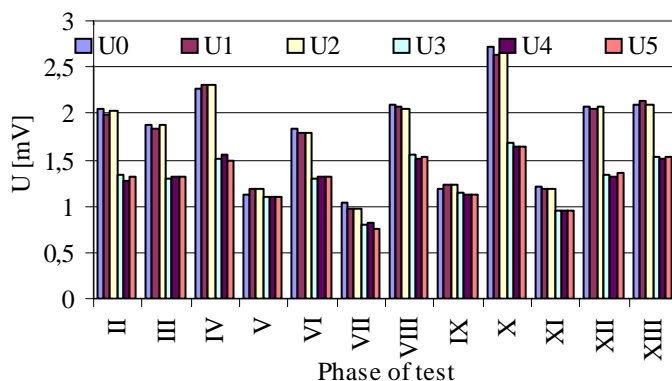

Fig. 2. Distribution of voltage signals during ESC test in measurement points U0–U5 in exhaust pipe with catalytically converter with 200 cpsi support [1].
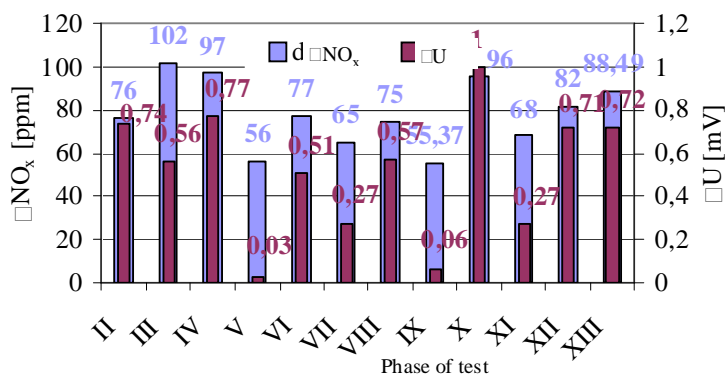

Fig. 3. Difference of voltage signals and NO_X concentration during ESC test in measurement points U0 and U5 in exhaust pipe with catalytically converter with 200 cpsi support [1].

A proper selection of the working parameters of the tested engine is an important analytical element in the aspect of the diagnostic monitor realisation in the onboard diagnosis system OBD. Phases II and X are most favourable from the point of view of the exact representation of the concentration values by voltages signals, however, they refer to the engine working parameters (n = 2400 rpm and n = 3670 rpm at 100% load) which could not occur during a typical operation of the vehicle. Similar conclusions can be referred to the phase VIII. In case of phases XII and XIII the range of loads is smaller and it is 75 and 50% of the maximum torque.

However, the crankshaft rotational speed is close to the maximum one. Taking the above analysis into account the most favourable parameters in the aspect of the realisation of the diagnostic monitor for the discussed system with the 200 cpsi carrier are those of the phase IV (fig. 4).

The working parameters of this phase reach the values possible to be obtained during the operation of the vehicle in urban drive. This is confirmed by the ETC test which represents the operation of the vehicle under different conditions. The operating parameters for the phase IV occur in that part of the test which represents operating the vehicle in urban drive. At this

stage of the ETC test the working parameters of 75% of the maximum crankshaft rotational speed and the maximum load are reached for 15 times. In case of phases II and X such parameters in urban drive (in turn: $M_o = 100\%$, $n = 58\%$; $M_o = 100\%$, $n = 89\%$) are reached only twice.
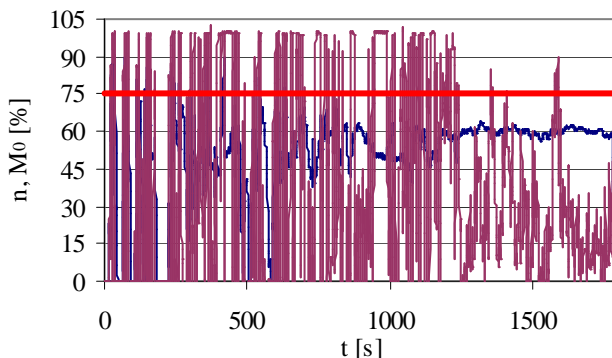

Fig. 4. Part of ETC test realization on test bad with presents using vehicle in urban driving; red line characterize parameters of runnig engine in part IV of ESC test [1].

In this connection it can be stated that the phase IV, in the aspect of the voltage signals generation and the possibility of starting the realisation of the diagnostic monitor, is most convenient for the described catalytic system and the engine which is subject to the test.

3. Conclusion

On the basis of the performed examinations and obtained test results the following conclusions can be drawn:
1. The analysis of the NO_x concentrations in exhaust gas from the compression-ignition engine can be based on the indications of the voltage probes with the modified electrodes of the oxygen pump;
2. The application of the reduction conditions in the voltage probes using the nitrogen oxides reduction by the electro-catalytic way depends on the exhaust gas parameters, the values of which change depending on the rotational crankshaft speed and engine load. For this reason obtaining the diagnostic signal for the whole engine operation range is impossible. The control of the correctness of the catalyst operation regarding the nitrogen oxides reduction can be realised for the defined operating parameters of the tested engine.

References

[1] RYCHTER, M. *Monitoring of compression ignition engine with OBD system on basis of exhaust emission in light of ecological manageability of engine*. Ph.D. dissertation, Poznań University of Technology, Poznań, 2004.

The Research on Railway Disc Brake with Closed Ventilation Canals of the Brake Disc

*Wojciech Sawczuk, **Grzegorz Szymański
* Poznan University of Technology, Faculty of Combustion Engines and Transportation Chair of Railway Vehicles, Piotrowo 3, 60-965 Poznan, Poland, wojciech.sawczuk@doctorate.put.poznan.pl
** Poznan University of Technology, Faculty of Combustion Engines and Transportation Chair of Railway Vehicles, Piotrowo 3, 60-965 Poznan, Poland, grzegorz.m.szymanski@put.poznan.pl

Abstract. A visual inspection of outside defects on brake discs is one of many activities made during overhaul of rail cars in accordance to technical and operational documentation. On this inspection outside defects on the disc caused by, among others, hitting by break stones are checked as well as thermal cracks on the friction surface and foreign matters in the ventilation canals [2].
The purpose of this article is to present the results of stationary tests with the disc brake with closed vane area by stimulating the presence of foreign matters in the ventilation canal.

Keywords: disc brake, ventilation canals, disc temperature, friction coefficient.

1. Introduction

Because of higher and higher speed, in most of rail vehicles disc brake is the prime operating brake. As distinguished from a traditional block brake, a disc brake thanks to better discharge of braking heat into the environment enables realization of stronger single pressures on the brake disc and obtaining bigger braking couple. The condition of quick exchange of braking energy into heat is strictly contingent upon impurities in inner ventilation canals and presence of break stones or other foreign matters in vane space of the disc. The concentration of heat energy on the brake disc has an effect on deterioration of braking process, what in extreme cases may lead to loss of braking power. During overhauls of braking systems in cars in accordance with technical and operation documentation, particular attention is paid to impurities and presence of foreign matters in ventilation canals of the disc.

The purpose of stationary tests was to determine selected characteristics of braking process on the brake disc with closed vane space by stimulating presence of foreign matters in ventilation canals.

2. Methodology and object of research

The tests were carried at an inertial station for testing rail vehicles brakes. A brake disc type 610x110 with ventilation vans and a set of matched brake linings type 200 FR20H.2 35 mm thick were the object of the test. Research program C (fast drive) was applied for the tests, according to [1] brakings were performed at speed of 120, 160 and 200 km/h, with lining pressure of 44 kN to the disc and braking mass of 7,5 t per disc. Disc temperature in the whole range of braking time was registered by six thermocouples; three of them were mounted on two sides of the disc and placed every 120º on three rays. The presence of foreign matters in

the area between the vanes was simulated by placing a band clamp on ventilation vanes. The way how the ventilation areas were covered is presented in Fig. 1.
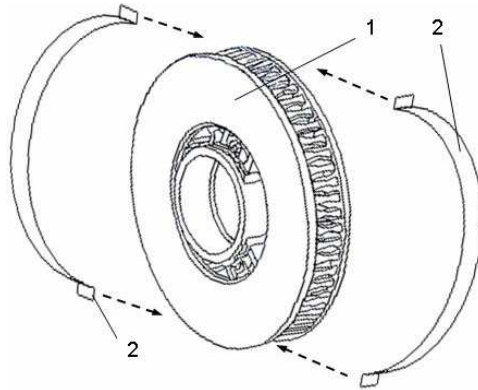

Fig. 1. Placing a band clamp on brake disc type 610×110: 1-brake disc, 2- right and left part of the band clamp.

Before main tests were carried out a series of identification tests had been made on the disc with open ventilation canals, thanks to which undisturbed flow of cooling was provided. For each speed at the beginning of braking eight repetitions of braking were performed.

3. Analysis of tests results

During tests the following parameters were measured: disc temperature at stoppage Fig. 2, average friction coefficient Fig. 3 and time of disc cooling to 60 ºC Fig. 4. Disc cooling was realized by simulating a car run at 100 km/h.
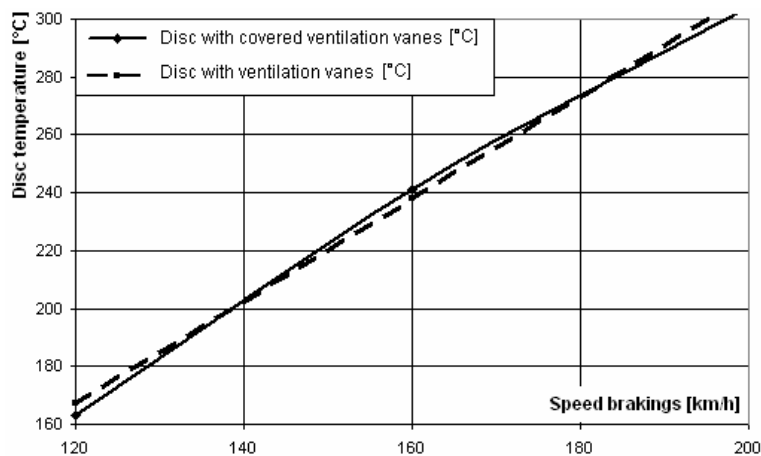
Fig. 2. Distribution of average temperature of brake disc type 610×110.
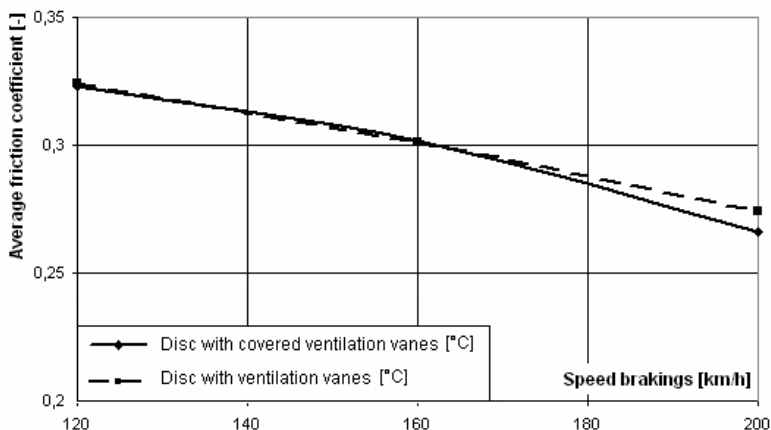
Fig. 3. Flow of average friction coefficient.
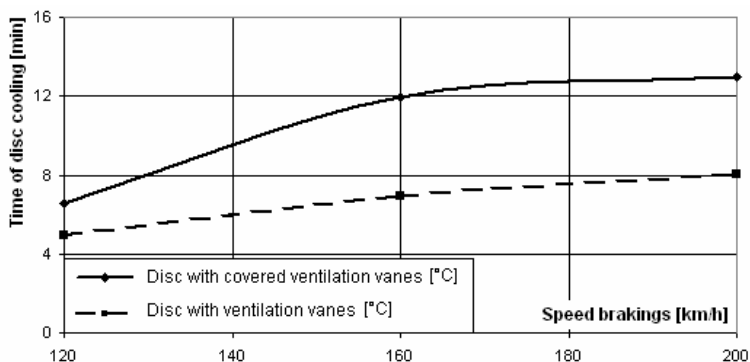
Fig. 4. Flow of cooling time of brake disc at 600rpm (100km/h) after stoppage braking

Brakings of a disc with covered ventilation vanes could lead to a change in the structure of the material as a result of strong thermal load. On the friction surface of the disc overheating occurred in a form of two rings in the area of inner and outer diameter of the disc. Discoloration of the friction area was observed yet after six brakings (Fig. 5).
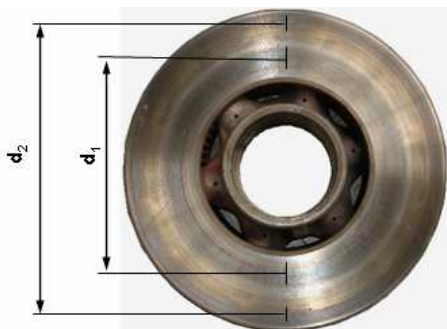
Fig. 5. View of the disc after series of brakings with covered ventilation vanes with visible surface overheating in a form of two rings of various diameters

During brakings on the disc with covered vane area, on one of the thermocouples overflow of temporary disc temperature over 400 °C was registered and reached scope between 403÷417 °C. According to [1] brake discs of rail vehicle on brakings should not reach

temporary temperature over 400 °C, because this causes disc deformation and loss of required resistance and flexibility.

4. Conclusion

After stationary tests it was found that covering the vane area simulating the presence of foreign matters between vanes has no substantial influence on temperature measured at stoppage and the value of friction coefficient in comparison to a disc with undisturbed ventilation. The changes in temperature and friction coefficient are contained in statistical error. The change in disc temperature with open and closed vane area has not been noticed, which may stem from long period of breaking heat discharge into the environment against time of singular braking, what was described in [3]. However, covering vane has significant influence on cooling time of the disc after braking. A disc ventilated during car run with a simulated speed of 100 km/h cools by 25÷40 % faster then a covered disc depending on speed at the beginning of braking.

Further usage of a disc with closed vane area because of longer cooling times may be the reason of faster disc wear as a result of strong heat load. On the friction surface of the disc discolors occur in a form of rings of various diameter. In further tests an analysis of disc material structure caused by overheating of friction area of the disc is planned.

Acknowledgement

References

[1] Kodeks UIC. *Hamulec – Hamulec tarczowy i jego zastosowanie. Warunki dopuszczenia okładzin hamulcowych.* Wydanie 6, listopad 2006.

[2] Rail Consult Gesellschaft für Verkehrsberatung mbH. *Wagon osobowy Z1 02, układ jezdny-tom2.* Dokumentacja Techniczno-Ruchowa.

[3] SOROCHTEJ M.: *Kształtowanie jakości zespołu ciernego hamulca tarczowego.* Przegląd Kolejowy 1/94.

Noise Reduction of Freight Rail Traffic

[*]Michal Striz

[*]University of Zilina, Faculty of mechanical engineering, Department for transportation and
manipulation machinery, Univerzitna 1, 010 28 Zilina, Slovak Republic
{michal.striz@fstroj.uniza.sk}

Abstract. This article describes the status of actual noise reduction methods in freight railway traffic. It shows the policies of different organizations which are relevant in railway business and also represents the measures taken to reduce noise of freight rail traffic across the EU.

Keywords: noise reduction, freight rail traffic, TSI, END.

1. Introduction

Freight trains are a strong source of noise emissions. Since the development of railway networks in Europe, the number of trains running on them constantly grew as a result to the industry and population growth.

The main sources of noise are currently used braking components on rolling stock (cast iron brake blocks, in the following as CI-blocks) and rolling noise (especially in sharp curves, where also the "squeezing" noise appears).

2. EU noise precautions

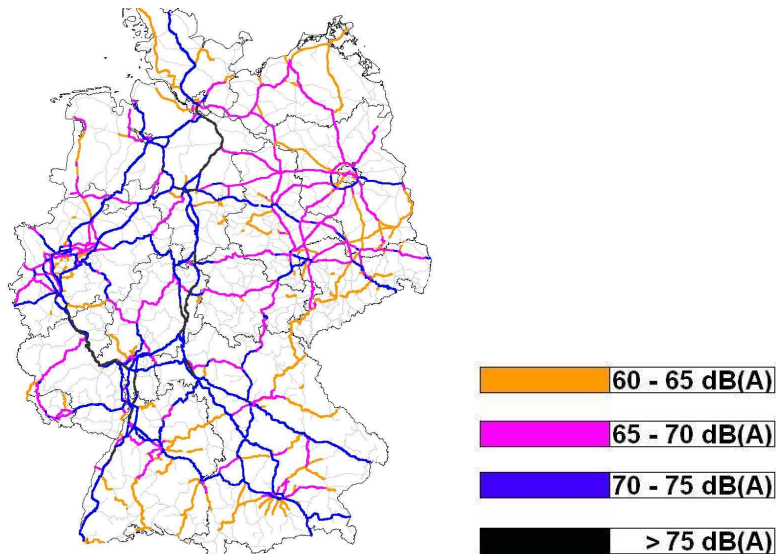As seen on Fig. 1, main railways are hot spots for noise emissions.

Fig. 1.   Noise emissions from major railway lines in Germany at night.

129

Thus the figure presents Germany; the situation is similar in every EU-country. The EU had to find a way how to reduce noise emissions from freight trains without jeopardising the competitiveness of rail transport. To do so, the EU was considering the measurement, which had the highest cost-effectiveness and health benefits ratio. The policy keeps following these major theses:

- Priority of rolling noise as the most predominant type of noise
- Freight wagons as most important source
- "Smooth wheels on smooth tracks"
- Noise emission limits for new vehicles
- Additional measures for the existing fleet
- Need for contributions of all relevant stakeholders to a common European strategy to reduce rail noise
- Need for development of affordable technologies to reduce noise at its source

Keeping these theses in mind, the measures at the source of the noise (rolling stock based measures) were identified more expensive than infrastructure based measures (such as noise barriers and insulating windows) as the retrofitting costs are estimated between 180 million to 1.8 billion Euros. The stakeholders do not have sufficient incentives, resources or direct influence to implement such cost-effective retrofitting programmes.

Yet, the EU released the Directive 2002/49/EC (Environmental Noise Directive, END). Also the Technical Specification of Interoperability (TSI) adopted in 2002 is setting noise emission limits for rolling stock. These are again opening the problem of retrofitting since the older rolling stock also has to fulfil the requirements of the directives mentioned above and is also a major contributor to noise emissions (Fig. 2 and Fig. 3).
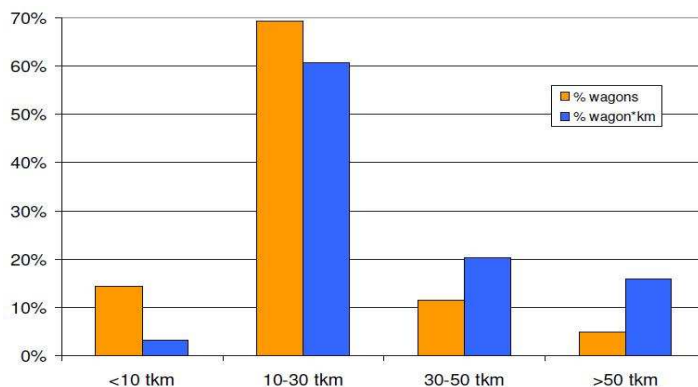

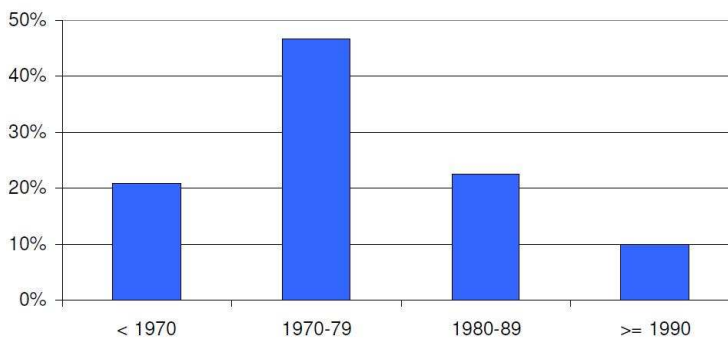**Fig. 2.** Mileage of wagons and their contribution to the overall noise emission.

Fig. 3. Age distribution of European freight wagons

130

The EU estimates, that there are about 360.000 wagons to be retrofitted in the 27 EU states, Switzerland and Norway.

Considering all the aspects the EU has made following conclusions to the noise reduction:

- European legal framework completed since December 2005
- Adoption of Communication of the European Commission in March 2008
- Additional measures at the source required: Retrofitting of freight wagons with low-noise brake blocks
- Keep ongoing study on impacts of policy options
- Need for clarification of the availability of affordable technical solutions and homologation procedures [1].

3. UIC measures

The UIC has started its own action programme in cooperation with the EU. The UIC action programme is divided into three work packages:

- Technology
- Funding and financing
- Communication and consensus finding

Technology

According to the UIC, the freight railway operation has to meet two basic requirements:

- Increase of railway traffic
- Reduce environmental impacts

The frameworks of action are the new legal aspects like the above mentioned TSI and END, but also the national legislations, like noise reduction action plans worked out by the local authorities, legislations based on noise reception limit values for new and upgraded lines in all European states and legislations suggested by residents challenging rail freight traffic along highly frequented corridors.

The UIC is also doing researches and came to the conclusion, that the railway noise is basically caused by rough wheels rolling on rough tracks, which corresponds with the theses mentioned in Chapter 2. The wheel roughness of freight wagons comes from CI-blocks rubbing the bearing surface of the wheel (Fig. 5). On the other hand, composite brake blocks keep the bearing surface of the wheel smooth and thus are reducing noise emissions (Fig. 4).

Fig. 4. Wheel using a composite block   **Fig. 5.** Wheel using a CI-block

Measurements are showing, that the noise reduction of a composite brake shoe "K"-type is 8-10 dB(A) – at this level the perceived noise is even halved. The noise reduction of "LL"-type is approximately of the same level.

As mentioned in Chapter 2 retrofitting is one of the most expensive measures in noise reduction, yet unequally to infrastructure measures, by retrofitting the whole net benefits from "low-noise" freight trains. At least in Belgium, in the Netherlands and in Germany the transport on rail to and from the harbours through populated areas will increase considerably until 2015. Without silent trains the necessary improvements of the capacity of the corridors will not be realized. Also, by that time almost 20% of the wagons will be newly purchased and more than 50% of the existing wagons should be retrofitted.

The conclusion of this package is that the technology of composite brake blocks is available and allows a significant reduction of rail freight noise emissions at the source.

Funding and financing

Although retrofitting may be more expensive than infrastructure based measures, the cost-effectiveness to health benefits ratio is very satisfying and – as mentioned above – silent rolling stock is a benefit for the whole infrastructure. Fig. 6 presents an UIC study to the costs of various measures in relation to people living under 60 dB(A) noise caused by freight rail traffic.
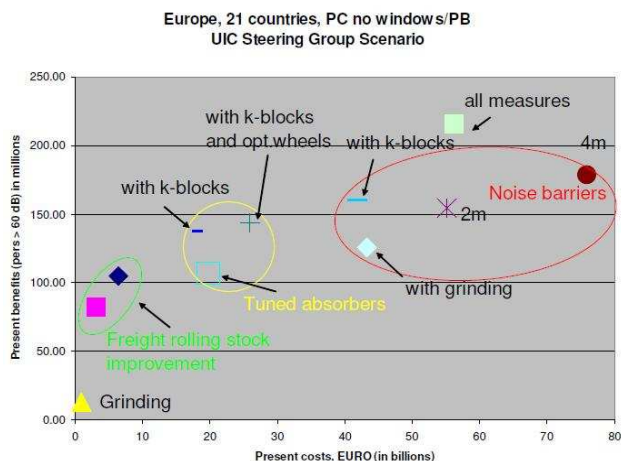

Fig. 6. Cost-Benefit-Analyses study results.

- On European level:
  - New Financial Instrument for the Environment, in force since June 2007 (LIFE+), which could finance pilot projects to railways via environmental agencies.
  - Cohesion funds, which could finance retrofitting in regions designated for development.
- On national level:
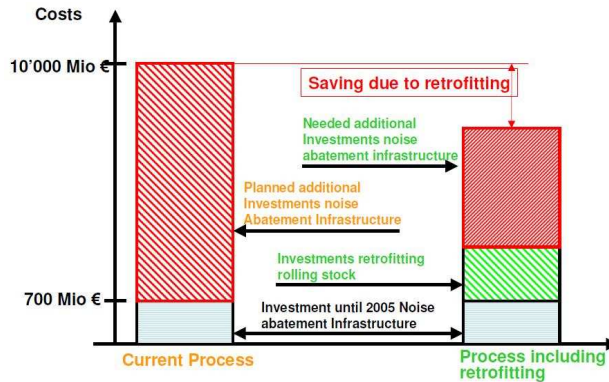 - Redirecting financial streams from noise screen construction to retrofitting rolling stock.

Fig. 7. Redirecting financial streams.

The diagram on Fig. 7 shows possible savings implementing retrofitting into the action plans made due the END (Chapter 2).

The conclusion of this package is that the EU countries spend a lot of money for infrastructure based measures. Instead, retrofitting would be more efficient at the same effect. Incentives for retrofitting have to be set.

Communication and consensus finding

The EU-Commission is about to propose instruments to reduce noise emissions of rolling stock, especially using retrofitting. European rail freight companies have reached consensus that retrofitting with composite brake blocks is the best option available to reduce noise emissions and a dialog between rail companies and wagon owners has been established. UIC members also have started national activities.

The conclusion of this package is that the railway companies and politicians have reached a consensus on the need to act. Now a consensus has to be found how to start the retrofitting process as soon as possible [2].

4. Noise reduction activities in Europe

EU-countries have started the noise reduction programmes on their own. While most of the countries like Norway, Sweden, Denmark, United Kingdom, France, Belgium, Austria, Poland and Slovakia are building noise barriers, some countries are doing combined measures. These countries are Netherlands, where track absorbers are being installed and also rolling stock is being retrofitted, Germany, where retrofitting, noise barriers and insulated house windows are being installed and Switzerland is also combining retrofitting with noise barriers.

The reasons why countries tend to use infrastructure measures (noise barriers) are listed below:

- Organizational obstacles: Separation of infrastructure and operation vs. noise is emitted from the whole system – operators and wagon owners is a complex system – infrastructure is simpler.
- Political obstacles: Local vs. global solutions – politicians are elected locally – return of investment for global solution is unclear.
- Legislative obstacles: Do EU-states aid rules applying retrofitting ? – national legislation: e.g. Italy.

- Philosophical obstacles: Symptoms vs. cause – individual comfort in short run vs. better solutions for everybody in long run.
- Incentives mainly for noise barriers: Local politics – included in budget of projects – "state of the art" – retrofitting may increase cost of operation.
- Lobbying support for noise barriers: Construction industry lobbies for noise barriers – road lobby against direct subsidies of railway operators.

The conclusions are, that current funding has to be redirected, because the savings from retrofitting are bigger if retrofitting starts sooner. Also EU or government support is needed [3].

5.   Conclusion

The article draws the actual problems in noise emission near. It presented some solutions and conclusions what has to be done if the current noise levels and invested funds have to be reduced.

References

[1]   KUNST H.: *EU noise policy*, UIC Workshop 2007.
[2]   MATHER M.: *UIC action plan*, UIC Workshop 2007.
[3]   OERTLI J.: *Overview of activities on railway noise*, UIC Workshop 2007.

Stress Analysis of Specimens for Multiaxial Fatigue Testing

*Andrej Udvorka, Miroslav Blatnický, Peter Kopas
*University of Zilina, Faculty of Mechanical Engineering, Department of Applied Mechanics,
Univerzitná 1, 01026 Žilina, Slovakia,
{andrej.udvorka, miroslav.blatnicky, peter.kopas}@fstroj.uniza.sk

Abstract. This paper contains the stress analysis of specimens for new multiaxial fatigue testing machine, which is prepared to make the combined loading by bending and torsion. Results of this analysis make possible to choose the testing mode and next final evaluation of this process.

Keywords: multiaxial fatigue, bending, torsion

1. Introduction

The fatigue crack of materials is one of the most frequent reasons of termination of mechanical parts and machines. The consequence of this fact is rising importance of monitoring of fatigue process, while fatigue behaviors of materials are the most considering factor in the design procedure to assure the safety and reliability of mechanical parts and constructions.

It is possible to say that prediction methods [1, 2] for the fatigue life of mechanical parts are subject of broad research and they have been published in many publications, but the results of these methods have not be found for practical applications and they are not regarded as universal yet. For this reason it is necessary to keep up the progress of these methods but also methods of fatigue testing of materials to make initial conditions for numerical computation of fatigue life by the prediction methods.

However, one factor of fatigue process must be considered. Many publications deal with researching of fatigue behaviors, but the most of them deal only with uniaxial fatigue testing. The problem of properly performing the fatigue assessment is further complicated by the fact that such failures are, in general, caused by multiaxial loadings. While the methods suitable for assessing components under uniaxial fatigue loading have already been investigated in deeply over the last century, the multiaxial fatigue criteria have not reached a satisfactory level yet, especially when variable amplitude loadings are involved [3].

2. Multiaxial fatigue testing

The fatigue loading system for testing specimens by combined bending-torsion loading, which is the subject of this paper, has been documented and published [4]. Generation of combined cyclic loading can be showed on Fig. 1. It is necessary to suggest that bending and torsion loading is independent from one another and also their measuring and control units are separate.

If we approximate loading by constant force which equals to the amplitude of loading force, then we can draw the concept of bending loading system by schema at Fig. 2. As a result on

that, computed stress approximately equals to the amplitude of stress in the case of bending and also torsion.
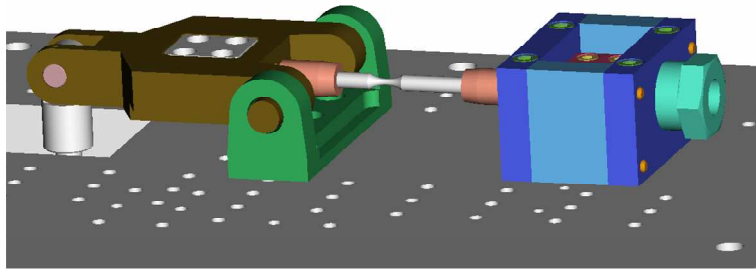

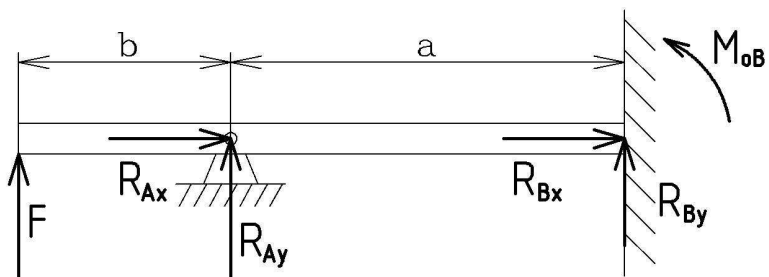**Fig. 1.** Multiaxial fatigue cyclic loading system.

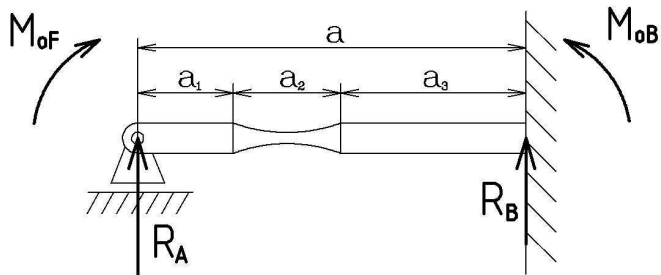**Fig. 2.** Scheme of the cyclic bending loading system.

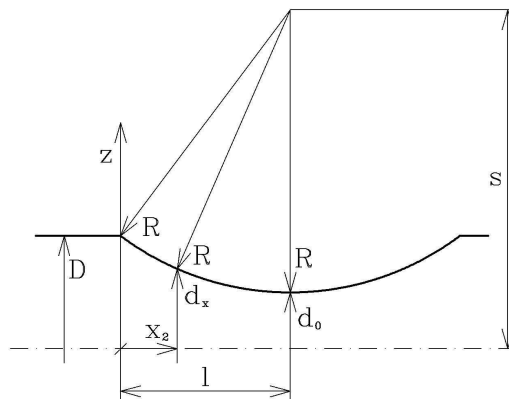**Fig. 3.** Simplified schema of the cyclic bending loading system with the design of specimen.

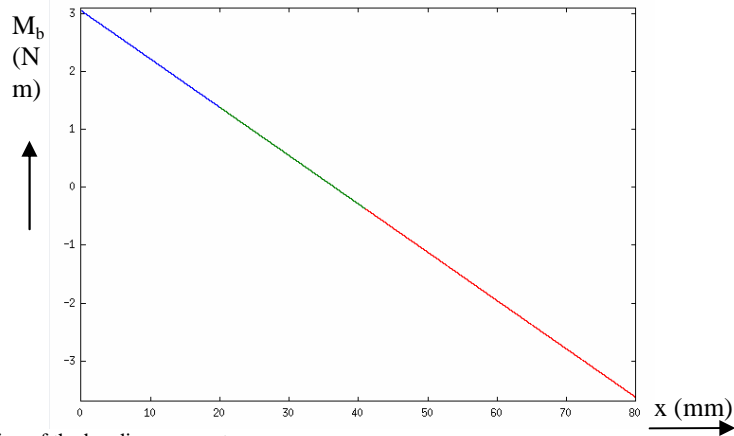**Fig. 4.** Design of the specimens contraction
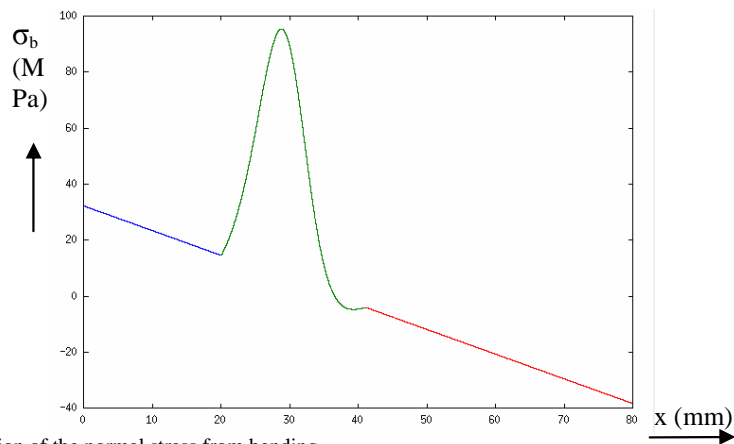
Fig. 5. Distribution of the bending moment

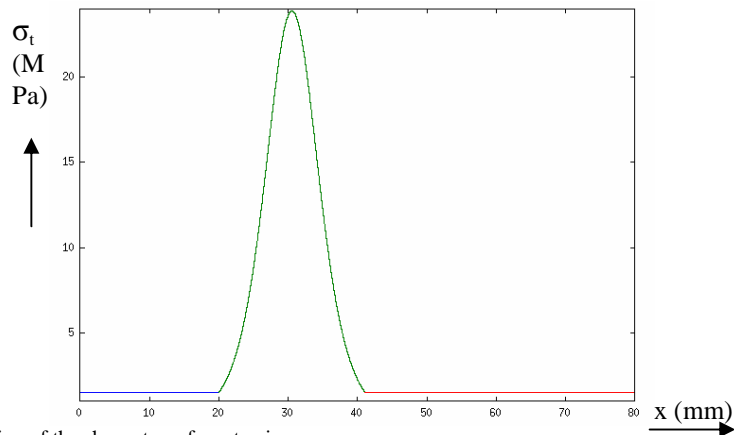**Fig. 6.** Distribution of the normal stress from bending

Fig. 7. Distribution of the shear stress from torsion

The simplified schema on Fig. 3 is the case of the static undetermined bend and its solution is a bit complicated because the cross section of the specimen has a contraction in the middle of the length as it is shown at Fig. 4. Its solution is shown at Fig. 5 and Fig. 6. The

torsion loading system is simpler because the distribution of torque is constant for the whole length of specimen and only the shear stress is depends on the cross section of the specimen (Fig. 7). The distribution of the equivalent von Mises stress from the combined bending and torsion loading is shown at Fig. 8 if the single loadings are in the phase.
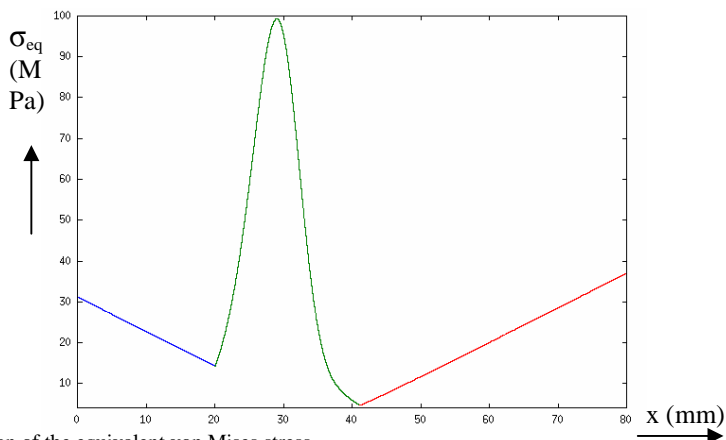

Fig. 8. Distribution of the equivalent von Mises stress

3. Conclusion

The stress distribution at the multiaxial cyclic loading has been analyzed for both cases separately as well as the combined loading if single loadings are in the phase. But we must remember that it is only a linear solution of this problem and it serves the purpose of design of specimen's geometry. The exact analysis require to using the final element method.

Acknowledgement

References

[1] PAPADOPOULOS, I. V. *A new criterion of fatigue strenght for out-of-phase bending and torsion of hard metals.* Fatigue Vol. 16, 1994, 377 – 384

[2] PAPUGA, J. - RŮŽIČKA, M. *Two new multiaxial criteria for high cycle fatigue computation.* International Journal of Fatigue 30, 2008, 58–66

[3] CRISTOFORI, A., SUSMEL, L., TOVO, R. *A stress invariant based criterion to estimate fatigue damage under multiaxial loading.* International Journal of Fatigue 30, 2008, 1646 – 1658

[4] UDVORKA, A., KOPAS, P. *Multiaxiálny únavový testovací systém.* In: Nekonvenčné technológie 2008, Žilina – Strečno, SR